IOWA STATE UNIVERSITY
Digital Repository

Retrospective Theses and Dissertations

Iowa State University Capstones, Theses and Dissertations

1984

Applications of NMR to the dynamics of carbohydrates: simplifying NMR spectra of proteins

Serge Lacelle
Iowa State University

Follow this and additional works at: https://lib.dr.iastate.edu/rtd

 Part of the Physical Chemistry Commons

Recommended Citation
Lacelle, Serge, "Applications of NMR to the dynamics of carbohydrates: simplifying NMR spectra of proteins " (1984). *Retrospective Theses and Dissertations*. 8183.
https://lib.dr.iastate.edu/rtd/8183

This Dissertation is brought to you for free and open access by the Iowa State University Capstones, Theses and Dissertations at Iowa State University Digital Repository. It has been accepted for inclusion in Retrospective Theses and Dissertations by an authorized administrator of Iowa State University Digital Repository. For more information, please contact digirep@iastate.edu.

www.manaraa.com

INFORMATION TO USERS

This reproduction was made from a copy of a document sent to us for microfilming. While the most advanced technology has been used to photograph and reproduce this document, the quality of the reproduction is heavily dependent upon the quality of the material submitted.

The following explanation of techniques is provided to help clarify markings or notations which may appear on this reproduction.

1. The sign or "target" for pages apparently lacking from the document photographed is "Missing Page(s)". If it was possible to obtain the missing page(s) or section, they are spliced into the film along with adjacent pages. This may have necessitated cutting through an image and duplicating adjacent pages to assure complete continuity.

2. When an image on the film is obliterated with a round black mark, it is an indication of either blurred copy because of movement during exposure, duplicate copy, or copyrighted materials that should not have been filmed. For blurred pages, a good image of the page can be found in the adjacent frame. If copyrighted materials were deleted, a target note will appear listing the pages in the adjacent frame.

3. When a map, drawing or chart, etc., is part of the material being photographed, a definite method of "sectioning" the material has been followed. It is customary to begin filming at the upper left hand corner of a large sheet and to continue from left to right in equal sections with small overlaps. If necessary, sectioning is continued again—beginning below the first row and continuing on until complete.

4. For illustrations that cannot be satisfactorily reproduced by xerographic means, photographic prints can be purchased at additional cost and inserted into your xerographic copy. These prints are available upon request from the Dissertations Customer Services Department.

5. Some pages in any document may have indistinct print. In all cases the best available copy has been filmed.

University
Microfilms
International

300 N. Zeeb Road
Ann Arbor, MI 48106

8505837

Lacelle, Serge

APPLICATIONS OF NMR TO THE DYNAMICS OF CARBOHYDRATES; SIMPLIFYING NMR SPECTRA OF PROTEINS

Iowa State University PH.D. 1984

University Microfilms International 300 N. Zeeb Road, Ann Arbor, MI 48106

PLEASE NOTE:

In all cases this material has been filmed in the best possible way from the available copy. Problems encountered with this document have been identified here with a check mark _✓_.

1. Glossy photographs or pages _____
2. Colored illustrations, paper or print _____
3. Photographs with dark background _____
4. Illustrations are poor copy _____
5. Pages with black marks, not original copy _____
6. Print shows through as there is text on both sides of page _____
7. Indistinct, broken or small print on several pages ✓
8. Print exceeds margin requirements _____
9. Tightly bound copy with print lost in spine _____
10. Computer printout pages with indistinct print _____
11. Page(s) _____ lacking when material received, and not available from school or author.
12. Page(s) _____ seem to be missing in numbering only as text follows.
13. Two pages numbered _____. Text follows.
14. Curling and wrinkled pages _____
15. Other _____

University
Microfilms
International

Applications of NMR to the dynamics of carbohydrates; simplifying NMR spectra of proteins

by

Serge Lacelle

A Dissertation Submitted to the
Graduate Faculty in Partial Fulfillment of the
Requirements for the Degree of
DOCTOR OF PHILOSOPHY

Department: Chemistry
Major: Physical Chemistry

Approved:

Signature was redacted for privacy.
In Charge of Major Work

Signature was redacted for privacy.
For the Major Department

Signature was redacted for privacy.
For the Graduate College

Iowa State University
Ames, Iowa

1984

TABLE OF CONTENTS

LIST OF FIGURES

LIST OF TABLES

GENERAL INTRODUCTION

Since the first experimental detection of NMR signals in the condensed phase in 1945 (1,2), tremendous progress has been made in application of this branch of spectroscopy to biological problems. Until 1969, less than 300 literature reports were found in this field (3). By 1981, over 8000 publications (3) appeared and today biological NMR studies are reported in greater number than ever before. This great success is due in part to technological advances which permit a variety of experiments to be performed routinely. From early studies of water bound to DNA (4), to the study of protein conformations by modern two-dimensional NMR techniques (5) and recent NMR imaging medical applications (6), a range of biological structures have been investigated.

In a magnetic field, the degeneracy of energy levels of nuclear spin magnetic moments is lifted. Transitions across these levels are stimulated with radio frequency (r.f.) radiation in the form of a pulse. The ensuing signal is detected by standard r.f. technology, digitized and stored in a computer memory. Since at equilibrium the population differences across the energy levels are of the order of parts per million, NMR is a rather insensitive technique. For this reason, it is necessary to accumulate signals in order to obtain a large signal to noise ratio. The methods of Fourier analysis are then applied to the time domain signal to yield the frequency spectrum. The power of NMR methods lies in the ability to provide microscopic structural details in the range of 1-500 Å. Dynamic processes

occurring over a time scale of months to picoseconds may be studied: time dependence of NMR spectral parameters such as relaxation constants, chemical shifts and lineshapes provide information about the nature and amplitude of such processes. This accounts for the widespread use of NMR techniques. The work presented in this dissertation makes extensive use of NMR data obtained both in the time and frequency domain representations.

The purpose of this dissertation is two-fold. In the first part, we study the dynamics in powders of carbohydrates with a variety of nuclear spin dynamics experiments. The NMR spectra of these systems are broad and somewhat featureless. Therefore time domain experiments are appropriate, since much more information is available in this representation than is obtained in the frequency spectrum. In the second part, we propose a new approach to the analysis of chemical shift data (in the frequency domain) of proteins and other biological systems. With modern two-dimensional NMR techniques, it is now possible to assign hundreds of resonances to particular atoms in proteins. The large data base generated by these experiments is reduced with statistical methods. In this way, we simplify or classify the information content of spectra.

Simple polysaccharides are made of carbon, oxygen, and protons, all of which have NMR active isotopes. ^{1}H is by far the most sensitive NMR probe. Cross-polarization techniques enhance ^{13}C signals but relaxation studies are somewhat difficult. In the solid state, the routine use of quadrupolar nucleus, ^{17}O still presents an

enormous challenge to the NMR spectroscopist. In the past, studies of carbohydrates in the solid state have been mainly limited to the water of hydration found in powders (7-8). Two major factors are responsible for this limitation: first, the overwhelming water signal in most cases obscures the carbohydrate signal; second, the polysaccharide protons usually experience strong dipolar coupling, and the signal lasts on the order of 50×10^{-6} seconds as opposed to 10^{-3} seconds for that of water of hydration. This fact poses stringent technical requirements upon experiments in solids. Recently, proton relaxation measurements were performed on cellulose and pectin (9). High resolution ^{13}C NMR techniques have been applied to cellulose (10-11). The detection of motions from kHz to MHz range is a difficult problem by other techniques. The role of molecular motions of carbohydrates in biological processes such as cell wall enlargement or enzyme catalysis of polysaccharides in storage granules has not been investigated. By beginning with simple model systems where the structure is known from x-ray crystallography, one may correlate relaxation parameters with certain segments of the molecules. These studies can then serve as a frame of reference for more complex systems (9).

The isotropic chemical shift has long been the single most used NMR spectral parameter by chemists. At the same time, it is one of the least understood interactions in NMR. Most of our knowledge in this area comes from empirical research. Within a molecule, different atoms have different chemical shifts, which accounts for their

popularity in structural determination. We propose the characterization of the collection of chemical shifts from a molecular point of view rather than the usual analysis of individual shifts of different atoms. In the past, the former approach has been used in conjunction with group theory (12) and graph theory (13). Molecular symmetry elements are needed for the application of group theory; for this reason, only relatively small molecules have been studied with this technique. Application of graph theory has been limited primarily to aromatic hydrocarbons which are amenable to correlation of structural connectivities with local and global molecular properties. We are interested in the chemical shifts of whole proteins. Clearly the previous approaches are inadequate. We propose to use statistical methods to analyze the distribution of the spacing between energy levels (or transitions), and the distribution of energy levels as a function of the energy. In this way, we qualitatively characterize the irregularity and the general appearance of the chemical shift spectra of proteins.

This dissertation follows the alternate style format. Sections 1 and 2 are to be submitted for publication to Biopolymers. Section 3 has been published in the Biophysical Journal 46, 181, (1984); the copyright belongs to the Biophysical Society. Section 4 is to be submitted for publication to the Biophysical Journal.

DYNAMICS OF CYCLODEXTRINS AND DEXTRAN BY SOLID STATE NMR.1

Serge Lacelle and Bernard C. Gerstein

Ames Laboratory, DOE* and Department of Chemistry
Iowa State University, Ames, Iowa 50011

*Operated for the U. S. Department of Energy by Iowa State University under contract No. W-7405-Eng-82. This research was supported by the Office of Basic Energy Sciences, Chemical Sciences Division.

SECTION I. DYNAMICS OF CYCLODEXTRINS AND DEXTRAN BY SOLID STATE NMR.1

Abstract

Broadline ^{1}H and high resolution ^{13}C solid state nuclear magnetic resonance (NMR) investigations of the dynamics of α and β cyclodextrins, and dextran B512F in powders are reported. In these polysaccharides, the homonuclear magnetic dipolar interactions and motions were monitored with relaxation measurements in the laboratory and rotating frames, and in dipolar local fields (T_1, T_{1d}, $T_{1\rho}$, T_2). Qualitative spectral density functions are obtained for motions in the kHz range from these relaxation measurements. From the relative proportions of the relaxation decays and lineshapes, it was possible to correlate the various time constants with different segments of the molecules. Water of hydration and its dynamics within the biopolymers were also examined. ^{13}C chemical shift variations indicate the interplay of local (1 glucose unit) and longer range (6-7 glucose units) conformations and order as important factors in determining these shifts. The temperature dependence of the ^{1}H lineshape and the dipolar spin-lattice relaxation time, T_{1d} were measured for α cyclodextrin yielding energies of activation. The results are discussed in the light of x-ray crystal and molecular structures. Hydrogen bonding is shown to play an important role in the dynamics of these systems.

Introduction

Biopolymers of carbohydrates form a wide and diverse range of chemical structures. They function in structural organization as in plant cell walls, and in food storage as found in cytoplasmic granules and seeds. Various biosynthetic pathways and regulatory mechanisms are involved in the conversion of monosaccharides $\rightleftarrows$ polysaccharides (1). The structure and dynamics of these biopolymers can be conveniently studied by NMR spectroscopy. In the present study, we investigate some static and dynamic properties of powders of α and β cyclodextrins, and the dextran B512F with transient techniques in NMR.

The low solubility of linear and branched carbohydrate polymers presents a major limitation to their characterization by standard high resolution liquid state NMR experiments. This stems from the extensive cooperative hydrogen bonding networks and cross-linking between chain segments which prevent the formation of solutions. In the presence of solvents, swollen gels composed of amorphous and crystalline regions have been observed with electron microscopy and x-ray diffraction (2). Within these structures, there is yet no clear picture of the distribution of conformations and motions of the chain segments. In powders, water of hydration exhibits heterogeneity in its interactions with polysaccharides. Bulk water, bound (physisorbed) water, and very tightly bound (chemisorbed) water have been postulated from the interpretation of ^1H NMR (3). NMR biophysical studies of these systems in the solid state (3-5) help our

understanding of the structures and dynamics of these polymers. Biological processes such as protein-polysaccharide interactions in cytoplasmic granules, seed germination and cell wall enlargement all occur in a condensed phase environment. Powders of carbohydrates serve as simple models of these substrates.

Cyclodextrins (CD) are cyclic oligosaccharides formed from α (1 → 4) linked D glucopyranose monomers; α CD (hexamer) and β CD (heptamer) are the smallest members of this class. The enzymatic degradation of the starch helix by an amylase of Bacillus macerans yields cyclodextrins with 6 to 12 glucose molecules per ring (6); the hydrophobic cavity of these torus shaped molecules can accomodate guests. The topology of the guest-host interactions has served as an enzyme model in view of the catalytic and binding properties (6-13) of CD. Molecular crystal structures of α CD·$6H_2O$ and β CD·$12H_2O$ have been reported (9-12). In the "empty state", both α and β CD have water enclosed within the cavity. α and β CD have respectively $2H_2O$ and $6.5H_2O$ inside the cavity, while the remaining water is incorporated into the lattice, hydrating the CD. On binding to other substrates, water is expelled from the cavity, and a conformational change occurs in α CD due to the relief of steric strain in the macrocyclic ring conformation. Such effects are not apparent in β CD. An induced fit mechanism has been proposed for the inclusion complex formation in α CD (9). The mechanism of inclusion and the forces responsible for driving complex formation are not yet understood. Dynamic properties of these inclusion compounds are not well

characterized in the solid state (14). Since the intermolecular arrangement of the cage-type crystal structure is relatively constant in α and β CD, differences in the behavior of NMR relaxation may be attributed mainly to intramolecular effects. Also, cross-linking between segments of the CDs is absent; only hydrogen bonding is present. Therefore stacking effects will be substantially different from those in polysaccharides such as cellulose and dextran.

Dextran B512F is a storage polysaccharide with D-glucose units linked in the α (1 → 6) positions with about 5% random branching in α (1 → 3). Chemical analysis gives a random distribution for the length of the side chains. The arrangements of the skeletal chains and the branching segments form comb-like, laminated and ramified types of structures, which in turn become intricate three-dimensional network structures. The molecular weight has been estimated in the range of 50 - 100 x 10^6 (15). Even if these biologically and commercially important polymers have been studied with many techniques, the nature and unequivocal assignment of configurations and conformations within the molecule are still not clear. The dynamics and types of motions are not understood.

It has been proposed that in proteins, the spatial and temporal correlation of conformational fluctuations generated by random processes might play an important role in enzyme catalysis (16-17). Typical lifetimes of enzyme-substrate complexes as detected by transient kinetic methods (18-19) range from 10^{-6} - 10^{-3} sec. During such a time scale, fluctuations of motions in the kHz to MHz range,

within the enzyme and/or substrate can affect the course of a reaction. The intrinsic complexity of these correlations makes their experimental detection difficult. As a first step to the solution of this problem, we report the observation of motions in this frequency range in polymeric carbohydrate substrates.

We propose to investigate the structures and the nature of molecular motions of solid cyclodextrins and dextran using a variety of nuclear spin dynamics probe, with reference to the above problems. Our approach involves the transformation of macroscopic heterogeneity (macroscopic magnetic polarization) into microscopic heterogeneity (microscopic magnetization). By following the time development of a non-equilibrium state, the spin ensemble which relaxes irreversibly to equilibrium, one can characterize average local fields and their dynamics. We wish to emphasize that in order to thoroughly understand these NMR experiments, we must rely upon the formalism of non-equilibrium quantum statistical mechanics (20). Nevertheless, such a treatment will not be essential to the interpretation of our results.

Experimental Section

The proton NMR experiments were performed on a homebuilt spectrometer operating at 220 MHz. The spectrometer design is similar to a 56 MHz system previously described (21). The recovery time of the probe receiver system from pulsed r.f. fields is 6 μsec. Free induction decays were obtained with 1.5 μsec 90° pulses, 410 μsec data acquisition time, and a 325 kHz filter, with an accumulation of 100 transients under an appropriate recycle time.

Relaxation measurements were obtained on resonance using standard pulse sequences. T_1s were measured using the inversion recovery sequence, 180_y-t-90_x. Dipolar relaxation times, T_{1d}, were monitored from the decay of the echo amplitude generated via the Jeener-Brockaert sequence 90_x-$t_1$$45_y$-$t_2$-$45_y$-$t_3$ (22). Measurements of the spin-lattice relaxation time in the rotating frame, $T_{1\rho}$, were performed with a 90_x r.f. pulse, followed by spin locking of the magnetization along the y direction for variable delay time, t, in an 11 Gauss r.f. field. In all experiments, the phase of the initial 90^o pulse was shifted by π for alternate decays in order to minimize baseline artifacts. In the measurements of T_1 and $T_{1\rho}$, the magnetization was sampled 6.5 μsec after the last pulse to accomodate recovery. The spin-spin relaxation times, T_2, were extracted from the lineshape analysis.

Low temperature measurements were done by blowing dried and cooled nitrogen gas over the sample. The temperature was monitored with a chromel-alumel thermocouple close to the sample in a homebuilt probe, and controlled by gas flow to $\pm$ .5°C. With a probe designed by Doty-Scientific, the temperature was controlled manually to $\pm$ 1°C with a copper-constantan thermocouple.

^{13}C cross polarization and magic angle sample spinning experiments were performed at 14.09 MHz on a homemade spectrometer described elsewhere (23). Rotating fields of 9.3 G for protons and 37 G for carbon satisfied the Hartman-Hahn match for optimum polarization transfer. A contact time of 1.5 msec, an appropriate

recycle time, 21 msec total data acquisition times, and a 6 kHz filter were used throughout for the co-addition of 30,000 transients. The phase of the proton preparation pulse was changed by π on alternate scans. Kel-F Andrew-Beams type rotors filled with about 300 mg of sample and rotated at the magic angle at 2.3 kHz permitted the averaging of the ^{13}C chemical shift anisotropy present in powdered samples. Water and adamantane served as external references for ^{1}H and ^{13}C respectively. Downfield shifts from the reference are negative.

Absorption lineshapes were fit using a non-linear least squares routine (24). A similar numerical procedure permitted the analysis of two component decays of magnetization in the relaxation measurements.

Samples of α and β cyclodextrins and dextran B512F were generously provided by Dr. P. Braun and Professor J. F. Robyt of the Biochemistry-Biophysics department at Iowa State University. The purity of the samples was monitored with ^{13}C NMR and ESR. Since relaxation measurements are particularly sensitive to paramagnetic impurities ESR measurements were carried out at 4 and 298 K on an ESR IBM/Bruker 200 D instrument operating at 9.5 GHz. Only at 4 K did the dextran reveal a weak signal at $g = 2.010$ which could be due to traces of copper.

Results and Discussion

^{1}H Free induction decays and lineshapes

The proton free induction decays (FID) for the cyclodextrins and the dextran taken with the carrier frequency at the center of the spectrum are shown in Figure 1. Data accumulation was initiated 6 μsec after the center of the pulse to avoid pulse breakthrough. In all cases, the FID displays a fast decaying component followed by a "beat or hump" which rides on a slowly decaying component. In these systems, the main interaction responsible for the dephasing of the macroscopic magnetization, as shown below, is the homonuclear dipolar coupling. The dynamics of the spins reflect the strength of such a homogeneous interaction. This interaction characterizes the average local environment, as the spatial part of the dipolar hamiltonian is dependent on r_{ij}^{-3} $(3 \cos^2 \theta_{ij}-1)$, with r_{ij} the distance between the spin pair i and j, and θ_{ij} the angle between $\vec{r}_{ij}$ and the magnetic field $\vec{B}_o$. The strongly coupled protons correspond to the fast decaying component. The slowly decaying portion of the FID represents a much weaker or averaged dipolar interaction. The origin of such behavior may be spatial, r_{ij} being large (isolated spins) or motional with θ_{ij} (t) being modulated to some average value. The latter is shown to be the case in Section 4. For the case of static dipolar coupled spins, a classical stochastic model of a gaussian distribution of local fields leads to the prediction of a monotonically decreasing decay (25). On the other hand, a quantum mechanical description of the FID of strongly coupled spins predicts a beat structure in the

Figure 1. Free induction decays. Total acquisition time is 410 μsec in all cases. a) α CD b) β CD c) dextran B512F

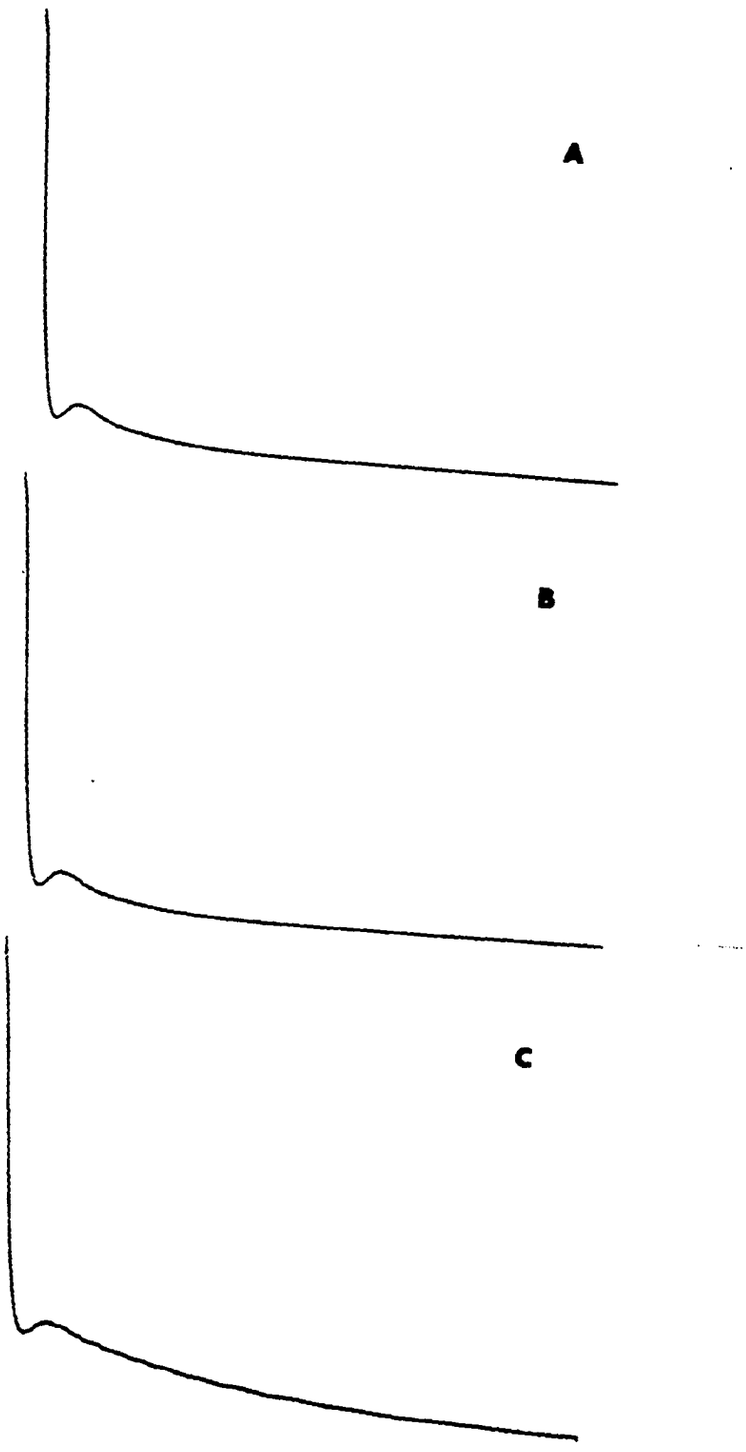
A
B
C

decay shape (26). This feature has been confirmed experimentally for crystalline and polycrystalline solids (26-27). Therefore, the beat in the FIDs confirms the fact that the dipolar interaction is dominant. If this feature were due instead to chemical shift interactions with non-zero isotropic values, the frequency spectra would show displaced peaks; these are not observed (see Figure 2).

Since we do not detect NMR signals in quadrature, Fourier transformation of an off-resonance FID is necessary to obtain the lineshape in the frequency domain. In Figure 2, we observed broad and narrow components, with the former corresponding to the fast decaying fraction of the FID and the latter to the slowly varying component. The presence of small shoulders at $\pm$ 250 ppm appeared after several months of drying the samples over drierite. These are reminiscent of the spectrum of powders of isolated pair of protons known as a Pake doublet (28). A typical Pake doublet has 2 extremities separated by 3/2 w_d and shoulders separated by 3 w_d with $w_d = (\gamma^2 h/r_{ij}^3)$, where γ is the magnetogyric ratio and h is Planck's constant. The shoulder splitting 3 w_d for an isolated pair of protons as in H_2O (r = 1.58 Å) is 91 kHz, and methylene protons (r = 1.77 Å) give a separation of 65 kHz. From the observed splitting, 110 kHz, one obtains a distance of 1.48 Å if this spectral feature is due to an isolated pair of protons. From the crystal structures of α and β CD, it is difficult to imagine the location of isolated pairs of protons, and similarly for dextran. Other possible sources of this feature include bulk surface water, a tightly interacting pair of hydroxyl

Figure 2. Broadline proton NMR frequency spectra. a) αCD b) βCD c) dextran B512F. oppm is H_2O

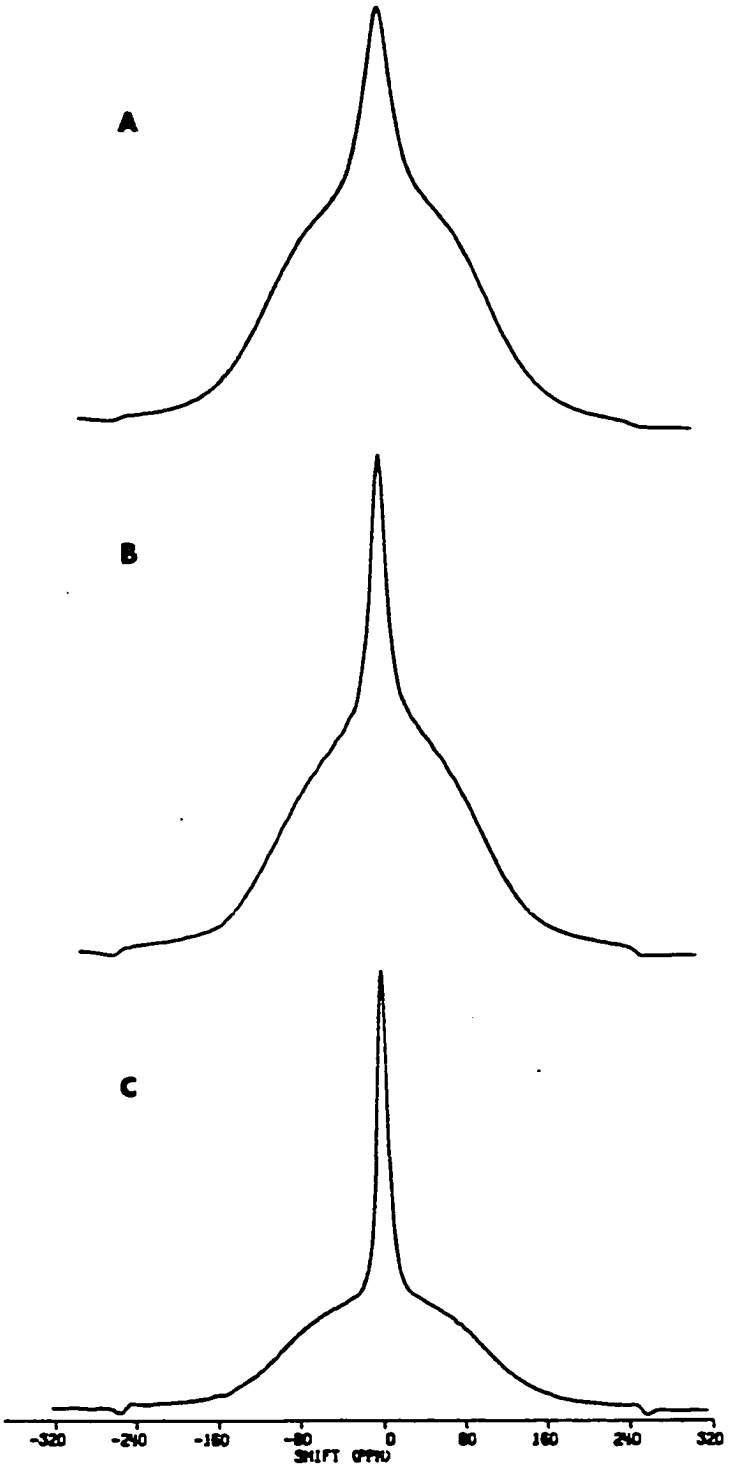
A
B
C
-320
-240
-160
-80
0
80
160
240
320
SHIFT (PPM)

groups due to stacking or surface effects, or water in pores or channels of the crystallites can be envisaged; but again the bulk of the protons, aliphatic or hydroxyl, would have to be separated from these water molecules. Further drying of the samples modified the spectra (see Figure 3), as shown by the disappearance of the small shoulders. Differences in the time constants T_1 and T_2, and their relative proportions were also observed. Numerical superposition of the absorption lineshapes with 2 components, both Gaussians for α and β CD, and Gaussian/Lorenztian for dextran are illustrated in Figure 4. The fits give reasonable agreement with the data. From these we obtain T_2, or the full width at half height, $\Delta\nu = (2\ln 2)^{1/2}/\pi T_2$ for a Gaussian, $\Delta\nu = 1/\pi T_2$ for a Lorenztian. The relative proportions of the broad and narrow components are listed in Table 1. Lineshape analysis in NMR has traditionally associated the Lorentz shape with spins in a liquid or gas which satisfy Bloch's equations of motion, and the Gaussian shape with a distribution of local static fields in rigid solids (29). For the calculated values of the relative number of protons in α CD and β CD (see Table 1), we assumed that the water inside the cavity gave rise to the narrow peak and the rest of waters of hydration were incorporated into the bulk of the other protons contributing to the broad peak. If the narrow component in dextran corresponds only to water, from the observed area ratio, we conclude that there is approximately one water per glucose in the dry sample, and one water per two glucose in the drier sample.

Figure 3. Broadline proton NMR frequency spectra of drier samples. The glitch on the left side of all spectra is an experimental artifact. a) α CD b) β CD c) dextran B512F

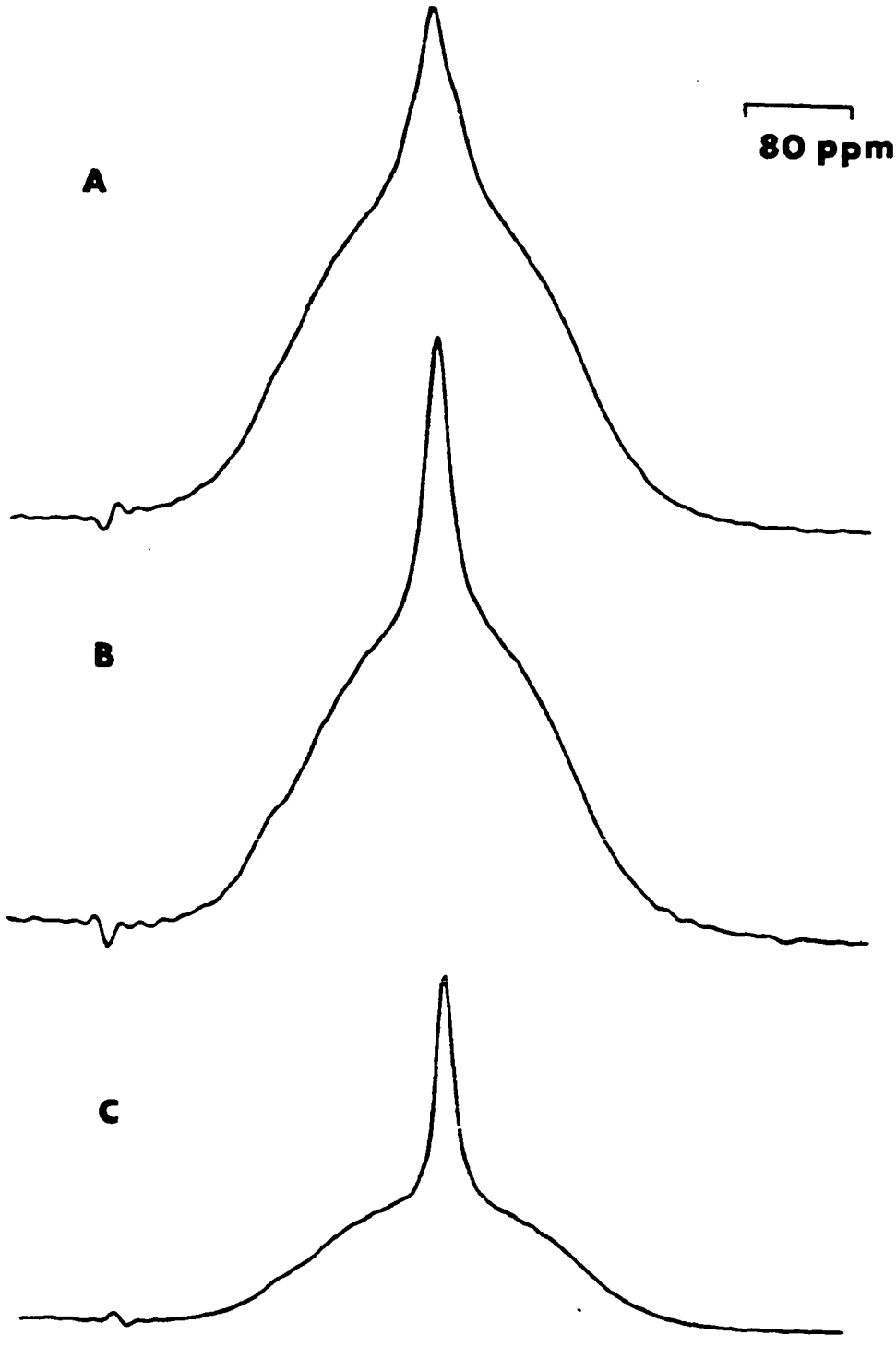
80 ppm
A
B
C

The water of hydration appears to display greater differences than the carbohydrate backbone when comparing linewidths. In dextran, where the backbone is expected to have a more porous structure than the cage-type packing arrangement of CD, the water displays more mobility. From x-ray crystal structure studies (9-12), it is known that the cavity waters in αCD are "ordered", and "disordered" in βCD. This picture agrees qualitatively with the T_2 results. In all cases, further drying decreased the long component T_2s (or broadened the narrow peak), implying more restrictions in the displacements of these water molecules, i.e., decrease amplitudes and/or frequencies of motions.

^{13}C cross polarization and magic angle sample spinning

The technique of proton enhanced nuclear induction spectroscopy has been applied to the detection of natural abundance ^{13}C in α, β CD and dextran. The sensitivity enhancement of cross polarization, in conjuction with high powered proton decoupling and magic angle sample spinning, give "high resolution" liquid like spectra (see Figure 5). The labeling of the glucose monomer is shown in Figure 6.

The ^{13}C magnetic shielding is a function of the local electronic environment and therefore sensitive to conformational changes. Chemical shifts of α, β CD and dextran are reported in Table 2. Our data agree with previous work (30) for α and βCD. Linewidths are partly due to a distribution of "frozen" conformations of the glucose ring, the macrocycle ring of cyclodextrins and tertiary structures for dextran. From our experience with solid state ^{13}C NMR, we believe

Figure 4. Numerical decomposition into broad (b) and narrow (n) components. Crosses represent experimental points and the solid lines represent the fit. Components and full widths are as follows:
a) α CD, 43.1 kHz (b), 5.6 kHz (n) b) β CD, 40.2 kHz (b), 3.6 kHz (n)
c) dextran B512F, 42.9 kHz (b), 2.7 kHz (n)

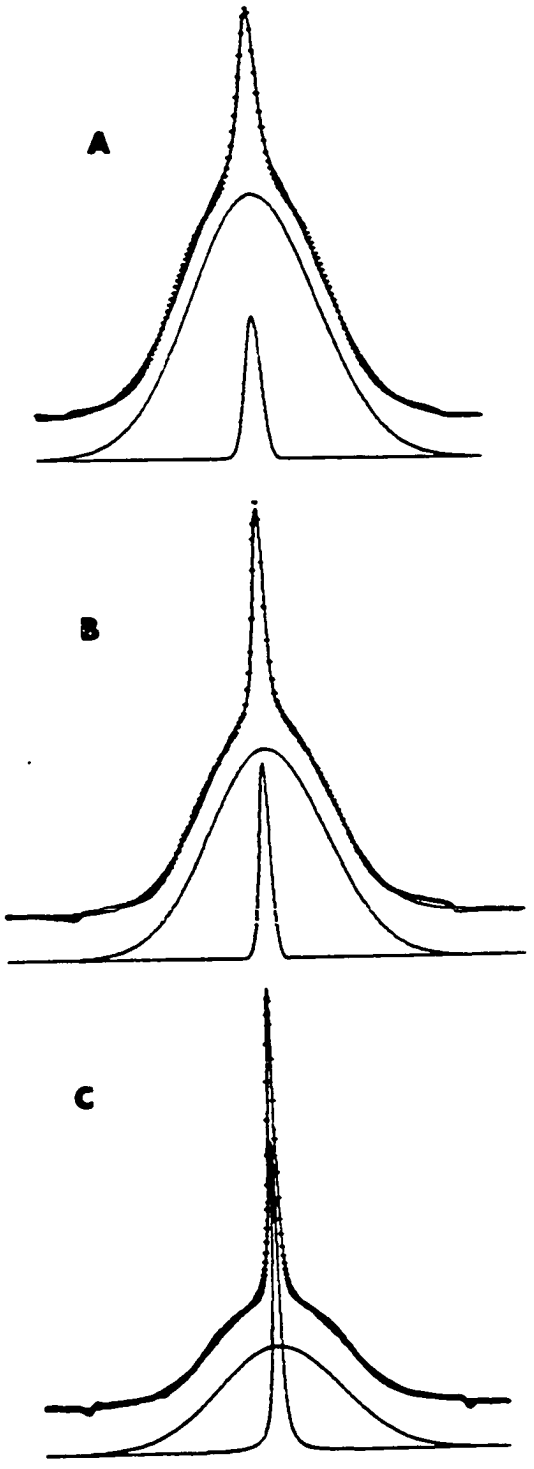
A
B
C

Table 1. Spin lattice and spin-spin relaxation times and their relative components

	T_1/msec		T_2/μsec		Calculated relative intensities	
α CD	520	100%	67	6.5%	$2H_2O$	5.6%
			8.7	93.5%	α CD·$4H_2O$	94.4%
*	1640	100%	62	4.5%		
			8.7	95.5%		
β CD	700	100%	100	8.1%	6·$5H_2O$	6.5%
			9.3	91.9%	β CD·5·5H20	93.5%
*	550	100%	89	6.3%		
			9.1	93.7%		
Dextran B512F	850	100%	140	18.6%	1 H_2O	16.7%
			8.7	81.4%	1 glucose	83.3%
*	1070	100%	112	10.2%	1 H_2O	9.1%
			9.0	89.8%	2 glucose	90.9%

*Kept over drierite for longer periods.

that the main contribution to the linewidth is from residual ^1H-^{13}C heteronuclear dipolar interaction arising from insufficient proton decoupling (H_1 = 9.3 G). Saito and Tabeta (30) obtained narrower resonance lines using a 14 G proton decoupling field in their ^{13}C studies of polysaccharides, which supports our contention in the case of CD. Missetting of the magic angle by .5° would broaden the linewidth by 2 ppm for a methylene carbon with a 60 ppm static shielding anisotropy.

Table 2. ^{13}C chemical shifts in ppm

	C_1	$C_{2,3,5}$	C_4	C_6
α CD	-104	-74	-82	-63
β CD	-104	-74	-84	-63
dextran B512F	-100	-74	-74	-74

Chemical shift differences in CD and dextran can be accounted for by a combination of motional and structural effects. Single crystal x-ray studies (9-12) of α, β CD and glucose show very small differences in average bond lengths ($\leq .05$ Å), and angles among these compounds. This invariance of the glucose geometry under variable external influences is peculiar to the solid state, where rapid conformational isomerism present in solution becomes hindered. ^{13}C NMR studies of polysaccharides (31) have shown that the C_1 and C_4 resonances are particularly sensitive to the glucosidic linkage (1 → 4) and its conformational changes. Even with the restrictions of the chain formation in the crystalline state, the torsion angles from C_3-C_4-C_5-O_5 (defined as the angle between C_3-C_4 and C_5-O_5 viewed along C_4-C_5) show a certain amount of conformational freedom with a range of about 10° (10). Distortions of the ring with frequencies as slow as 300 Hz accounts for the observed differences in ^{13}C chemical shifts. In α CD, well resolved ^{13}C resonances are observed for C_1, C_4, C_6 because of the constrained and rigid macrocycle conformation. For β CD, the increased freedom of motion associated with the unstrained

Figure 5. High resolution ^{13}C CP/MAS spectra a) α CD b) β CD c) dextran B512F. oppm is TMS

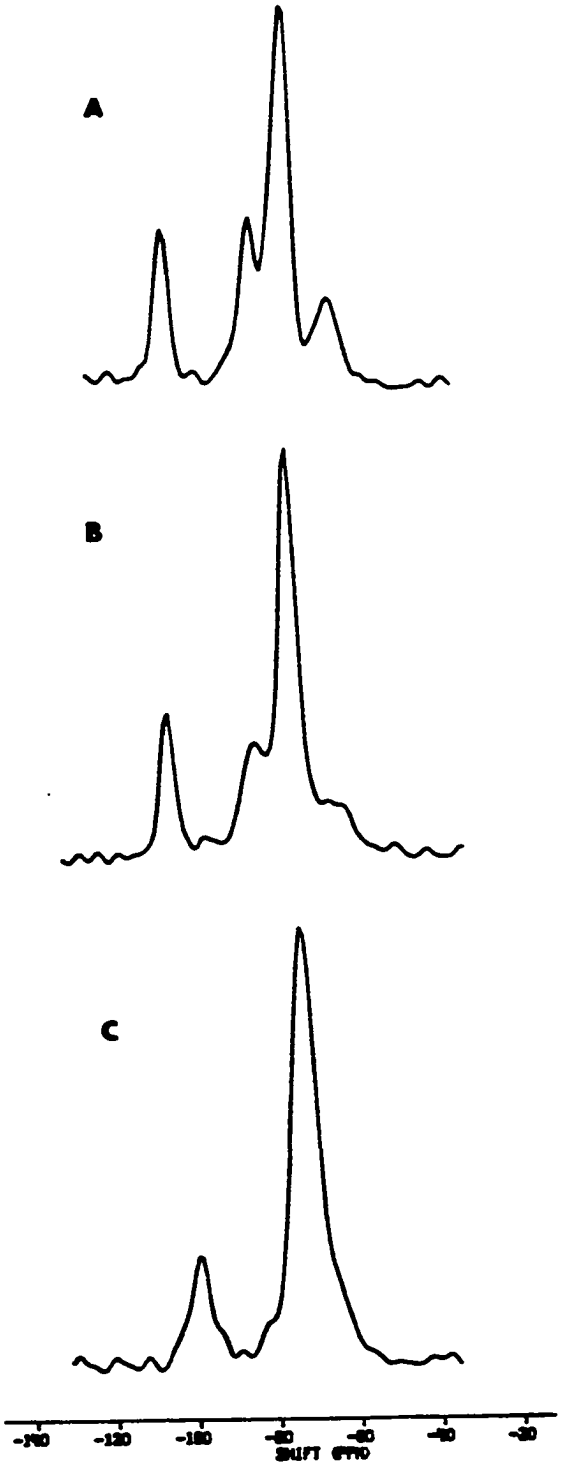
A
B
C
-140
-120
-100
-80
-60
-40
-20
SHIFT (PPM)

Figure 6. Labeling of the glucose monomeric unit of the cyclodextrins according to the x-ray convention

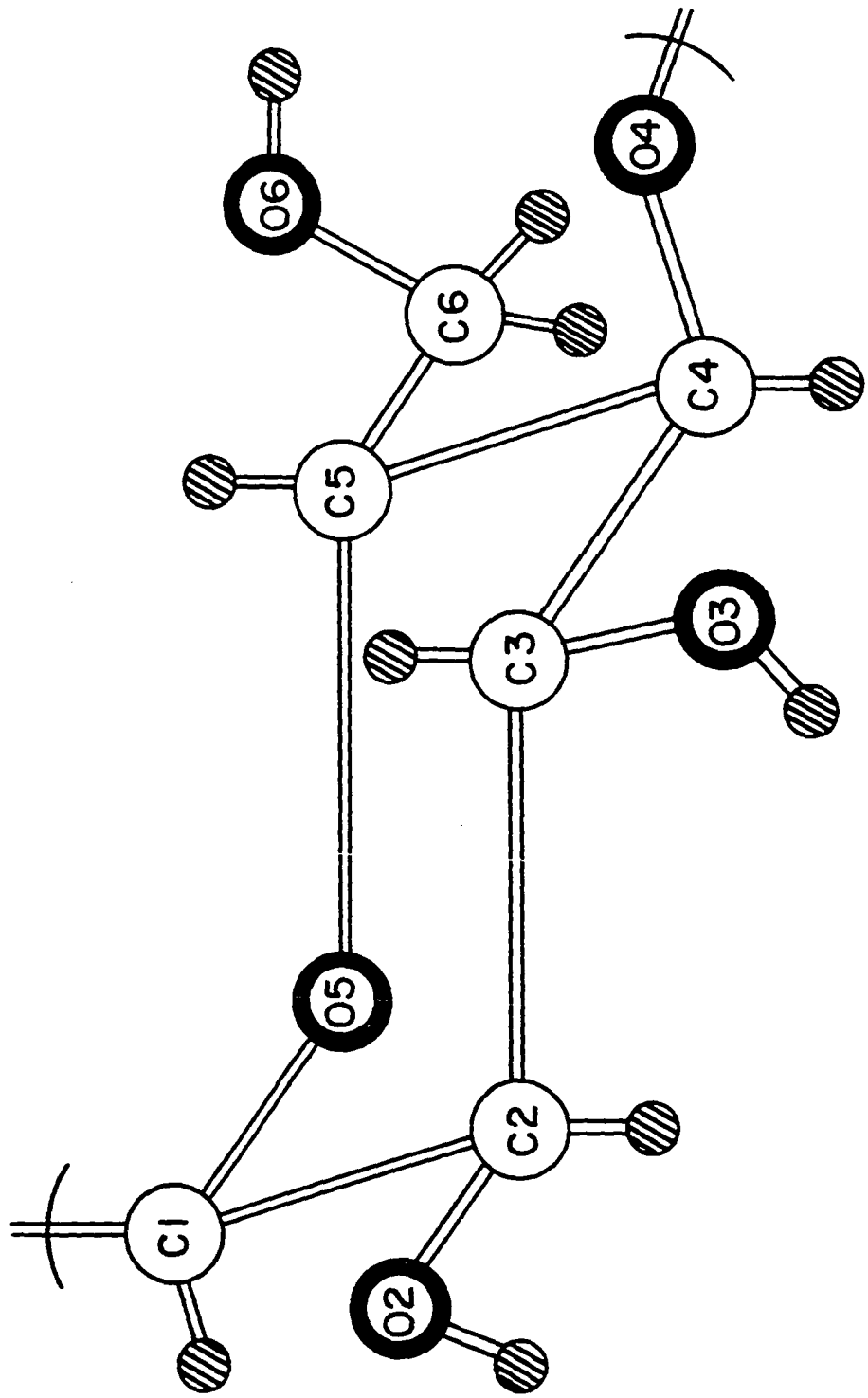
O6
O4
C6
C4
C5
C3
O3
O5
C2
C1
O2

macrocycle causes the $C_{4,6}$ resonances to coalesce with the $C_{2,3,5}$ resonances. These low amplitude motions must be in the range 0-1 kHz, as the chemical shift differences between C_4 and C_6 is 150 Hz. These slow motions of the backbone or the individual glucose rings are too slow to affect the ^1H linewidths arising from the strong ^1H dipolar coupling. Local distortions of a few hundred hertz for the individual glucose ring at C_4 and C_6 would collapse these resonances if both sites sample in their motions each others average electronic environment. Conformation dependent modulations of ^{13}C chemical shifts have been observed in complexes of cyclodextrins, and have been interpreted in terms of changes occurring in the dihedral angles of the glucosidic linkage (31).

In ^{13}C CP/MAS studies of cellulose (32-33), a β 1 → 4 glucose polymer, the lineshapes broadened for all resonances on passing from a crystalline to an amorphous samples. Slight chemical shift changes were also noted, but there was no collapse of the C_4, C_6 resonances with $C_{2,3,5}$ as we observed in the hydrated dextran. This effect is easily understood in terms of the conformations of polysaccharide chains (34). In cellulose, the β glucosidic linkage energetically constrains glucose units to extended linear chain conformations, and further stabilization is provided by interchain hydrogen bonding. The rigidity and long range order of such arrangements permits the formation of strong fibers. In the case of α glucosidic linkages as in dextran, one finds helical structures with 6-7 glucose units per turn. This intermediate range order allows local distortions of the

glucose ring which give rise to the observed coallescing of ^{13}C resonance lines. Therefore, local motions of the individual glucose ring and constraints imposed by the rigidity of the macrocycle in CD both play important roles in determining the ^{13}C chemical shifts. For dextran, higher frequencies and/or amplitudes of these local ring motions reflect the flexibility of chain segments on a scale of several (6-7) glucose units.

Relaxation

Review of relevant relaxation principles

The purpose of this section is to present to those unfamiliar with the details of NMR relaxation theory, the necessary background to understand the interpretation of the relaxation experiments and data.

Introduction

Relaxation measurements consist of placing an ensemble of spins into a non-equilibrium state and monitoring its decay. Depending on the preparation of such a state, the relaxation constants will have definite characteristic time scales and will depend on the frequencies of the processes as well as the spatial arrangements of the spins. In solids, the classical interpretation of relaxation of precessing magnetization of independent spin isochromats is invalid because of the strong dipolar coupling among spins. Rather than treating individual spins, we may consider collective properties. In the literature, such approaches as the spin temperature or the method of the moments treat ensembles of spins without detailed knowledge of their microscopic interactions (35).

Spin-lattice relaxation implies an energy exchange by the precession of the spin system with the other degrees of freedom, i.e., the motions of the lattice. Spin-spin relaxation also has a component that represents entropy effects or redistribution of energy, but now within the spin system. Thus one speaks of internal quasi-equilibrium within the spin energy levels, and thermal equilibrium when these levels attain the lattice population distribution.

Relaxation rates (36) are dependent on the spectral density functions, or the frequency spectrum of the motions and the strength of the interaction. These functions carry information regarding the nature of the motions, such as rates and amplitudes. The fluctuations of interactions about average value are characterized by the correlation time, t_c, the average time between fluctuations. For a Lorenztian spectral density function, different regimes of interest exist that depend on the frequencies being sampled (37). The motionally narrowed limit condition $\omega t_c << 1$ corresponds to the situation normally encountered in liquids where t_c is shorter than the Larmor period; $\omega t_c >> 1$ corresponds to the solid regime; and for the intermediate regime, $\omega t_c = 1$.

In solids, different types of nuclear relaxation offer additional information not usually found in solution. Next, we will briefly examine the different types of relaxation investigated in the present study.

T_1-spin lattice relaxation in the laboratory frame The longitudinal relaxation of the magnetization along a strong magnetic field B_o is an irreversible process by which the spin system comes to equilibrium with the lattice. Different mechanisms, such as dipole-dipole interactions, can couple the spins to the lattice. The relaxation rate is maximal when the correlation time is on the order of the inverse Larmor frequency, ω_o^{-1}. Theoretical expressions for relaxation rates of spin pairs have been derived in the weak collision regime using perturbation theory (38). In this case, many correlation times are required before the relaxation of one spin occurs. The spectral density function is dependent on ω_o and $2\omega_o$; in the experiments reported here, this represents motions of 220 and 440 MHz.

$T_{1\rho}$ -spin lattice relaxation in the rotating frame The observation of NMR signals involves the detection of a low frequency modulation on the MHz Larmor frequency. In order to detect this modulation, a transformation from the laboratory frame to the rotating frame is performed. In the rotating frame, the effective magnetic field is also transformed. On resonance, the effective Larmor frequency becomes $\vec{\omega} = \gamma \vec{H}_{eff}$ where $\vec{H}_{eff} = \vec{H}_d + \vec{H}_{rf}$, and where H_d is the local dipolar field, H_{rf} is the radio frequency field. This permits sampling of motions slower than ω_o, i.e. motions in the range of tens to hundreds of kHz (39). A spin temperature approach treating the strong collision regime, where the spins relax over one correlation period, has been developed (40) for $T_{1\rho}$ relaxation in solids. $T_{1\rho}^{-1}$ relaxation rates valid for the weak collision regime

are also found in the literature (41).

When using spin locking fields where $H_{rf} \leq H_d$, spin-spin contributions to $T_{1\rho}$ complicate the interpretation of the experiment (42). It has been shown (43) for the case of a Gaussian lineshape that the local field, $H_d = \Delta H/\sqrt{i2}$, where ΔH is the linewidth at half intensity. For the systems investigated here, ΔH = 40 kHz, which gives H_d = 11.5 kHz, while $H_{r.f.}$ = 47 kHz which satisfies $H_{rf} > H_d$. Therefore, the spin-spin contributions to $T_{1\rho}$ should be minimized under such experimental conditions. Under spin-locking times of the order of T_2, and with the condition $H_{rf} > H_d$, it is possible to observe a coherence phenomenon. The magnetization oscillates at a frequency of 2 ω_{rf}, where $\omega_{rf} = \gamma H_{rf}$, for periods on the order of T_2 (42,44). In the event of $H_{rf} \leq H_d$, the oscillations become faster and are difficult to observe (45). These oscillations are the result of non-equilibrium cross relaxation between the Zeeman energy in the rotating frame and the dipolar energy. The dipolar spin fluctuations present under r.f. irradiation dampened these oscillations, and are characterized by a time constant T_2'.

T_{1d}-spin lattice relaxation in local dipolar fields By transforming Zeeman order (entropy) into dipolar order it becomes possible to monitor dipolar spin lattice relaxation (22). The motions responsible for this relaxation will typically have frequencies in the range $\omega_d = \gamma H_d$, which are somewhat slower than those detected by $T_{1\rho}$ in solids. The shape of the echo depends on the character of the interaction. Homogeneous interactions such as strong dipolar coupling

give a single echo proportional to the derivative of the FID, while in homogeneous interactions such as chemical shift and localized heteronuclear dipolar interactions give rise to at least 3 echoes, one of which becomes distorted as a function of the spacing time between pulses (46). Multiple quantum coherences have been shown to introduce "humps" into the relaxation decay (47).

T_2-spin-spin relaxation The decay of the magnetization perpendicular to the strong magnetic field $\vec{B}_o$ following a single pulse is characterized by a time constant T_2, the transverse relaxation time. The spectral density function in this case depends upon components of motions at ω_o and $2\omega_o$, but most important for solids are the motions at $0\omega_o$, which are very slow cooperative molecular motions with respect to ω_o (48).

Relaxation data In order to assign motions with relaxation measurements, a model of the spectral density function and the energies of activation are required. In this section we describe the spectral density function for the carbohydrate systems, while in the next section we deal with energies of activation in α CD. The availability of molecular crystal structures for α and β CD permits a correlation of the relaxation rates with certain segments of CD; these serve as bench marks for dextran, where the structure is known in less detail.

The relaxation data are presented in Tables 1 and 3. The precision of all relaxation times has been estimated to be well within ± 5%. Relaxation decays have been fitted with single exponentials for

T_1, and biexponentials for T_{1d} and $T_{1\rho}$, and T_2 has been obtained from the lineshape analysis.

A general trend in the relaxation times is observed for all samples. T_1s display a single component decay, while T_{1d}, $T_{1\rho}$ and T_2 all have a two component decay. An interesting observation is that for the smaller fractions $T_2 < T_{1\rho} < T_{1d}$, while for the larger component of the decays, $T_2 < T_{1d} < T_{1\rho}$. Since T_2, T_{1d} and $T_{1\rho}$, all sample very slow motions, we are able to use these parameters to obtain a qualitative picture of the spectral density function in the kHz frequency regime at o, ω_L, $\omega_L + \omega_{rf}$, $2\omega_L$, $2(\omega_L + \omega_{rf})$, where ω_L is of the order of the local field precession, ω_{rf} is the precession frequency in the r.f. field. T_1 is sensitive to 220 and 440 MHz motions.

In all cases, T_1 is 300-1000 times longer than the slowest of the low frequency constants. This implies a low intensity of MHz motions compared to those of kHz frequencies if the relaxation mechanism is the same. We note that even if molecular packing exhibits differences between CD and dextran, the T_1s are within a close range. Water of hydration in these systems influences the overall spin lattice relaxation (see Table 1). Further drying increased T_1 for α CD and dextran, while decreasing it for β CD. The nature of the motions responsible for the T_1 relaxation are characterized in the following paper (49).

Table 3. Relaxation in dipolar and radio frequency fields and their relative components

	T_{1d}/μsec		Calculated relative intensities	T_1 /μsec		Calculated relative intensities
α CD	1900	29%	31%	210	13%	14%
	21	71%	69%	4400	87%	86%
β CD	950	39%	37%	350	3.3%	2.1%
	24	61%	63%	2900	96.7%	97.9%
dextran B512F	560	31%		350	27%	
	20	69%		3900	73%	

Slow motions can be represented by long range cooperative modes involving several spins. Our data demonstrate this effect clearly in the case of the smaller component of the decays in the $T_{1\rho}$, T_{1d}, T_2 experiments for CD. Motions of the guest molecules other than water in the cavity of CD have been inferred from NMR measurements (14). For α CD, $2H_2O$ can be found in the cavity which represents 5.6% of the total protons in α CD·$6H_2O$. From the x-ray data, it is known that the CH_2OH group of glucose 1 and 5 are interacting by hydrogen bonds with one of the cavity water molecules. Here, $2H_2O$ and $2CH_2OH$ correspond to 14% of the protons. If we add to this the glucose ring protons of C_3 and C_5, which are present within the cavity, the sum represents 31% of the total protons. These proportions have been associated with the

smaller fraction of relaxation decays in Table 3. The following picture emerges from relaxation data for the nature of motion of protons in the cavity of α CD. The observed fraction 29% (T_{1d} = 1.9 msec) would correspond to some slow cooperative or correlated motion inside the cavity involving the $2H_2O$, $2CH_2OH$ and 6 pairs of protons from C_3 and C_5. $T_{1\rho}$ would reflect a faster motion than the one detected by T_{1d}, involving the $2H_2O$ and the $2CH_2OH$ groups. Finally T_2 samples the faster motions of the included water molecules. If we assume that the dominant relaxation mechanism is the dipolar interactions, then the relative relaxation rates indicate that spectral density functions decrease rapidly as a function of kHz frequency for the protons on the "outside" of the torus (see below). A similar picture is obtained for the protons on the inside, but the spectral density function extends to higher frequencies of motions due to the two guest water molecules. A jump frequency of 66 kHz at room temperature has been inferred for the motions of all the protons inside the torus from the temperature dependence of T_{1d} (see Section 4). This motion must be anisotropic and limited to displacements since it does not average the 40 kHz linewidth.

A similar analysis is possible for β CD. It is known that $6 \cdot 5H_2O$ molecules are found in the cavity, which corresponds to 6.5% of the total protons of β CD$\cdot 12H_2O$. Of these guest water molecules, only one has a tetrahedral arrangement of hydrogen bonds. This result would imply a higher barrier to motion and represents 2.1% of the total protons. Three CH_2OH groups interact with the interior water;

together with the 7 pairs of protons on C_3 and C_5, this interaction accounts for 37% of the protons. Therefore a slow collective interaction of the $6 \cdot 5H_2O$, $3CH_2OH$ groups and the ring protons is responsible for T_{1d} relaxation. If this case were analogous to that of α CD, we would expect motions of the CH_2OH groups and the guest water molecules to be responsible for relaxation sampled by $T_{1\rho}$. Because of the disordered water, this is not the case; T_1 seems to sample only the slower motion of the tetrahedrally bound H_2O (or $2H_2O$ which is 4.2%), while T_2 monitors the faster motions of the $6 \cdot 5H_2O$. The ratio of relaxation rates supports the same kind of spectral density function as proposed for α CD, assuming that the dipolar interaction is the dominant relaxation mechanism, and that the spectral density functions are Lorenztian-like. Depending upon the extent of the distributions of correlation times or the degree of cooperativity, the form of the spectral density function might not necessarily be Lorenztian (50).

The difference in T_{1d} of α and β CD is qualitatively in accord with the x-ray crystal structure data regarding the premise that ordered and disordered guest water molecules interact differently within the torus of CD. If the same premise applies to the dextran, the water in that system should exhibit even greater heterogeneity. We witnessed a four-fold increase in the dipolar spin lattice relaxation rate over that of α CD. This hypothesis is further supported by the relatively long T_2 of water in dextran. The interpretation of the component of $T_{1\rho}$ (27%) of dextran probably

implies participation of some free side chain, or the CH_2OH of terminal glucose in such a chain or even tetrahedrally bound water in the lattice. A temperature dependent study of $T_{1\rho}$, T_{1d}, T_2 and frequency dependent study of $T_{1\rho}$ are needed to define such possible interactions.

The larger fraction of the decays in the $T_{1\rho}$, T_{1d}, T_2 experiments display the same behavior characteristic of strongly dipolar coupled spins. Spin diffusion or spatial diffusion of the longitudinal magnetization without physical displacement of the spins permits a fast equilibration of the magnetization over distances of 10-200 Å (51). This interaction represents the zero frequency component of the spectral density function. The T_2 macroscopic effect of spin diffusion is to decrease the transverse magnetization while keeping the longitudinal magnetization constant. In the cyclodextrins, the region covered by spin diffusion represents the protons on the outside of the torus which interact with each other and with the ring protons inside the cavity. It is interesting to note that for cyclodextrins, the inner diameters are about 5 Å (α) and 6.2 Å (β), and the outer diameters range from 11-15 Å (9-12). Helical structures have been postulated for dextran (2). These facts allow a distinction to be made between the "inside" and "outside" of such structures, as demonstrated by the distribution of the spins giving rise to the 2 components in the T_{1d} experiments. Therefore one may speak of strong dipolar coupling in the outside domain which is spatially separated from the inside cavity. This distance in turn permits an attenuation

(or decoupling) of the dipolar fields between these local regions which display different dynamics. The presence of networks of intra- and intermolecular hydrogen bonds favors collective modes (52-53); this view is supported by the very small T_{1d} which implies a high density of ultra-slow motions of hydroxyl and ring protons on the outer region of the torus. For all the samples, the larger component $T_{1\rho}$s are rather long. Again, the assumption that the mechanism of relaxation is through dipolar interactions implies that the intensity of the spectral density function for frequencies above ω_L and $2\omega_L$ decreases. The temperature dependence (see next section) of T_2 also indicates the presence of higher frequency motions which could be easily accounted for by small amplitude distortions of hydrogen bonding, such as protons hopping between two sites (or potential wells) within a hydrogen bond.

In Figure 7, we present the echo from the Jeener-Brockaert sequence as function of pulse spacing. For a sample with several distinct phases, e.g., crystalline and amorphous regions, we would expect each domain to have its respective T_{1d}, which should lead to a distortion and appearance of three echoes (47). There is no such evidence and the samples are therefore inferred to be macroscopically homogeneous. Establishment of the dipolar order in the samples occurs over a period of less than 10 μsec. The fact that the smaller T_{1d} of α CD (21 μsec) is temperature dependent (see next section) implies that the shorter T_{1d} reflects spin lattice processes rather than equilibration of the dipolar energy (54).

In Figure 8, we show the results of the spin locking experiment with $H_{rf} > H_d$, on a T_2 time scale. These transient oscillations of $2\omega_{rf}$ are dampened by proton spin fluctuations, and are characterized by a decay constant T_2' during irradiation. The spectral density functions for these fluctuations in organic solids is represented by a decaying exponential (42), as opposed to a Lorenztian function. The oscillations' initial amplitudes are roughly 15% of the spin lock magnetization, and decay in about 25 sec; this implies $T_2' < T_2$ for all samples.

Temperature dependence of the lineshape and T_{1d} for α CD

NMR measurements as a function of temperature cannot provide details of the geometrical arrangements of spins with the exception of single crystal studies and powders of simple model compounds. Nevertheless, relaxation studies can reveal the lifetime of molecular arrangements and the energy of activation of the process responsible for relaxation. In this section, we present a qualitative analysis of the ^1H lineshape and the dipolar relaxation times, T_{1d}, as function of temperature for α CD.

A description of the redistribution or modulation of the spectral intensity due to molecular motions provides insight into the time dependence of the interactions giving rise to these spectral features. In Figure 9, the ^1H lineshape of α CD is presented for various temperatures. The chemical shift anisotropy interaction, H_{cs}, and the homonuclear magnetic dipolar interactions H_d, are the principal

Figure 7. Jeener-Brockaert echoes from the pulse program 90_x-t_1-45_y-t_2-45_y-t_3 with t_2 = 20 μsec for a,c,e and 100 μsec for b,d,f; t_1 = 10 μsec in all cases. Total acquisition time 410 μsec. a),b) α CD, c),d) β CD, e),f) dextran B512F

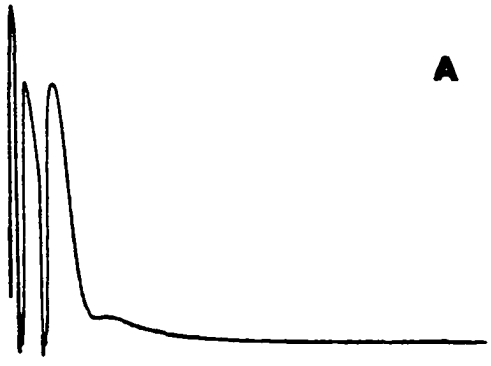
A

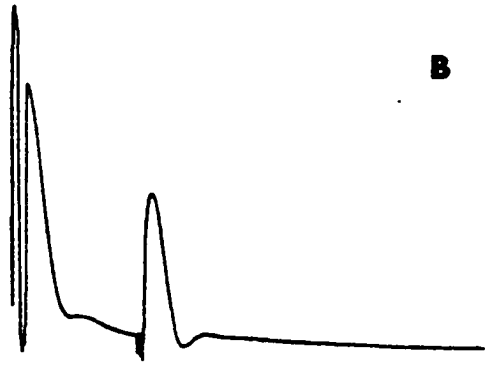
B

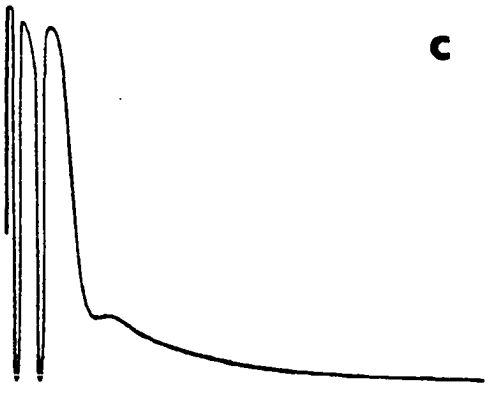
C

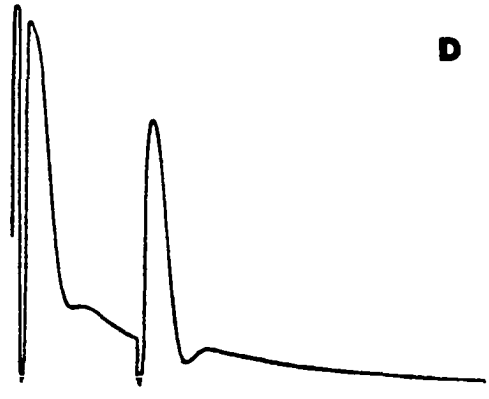
D

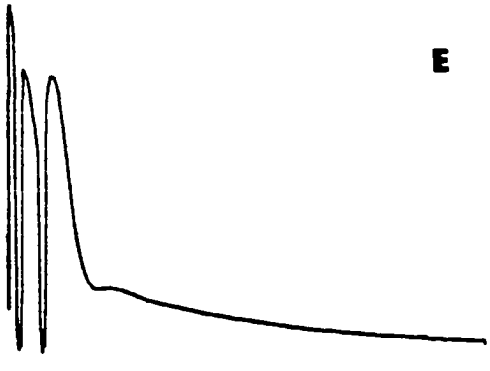
E

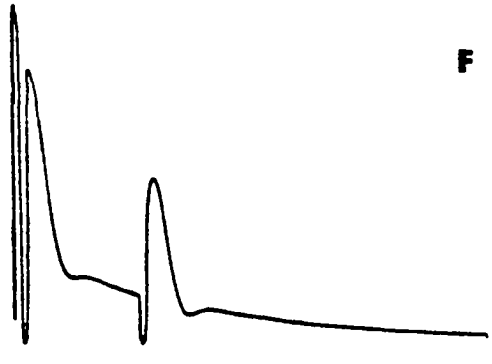
F

Figure 8. Spin locking in a 39G field for periods of T_2*. Initial amplitudes (arbitrary units) versus spin locking time in sec. Expected period of oscillation 5.7 sec. a) α CD, b) β CD, c) dextran (D.C. decay is associated with $T_{1\rho}$)

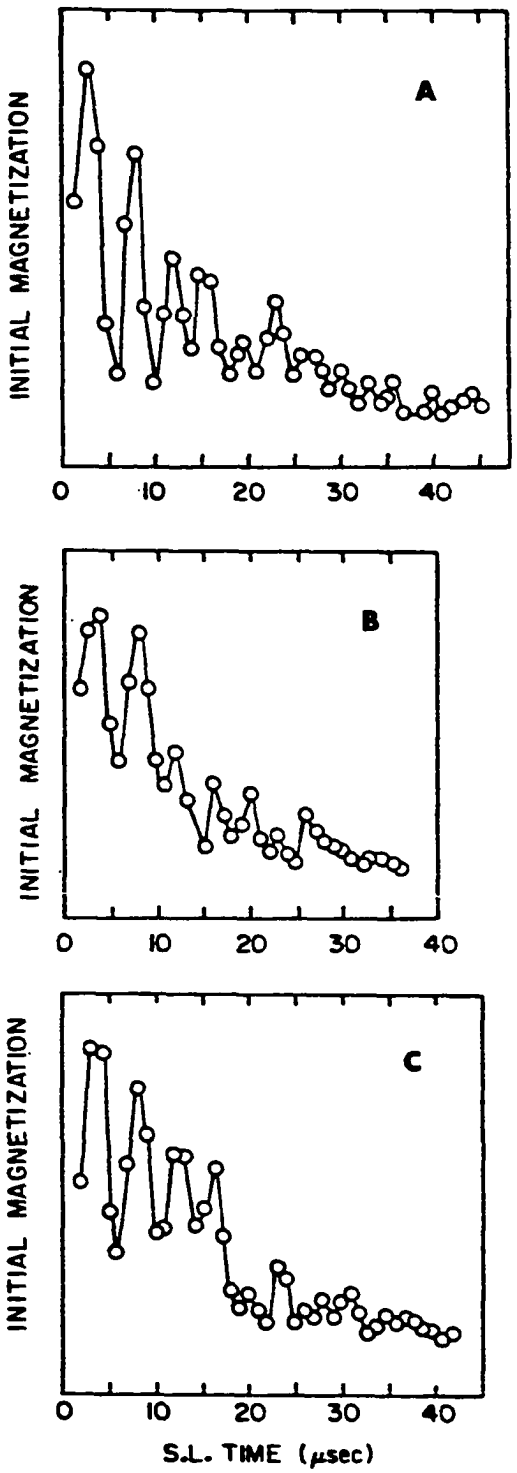
INITIAL MAGNETIZATION
A
0
10
20
30
40
INITIAL MAGNETIZATION
B
0
10
20
30
40
INITIAL MAGNETIZATION
C
0
10
20
30
40
S.L. TIME (μsec)

sources of broadening in the spectra, with $H_d > H_{cs}$. At room temperature, H_d = 42 kHz dominates the broad component. The full width at half maximum of the narrow component, 5.6 kHz, reflects motional averaging of the dipolar interaction with frequencies greater than 43 kHz.

For thermally activated processes, an Arrhenius expression can be written of the form, $k = A \exp - (E_a/RT)$. The interpretation of this equation in terms of the transition-state theory of chemical kinetics implies that k is a relaxation rate, A is a constant proportional to the entropy of activation, E_a is the energy of activation (enthalpy), and T is the temperature. For a process with a single correlation time t_c characterizing the random fluctuations of the interaction responsible for relaxation, expressions have been derived (38) for the BPP model relating the relaxation rates T_1^{-1}, T_2^{-1} to t_c and ω_o. For this model, at the maximal spin lattice relaxation rate in dipolar fields (55), $\omega_L t_c = 1$, where ω_L is the average dipolar frequency, which is proportional to the full width at half intensity of the spectrum. Extensions of this model to different types of relaxation rates, e.g., $T_{1\rho}^{-1}$, are found in the literature (41). It is noteworthy that the strong collision treatment of relaxation in the rotating frame gives a maximal rate when $\omega_L t_c = 1/2$ for $\omega_L = \omega_{rf}$ (40,56). In our analysis, the BPP model will be employed because of its simplicity, although it may not be exact for carbohydrates as distributions of correlation times and cooperative motions are expected (57).

Figure 9. ^{1}H absorption lineshape of αCD as function of temperature (^{o}C)

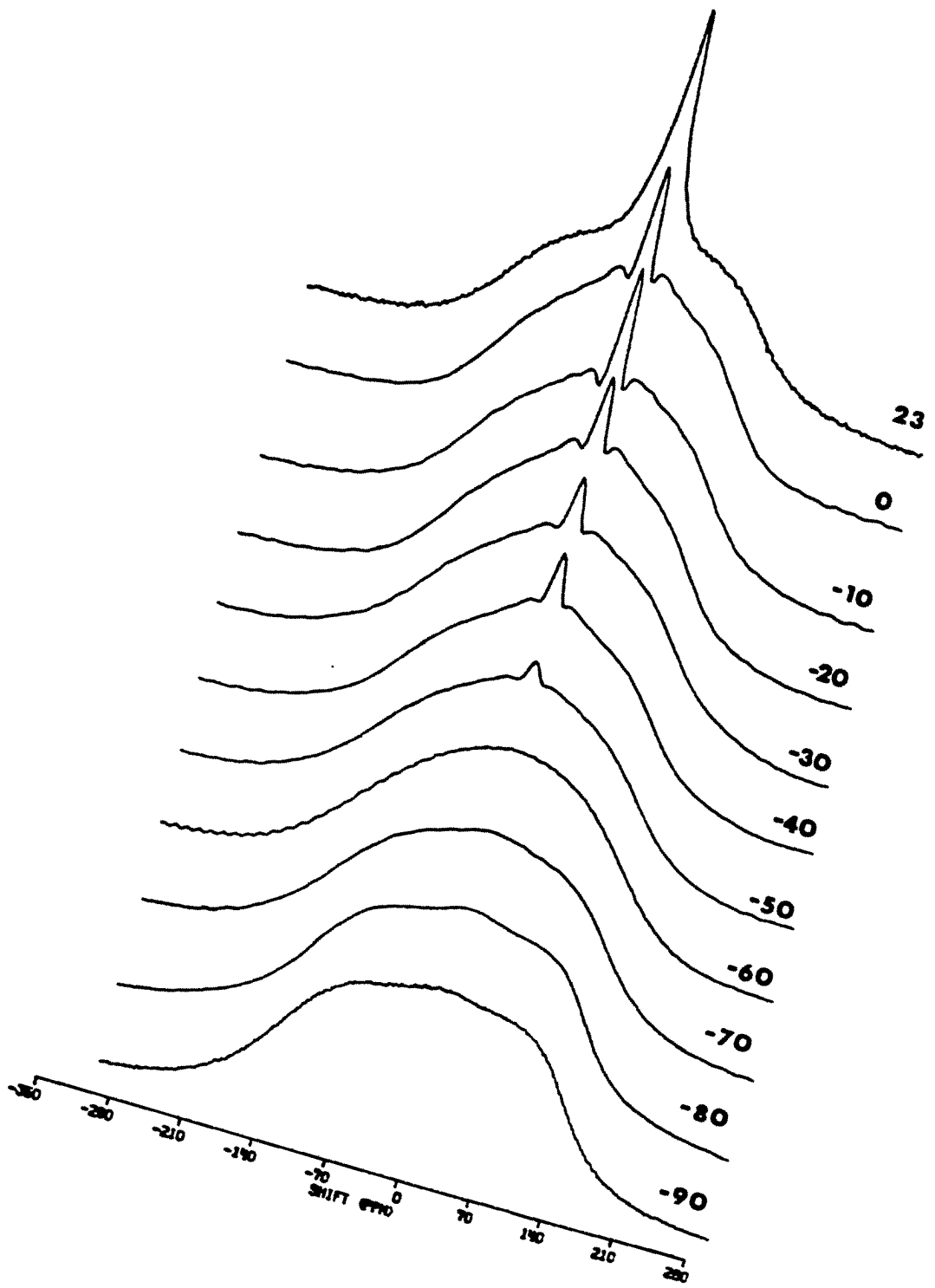
23
0
-10
-20
-30
-40
-50
-60
-70
-80
-90
-280
-210
-140
-70
0
70
140
210
280
SHIFT (PPM)

The observed lineshapes of Figure 9 have been fit to a superposition of two Gaussian curves in order to obtain the linewidth from which T_2 will be extracted. For each component, plots of ln T_2 versus the reciprocal temperatures are reported in Figures 10 and 11.

For the broad component we neglect H_{cs}, which might be on the order of 7 kHz at 220 MHz for hydroxyl groups (58) compared to H_b. Under the experimental range of temperatures, H_d varies between 43 and 63 kHz; this magnitiude justifies our neglect of H_{cs}, at least as a first approximation. The apparent energy of activation of 0.40 ± 0.02 kcal/mole is obtained from the slope of Figure 10. Since we have assigned the broad component to the ring and hydroxyl protons of glucose and to lattice water molecules, such a small energy of activation could correspond to fluctuations in the easily deformable hydrogen bond network. Energies of activation of 1/4 - 1/2 kcal/mole have been observed for protons hopping between hydrogen bonded dimers of carboxyl groups of organic acids in the solid state (59). It is to be noted that the linewidth has not reached the rigid lattice limit even at $-80^{\circ}C$, which implies that motion is still present, an observation consistent with the behavior of hydrogen bonds at very low temperatures. The shoulder and its shape in the high temperature region of Figure 10 can be interpreted qualitatively (60-61). Systems with several phases or high energy sites lead to these spectral features. We can eliminate the first possibility, as the dipolar relaxation with the Jeener-Brockaert sequence demonstrated that the carbohydrate systems were homogeneous in terms of phase. A more

Figure 10. Plot of ln T_2^* versus (temperature, $^{o}K)^{-1}$ from the full width at half maximum of the broad component

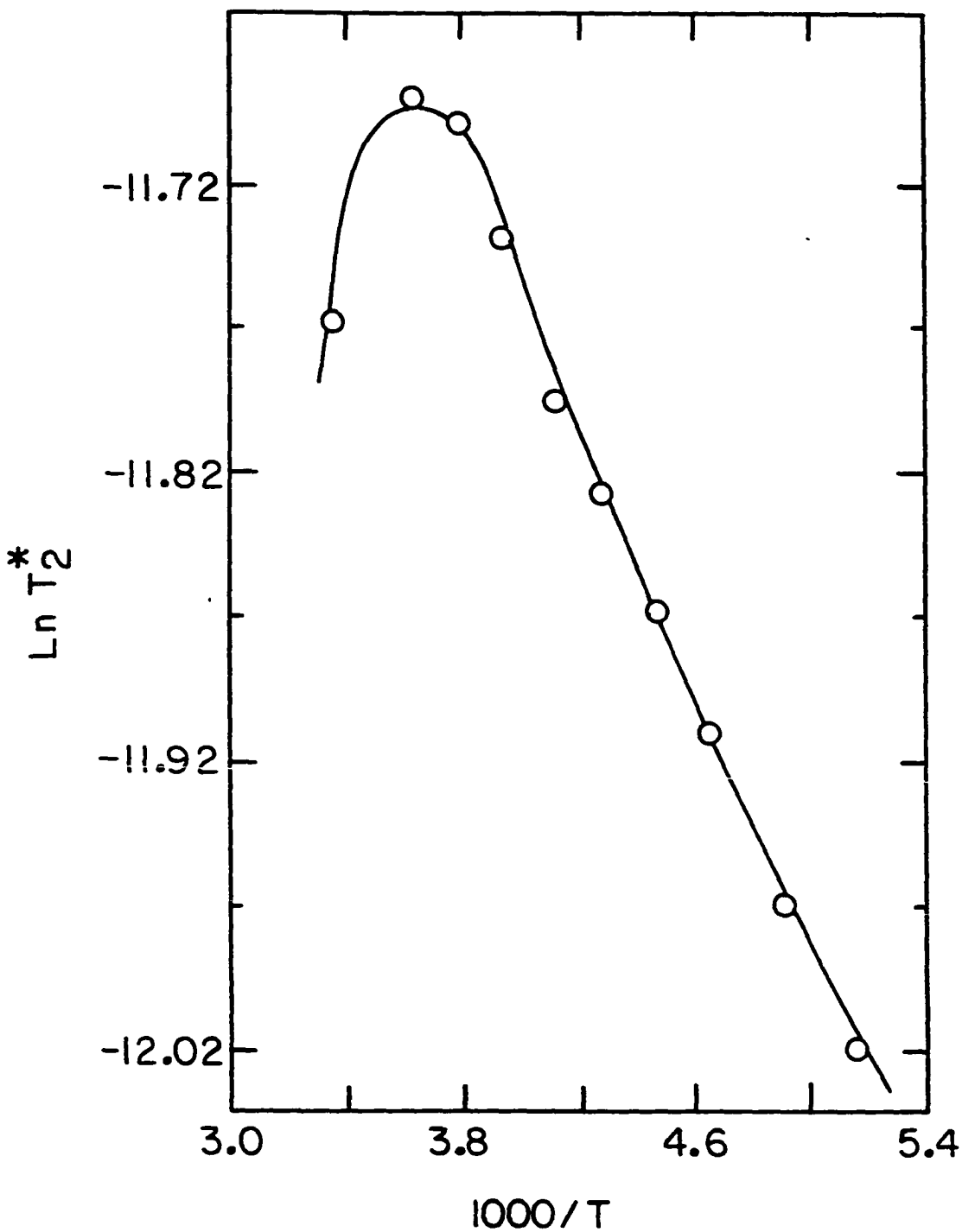
-11.72
-11.82
-11.92
-12.02
Ln T2*
3.0
3.8
4.6
5.4
1000/T

Figure 11. Plot of ln T_2^* versus (temperature, $^{o}K)^{-1}$ from the full width at half maximum of the narrow component

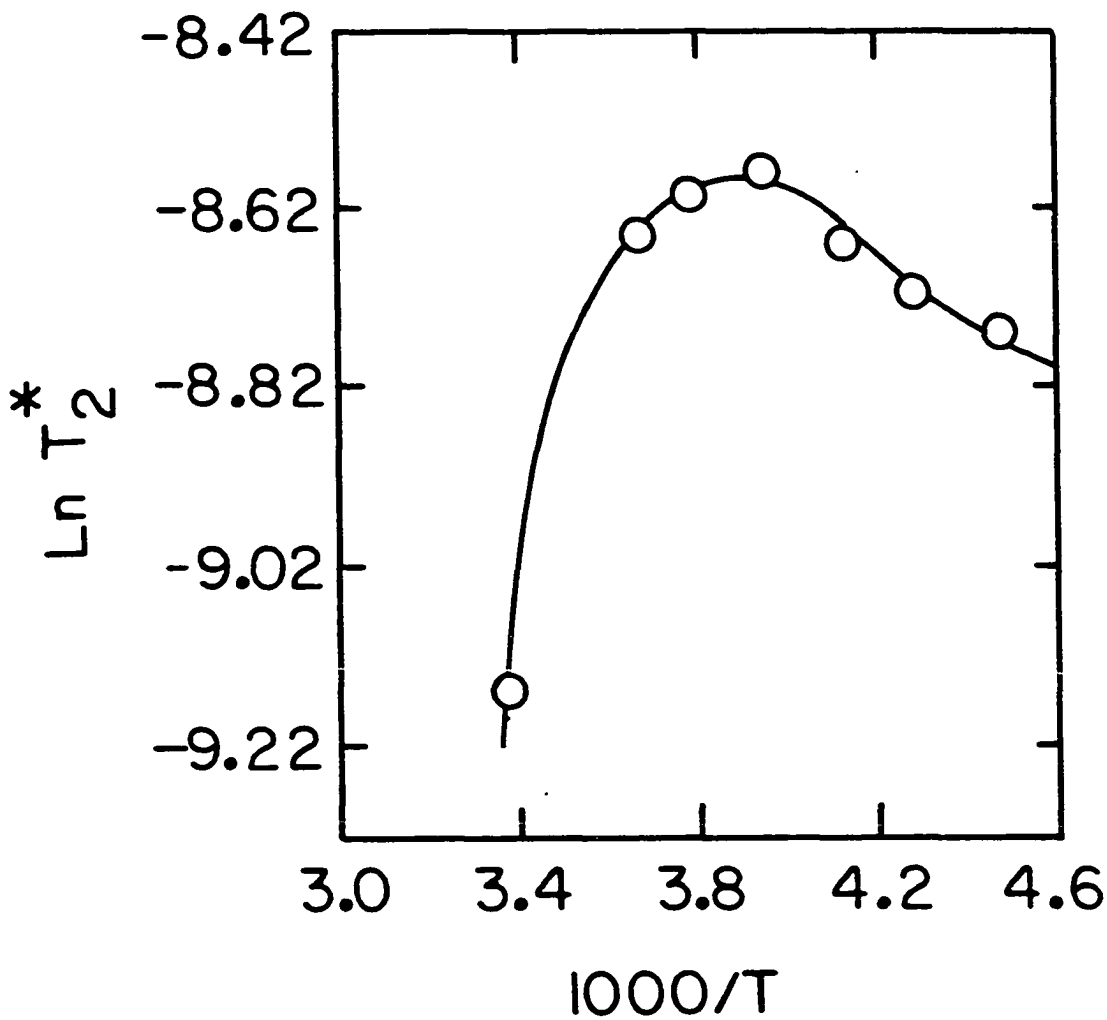
-8.42
-8.62
-8.82
-9.02
-9.22
Ln T2*
3.0
3.4
3.8
4.2
4.6
1000/T

likely explanation would be a distinction between intra- and intermolecular hydrogen bonds corresponding to the different energetic sites. It is well known that intramolecular hydrogen bonding in α CD is somewhat stable to solvent exchange (62). The cooperative interaction of the proton donor and proton acceptor functions of hydroxyl groups has been observed in carbohydrate crystal structures (52-53). This interaction leads to a systematic relationship between the hydrogen bond length and the type of OH···H interaction. The case in which the hydroxyl oxygen is both a hydrogen bond acceptor and bond donor yields the shortest hydrogen bond lengths. The ring of interglucosidic O(2)···O(3) hydrogen bonds within CD is an example of such cooperativity. The entire hydrogen bonding network in α CD has not been completely described.

The data cannot entirely rule out the possibility that the relaxation of the broad component is dominated by spin diffusion to rotating CH_2OH groups present on each glucose, and that the rest of hydroxyl and ring protons are relaxed by this methyl-like rotor. This model is not favored, since a similar value of T_2 is observed for the broad component of dextran where the C_6 groups is involved covalently in the glucosidic linkage. Furthermore, the fraction of area of the different components in the lineshape is incorrect if we assume that the narrow component arises from CH_2OH groups. A distribution of barrier heights accounts for the shape of the shoulder in Figure 10. For the narrow peak (see Figure 11), the plot of ln T_2* versus the reciprocal temperature exhibits a broader shoulder than the one in Figure 10. This indicates a greater distribution in the energy of

activation for the 2 water molecules inside the CD torus. From the crystal structure, it is known that one of the H_2Os is hydrogen bonded to the hydroxyls of C_6 from the ring glucose 1 and 5. This same water served to stabilize the distorted macrocycle ring conformation by Van der Waals contact with the ring. Therefore, the water A seems well anchored in the torus cavity. It is postulated (9-10) that the second inner water molecule B forms, through its oxygen, one hydrogen bond to water A. From such a bonding pattern, water B would be expected to be held less tightly. The broader shoulder of the T_2 results agrees qualitatively with this picture.

The redistribution of the spectral intensity about the narrow peak as a function of temperature can be modeled through modulation of the dipolar and chemical shift anisotropy interactions by assuming a certain model of motion (63) for the waters in the cavity of α CD. The nature of the motion could be a random rotation of the waters. Possible models include rotational Brownian motion characterized by average angle and jump frequency, or rotational random jumps which occur through random angles with all angles equally probable. A model of symmetry-related jumps may also be applicable. The thermal anisotropy parameters obtained in the crystal studies showed that the oxygen atoms of cavity water were fixed in α CD and disordered in β CD. This eliminates "rattling" of the water inside the α CD cavity. We have attempted unsuccessfully to simulate the spectral features at $-10^{\circ}C$ by assuming that a single H_2O was responsible for the redistribution of the spectral intensity. Our lack of success was

likely a result of this simple-minded assumption. Cooperativity of motion involving 2 water molecules makes modeling difficult. Multiple quantum spectroscopy has been used to probe the energy level structure of these 2 water molecules (49).

The results of the smaller fraction (29%) of the T_{1d} decay are plotted in Figure 12 as function of the reciprocal temperature. We obtain a value of 3.25 $\pm$ 0.33 kcal/mole for the energy of activation of the process causing this T_{1d} relaxation. By assuming a BPP-type behavior for the dipolar spin lattice relaxation, and $H_{Loc} = \Delta H/\sqrt{12}$ (43), we find a correlation time of 69 μsec at the T_{1d} minimum ($\omega_{Loc}t_c = 1$). The apparent asymmetry of the experimental data with respect to a motion with a single correlation time (BPP model - solid line in Figure 12) suggests the possibility of two minima: one at $-25^{o}C$ and the other at about $-50^{o}C$. This feature might represent the separate "freezing" temperatures of the motions of H_2O A and H_2O B inside the cavity. More data are needed to verify this suggestion. For the larger fraction of the T_{1d} decay, the energy of activation is found to be 1.06 $\pm$ 0.09 kcal/mole (see Figure 13).

These very low energies of activation indicate the participation of hydrogen bonds such as proton hopping between wells, and agrees with other measurements on similar systems (59). Several studies of the dynamics of H_2O in biological systems (61) point out that a distribution of correlation time leads to an underestimate of the energy of activation. Nevertheless, the correlation time obtained above agrees well with those for H_2O on bacterial cell walls, where

Figure 12. Plot of log T_{1d} versus (temperature, $^{o}K)^{-1}$ for the smaller component of the T_{1d} decay

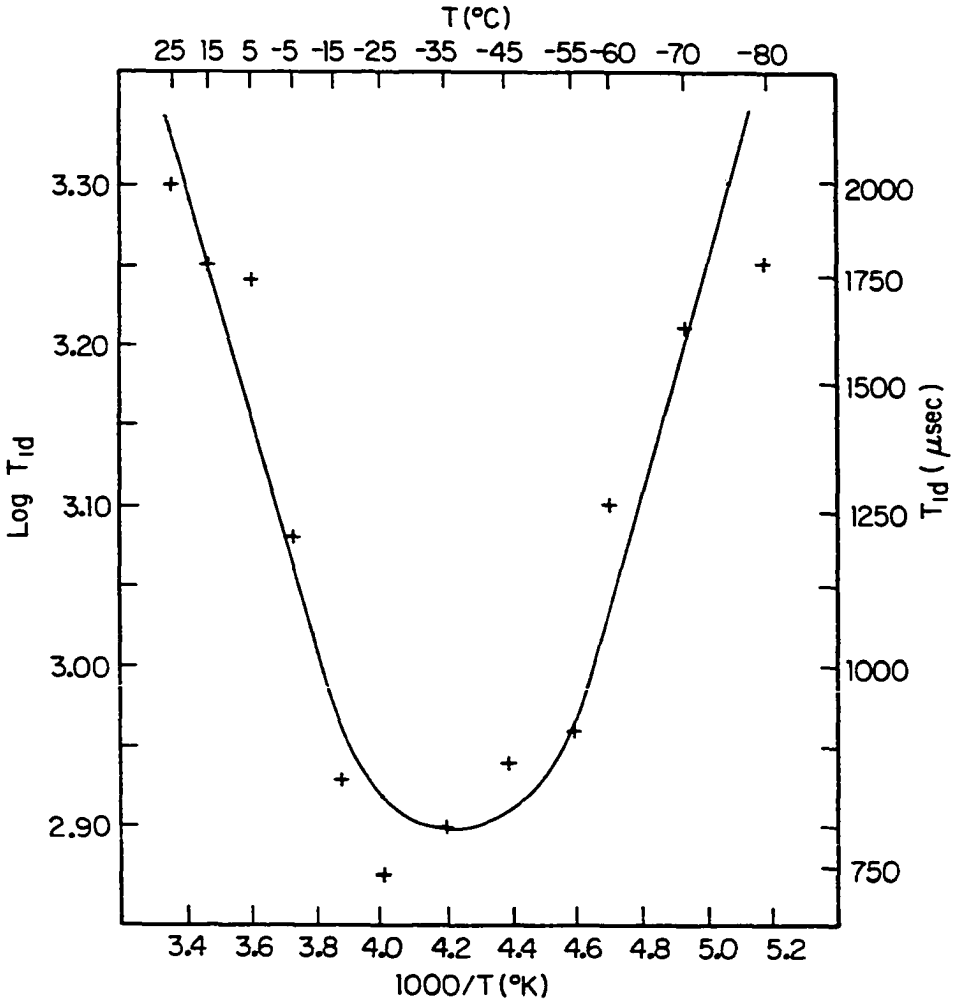
T(°C)
25 15 5 -5 -15 -25 -35 -45 -55 -60 -70 -80
3.30
3.20
3.10
3.00
2.90
Log T_{id}
2000
1750
1500
1250
1000
750
T_{id} (μsec)
3.4 3.6 3.8 4.0 4.2 4.4 4.6 4.8 5.0 5.2
1000/T(°K)

the structure is composed of peptides and polysaccharides. These systems exhibit a broad range of correlation times with typical values from solid to liquid water, i.e., 10^{-5} - 10^{-11} seconds. In charcoal, cavities with radii of 12-15 Å contain about 25-30 water molecules (60-61). The hydrophobic character of the graphite surface prevents strong interaction with H_2O, which displays mobility of bulk water in these micropore environments. On the other hand, the smaller cavity size of CD permits stronger interactions between guest and host. This effect hinders motion of the guest, as in the case of hydrogen bonded water in CD as shown by T_{1d} measurements.

Conclusions

In the present study, we have used transient techniques in NMR to investigate motions in solid cyclodextrins and dextran. A qualitative picture of the spectral density function in the kHz range emerged from the $T_{1\rho}$, T_{1d}, T_2 experiments. From the proportions of relaxation decays, it was possible to associate the various protons of cyclodextrins with particular time constants. Indeed, we observed a distinct difference in relaxation behavior of protons inside the CD cavity and those on the outside. The spectral density function in the kHz range rapidly decreased as a function of frequency for the protons on the outside of the torus. Extended spectral density functions characterized the motions of the protons inside the torus. This picture relies on the assumption that the dipolar interaction is the main mechanism of relaxation. ^{13}C chemical shifts modulated by slow motions due to local ring fluctuations and distortions accounted for

Figure 13. Plot of log T_{1d} versus (temperature, $^{o}K)^{-1}$ for the larger component of the decay due to dipolar spin lattice relaxation

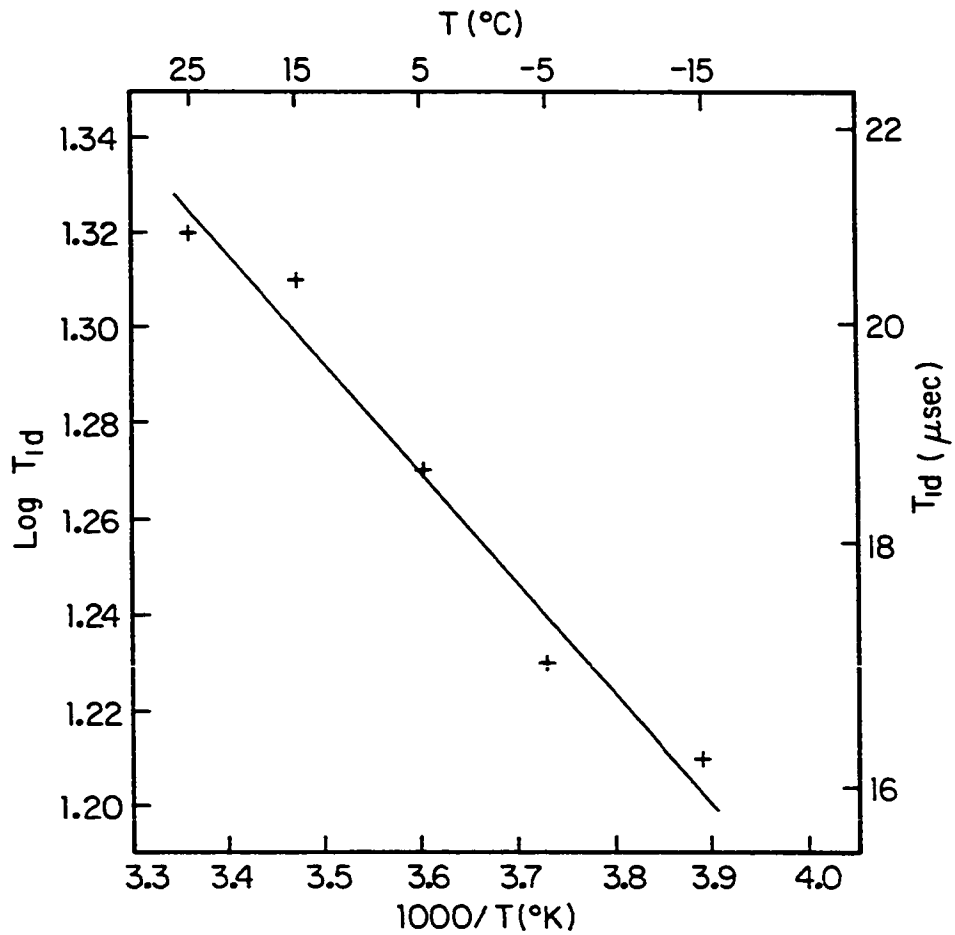
T (°C)
25
15
5
-5
-15
1.34
1.32
1.30
1.28
1.26
1.24
1.22
1.20
Log T_{Id}
22
20
18
16
T_{Id} (μsec)
3.3
3.4
3.5
3.6
3.7
3.8
3.9
4.0
1000/ T(°K)

the observed changes in the spectra in passing from α CD to β CD to dextran. The presence and role of hydrogen bonds were detected by the small energies of activation, and in the dispersion of "shoulders" in the variations of T_2 as a function of temperature in α CD.

To further our picture of dynamics within these polysaccharides, we have studied the effect of deuteration on the spectral density functions (49). The energy level structure of the two included water molecules in α CD was probed with multiple quantum spectroscopy in order to determine the extent of correlation between these waters. Frequency- and temperature-dependent studies of T_1, which should help to characterize the nature of the high frequency motions, are also reported in the following paper.

Degradation of starches in granules occurs during seed development. If the enzymes responsible for this breakdown work in an hydrophobic domain of the polysaccharides as that of dextran in the present investigation, motions and fluctuations of the substrate could play an active role in catalysis. Our NMR results have shown the existence of kHz motions in such substrates. Therefore the mechanism of action of enzymes operating in solid state-like environment might be substantially different from the same reaction in solution.

Acknowledgments

We would like to thank T. H. Apple, C. G. Fry, J. H. Iwamyia and L. Pierce for their help during this work.

References Cited

1. Roehring, K. L., Carbohydrate Biochemistry and Metabolism (Avi, Westport, 1984).

2. Sidebotham, R. L., Adv. Carbohydrate Chem. and Biochem, R. S. Tipson, D. Horton (eds.), (Academic Press, New York, 1974), Vol. 30, p. 371-444.

3. Ablett, S., P. J. Lillford, S. M. A. Baghdadi and W. Derbyshire, J. Colloid Interface Sci. 67, 355, (1978).

4. Mackay, A. L., M. Bloom, M. Tepfer and I. E. P. Taylor, Biopolymers 21, 1521, (1982).

5. Forslind, E. in NMR Basic Principles and Progress, P. Diehl, E. Fluck, R. Kosfeld (eds.), (Springer Verlag, New York, 1971), Vol. 4, p. 145.

6. Saenger, W., Angew. Chem. Int. Ed. Engl. 19, 344, (1980).

7. Bender, M. L. and M. Komiyama, Cyclodextrin Chemistry (Springer Verlag, New York, 1978).

8. Szejtli, J., ed. Proc. of the 1st Int. Symp. on Cyclodextrins (Reidel, Boston, 1982).

9. Saenger, W. and N. Noltemeyer, P. C. Manor, B. Hingerty, B. Klar, Bioorg. Chem. 5, 187, (1976).

10. Manor, P. C. and W. Saenger, J. Am. Chem. Soc. 96, 3630, (1974).

11. Lindner, K. and W. Saenger, Angew. Chem. Int. Ed. Engl. 17, 694, (1978).

12. Lindner, K. and W. Saenger, Carbohydrate Res. 99, 103, (1981).

13. Tabushi, I., Acc. Chem. Res. 15, 66, (1982).

14. Okazaki, M. and C. A. McDowell, Chem. Phys. Lett. 102, 20, (1983).

15. Walker, G. J., Biochemistry of Carbohydrates II, 16, 75, (1978).

16. Careri, G., Order and Disorder in Matter, (Benjamin Cummings, Reading, MA, 1984), p. 115-135.

17. Careri, G. in Quantum Statistical Mechanics in the Natural Sciences, S. L. Mintz, S. M. Widmayer eds., (Plenum Press, New York, 1974), p. 15-35.

18. Eigen, M., in Quantum Statistical Mechanics in the Natural Sciences, S. L. Mintz, S. M. Widmayer eds., (Plenum Press, New York, 1974), p. 37-61.

19. Bernasconi, C. F., Relaxation Kinetics (Academic Press, New York, 1976), p. 207-209.

20. Lenk, R., Brownian Motion and Spin Relaxation (Elsevier, New York, 1977), p. 217-240.

21. Gerstein, B. C., C. Chow, R. G. Pembleton and R. C. Wilson, J. Phys. Chem. 81, 565, (1977).

22. Jeener, J. and P. Brockaert, Phys. Rev. 157, 232, (1967).

23. Cheung, T. T. P., L. Worthington, P. D. Murphy, B. C. Gerstein, J. Magn. Res. 41, 158, (1980).

24. Murphy, P. D. and B. C. Gerstein, Computerized Techniques for Digital Filtering and Spectral Decomposition with Applications to NMR. DOE Report IS-4620, (1979).

25. Herzog, B. and E. L. Hahn, Phys. Rev. 103, 148, (1956).

26. Lowe, I. J. and R. E. Norberg, Phys. Rev. 107, 46, (1957).

27. Barnaal, D. E. and I. J. Lowe, Phys. Rev 148, 328, (1966).

28. Pake, G. E., J. Chem. Phys. 16, 326, (1948).

29. Pake, G. E. and E. M. Purcell, Phys. Rev. 74, 1184, (1948).

30. Saito, H. and R. Tabeta, Chem. Lett. 713, (1981).

31. Saito, H., G. Izumi, T. Mamizuka, S. Suzuki and R. Tabeta, J. Chem. Soc. Chem. Commun. 1386, (1982).

32. Atalla, P. H., J. G. Gast, D. W. Sindorf, V. J. Bartuska and G. E. Maciel, J. Am. Chem. Soc. 102, 3249, (1980).

33. Earl, W. L. and D. L. VanderHart, J. Am. Chem. Soc. 102, 3251, (1980).

34. Metzler, D. E., Biochemistry (Academic Press, New York 1977), p. 88-91.

35. Abragam, A., The Principles of Nuclear Magnetism (Oxford Univ. Press, London 1961), p. 97-158.

36. Jardetsky, O., G. C. K. Roberts, NMR in Molecular Biology (Academic Press, New York 1981), p. 52-60.

37. Carrington, A., A. D. McLachlan, Introduction to Magnetic Resonance (Wiley, New York 1979), p. 176-201.

38. Bloembergen, N., E. M. Purcell and R. V. Pound, Phys. Rev. 73, 679, (1948).

39. Fukushima, E. and S. B. W. Roeder, Experimental Pulse NMR - A Nuts and Bolts Approach (Addison-Wesley, Reading 1981), p. 261-270.

40. Slichter, C. P. and D. Ailion, Phys. Rev. 135, 1099, (1964).

41. Look, D. C. and I. J. Lowe, J. Chem. Phys. 44, 2995, (1966).

42. Garroway, A. N., J. Magn. Res. 34, 283, (1979).

43. Cheung, T. T. P. and R. Yaris, J. Chem. Phys. 72, 3604, (1980).

44. Deininghaus, U. and M. Mehring, Phys. Rev. B24, 4945, (1981).

45. Thompson, R. T., D. W. Kydon and M. M. Pintar, J. Chem. Phys. 67, 5914, (1977).

46. Packer, K. J., Mol. Phys. 39, 15, (1980).

47. Emid, S., J. Konijnendijk, J. Smidt and A. Pines, Physica 100B, 215, (1980).

48. Lenk, R., N. Bernardini, M. Bonzon and H. Greppin, Chem. Phys. Lett. 88, 119, (1982).

49. Lacelle, S. and B. C. Gerstein, following paper, herein.

50. Connor, T. M., Trans. For. Soc. 60, 1574, (1964).

51. Bloembergen, N., Physica 15, 386, (1949).

52. Jeffrey, G. A., M. E. Gress and S. Takagi, J. Am. Chem. Soc. 99, 609, (1977).

53. Tse, Y. C. and M. D. Newton, J. Am. Chem. Soc. 99, 611, (1977).

54. Punkkinen, M. and L. Osterberg, J. Magn. Res. 31, 377, (1978).

55. Gaspar, R., E. R. Andrew, D. J. Bryant and E. M. Cashell, Chem. Phys. Lett. 86, 327, (1982).

56. Connor, T. M., NMR Basic Principles and Progress P. Diehl, E. Fluck, R. Kosfeld (eds.), (Springer Verlag, New York 1971), Vol. 4, p. 247-270.

57. Connor, T. M., J. Polymer Science B6, 711, (1968).

58. Ryan, L. M., R. C. Wilson and B. C. Gerstein, Chem. Phys. Lett. 52, 341, (1977).

59. Meier, B. H., R. Meyer, R. R. Ernst, P. Zolliker, A. Farrer and W. Halg, Chem. Phys. Lett. 103, 169, (1983).

60. Resing, H. A., Adv. Mol. Relaxation Processes 1, 109, (1968).

61. Resing, H. A., Adv. Mol. Relaxation Processes 3, 199, (1972).

62. Casu, B., M. Reggiani, G. G. Gallo and A. Vigerani, Solution Properties of Natural Polymers, Special Publication No. 23, Chemical Society, 217-226, (1968).

63. Cheung, T. T. P. and B. C. Gerstein, Modulated NMR Powder Spectra: Two-Site Jump Model, DOE Report IS-4814, UC-13.

DYNAMICS OF CYCLODEXTRINS AND DEXTRAN BY SOLID STATE NMR.2

Serge Lacelle and Bernard C. Gerstein

Ames Laboratory, DOE* and Department of Chemistry
Iowa State University, Ames, Iowa 50011

*Operated for the U. S. Department of Energy by Iowa State University under contract No. W-7405-Eng-82. This research was supported by the Office of Basic Energy Sciences, Chemical Sciences Division.

SECTION II. DYNAMICS OF CYCLODEXTRINS AND DEXTRAN BY SOLID STATE NMR.2

Abstract

Further ^{1}H nuclear magnetic resonance (NMR) spin dynamics experiments are performed to monitor motions in powders of α, β cyclodextrins (CD), dextran B512F, and their deuterated analogues. The frequency dependence of the spin lattice relaxation times T_1 in the laboratory frame is interpreted in terms of the reptation model and chain backbone motions. Extrapolation of T_1 to frequencies of the order of those arising from the local dipolar fields give values in agreement with the measurements of the spin lattice relaxation T_{1d} in local dipolar fields. These results permit assignment of motions to particular segments of the molecules. The temperature dependence of T_1 yields an apparent energy of activation for motions in α CD. Goldman-Shen experiments show that the water molecules occur in small clusters rather than domains, and that their motions can be characterized by a correlation time shorter than 10 μsec. Double quantum coherences have been excited and detected in α CD. Deuteration of these carbohydrate systems leads to unpredictable changes in the relaxation parameters T_1, T_{1d}, $T_{1\rho}$, T_2, and indicate that the kinetics of exchange might not be as rapid as was previously believed.

Introduction

Solid state NMR investigations of carbohydrates in biological systems have proven difficult because of the overwhelming water signal (1). On the other hand, high resolution liquid state NMR of polysaccharides are time consuming because of their low solubility. The results obtained in solution might not truly reflect dynamic properties of carbohydrates as found in storage granules, cell wall structures or bacterial dental plaque. For this reason, we believe that powders of carbohydrates serve as better models for an understanding of the structures and dynamics of these biopolymers as found in nature. In the present paper, we continue to characterize the nature of the dynamics in powders of α and β cyclodextrins (α, β CD) and dextran B512F with transient techniques in NMR.

In particular, we address the problem of determining the role of water and exchangeable protons in the relaxation processes in carbohydrate powders. The measurement of the spin-lattice relaxation T_1 as a function of the temperature yields the energy of activation of the molecular motions for the case of α CD. The frequency dependence of T_1 permits sampling of the spectral density functions at ω_o and $2\omega_o$, where ω_o represents the MHz Larmor frequency. In this way, the determination of the power spectrum is extended to a higher frequency range than the kHz motions studied in the previous paper. Relaxation processes involving water and exchangeable protons are investigated by monitoring the relaxation parameters T_1, $T_{1\rho}$, T_{1d}, T_2. The amount of water present in the powders of these carbohydrates affects T_1.

Deuteration by solvent exchange will show similar effects for most of the relaxation parameters. The spin energy level structure of the water included in α CD is probed with the detection of multiple quantum coherences. Depending on the homogeneous or inhomogeneous character of the interactions responsible for the width of the narrow line in the spectrum of αCD, we can selectively probe the extent of couplings for the included water protons with this technique. When this approach is applied to the remaining protons, local fields may be described as relatively ordered or random on the time scale of the experiment. We also measure the extent of coupling or communication via spin diffusion between the water molecules responsible for the narrow peak in the spectra and the carbohydrate protons giving rise to the broad peak. The interpretation of the results of the Goldman-Shen experiments are discussed in terms of the domain size occupied by waters in the polysaccharides. The calculation of spin diffusion on the carbohydrates restricted by spin lattice interactions gives an upper limit on the distance over which spin diffusion can occur. From these results, estimates of the carbohydrate domains are proposed.

In α, β CD, the conformations of the polysaccharide chains on length scales of the order of 10-20 Å (1-2 mm) bear some resemblance to those of starch, as the cyclodextrins are degradation products of the starch helix. Therefore it will be of interest to compare our NMR relaxation results with those of MacKay et al. (2) who investigated ^{1}H relaxation in cellulose, which has linear extended chains. Linear starch molecules with double helical conformations of 6 glucose per

turn have been proposed (3) for amylose. These helices would form hairpin fold structures with length scales greater than 15 Å. It is generally assumed (4) that dextran has a ramified structure of the chains, involving different branching and segment lengths. Helical conformations have been suggested to occur in dextran (4).

Experimental Section

Most experimental methods have been described in detail in the previous paper (5).

Low field spin lattice relaxation measurements, T_1, were performed at 12, 40, 56 MHz, on homemade spectrometers. The design of the 12 and 40 MHz spectrometers is outlined elsewhere (6). With these spectrometers, 90° pulse lengths were between 2 and 3 μsec. All measurements were obtained with a 0.5-1 MHz filter, and an appropriate recycle time.

The Goldman-Shen pulse sequence (7), $90_x\text{-}t_1\text{-}90_{\bar{x}}\text{-}t_2\text{-}90_x\text{-}t_3$ served to monitor magnetization transfer between domains with different T_2s (8-9). With a delay t_1 chosen to be $6T_2$ of the fast component, magnetization was selectively "destroyed" for the spins in this domain. By bringing the residual magnetization of the slow component T_2 along the Zeeman field one can measure the transfer of magnetization due to spin diffusion back into the domain with the fast T_2. When t_2 is varied on a time scale shorter than 10^{-2} T_1, energy is conserved within the spin system, and spin lattice effects can be safely ignored. From the recovery of the magnetization after the third pulse, the dimension and sizes of the domains can be inferred

(8-9).

Double quantum free induction decays (FID) were measured on α CD with an off-resonance Jeener-Brockaert pulse program (10-12), 90_x-t_1-$45_{y,\bar{y}}$-t-45_y-t_2. The magnetization was sampled at $t_2 = t_1 = T_2$, with a 24 kHz offset for the long T_2, and a 40 kHz offset for the short T_2. When the signal obtained with the first 45° along $\bar{y}$ was added to the signal observed with the same pulse being along y, odd quantum coherences were detected by an oscillation of the magnetization, of frequency $n\Delta\omega$, where n is the order of the coherence, and $\Delta\omega$ is the resonance offset. When the signal obtained with a 45_y was subtracted from that observed with a $\bar{y}$ phase, even quantum coherences were selected. In both cases, the decay of the oscillations was due to the T_2 interactions present during the evolution period, t.

Deuterated α, β CD and dextran were prepared by dissolving 0.5 g of sample in 30-40 ml of D_2O (99.8%, Isotopes KOR, Cambridge), followed by an exchange period of one to two hours at room temperature and lyophillization. Three such cycles were performed for α and β CD, while two cycles were used for dextran.

Results and Discussion

Frequency dependence of T_1 : $T_1 \alpha\omega_o^m$

The results of the frequency dependence of T_1 are shown for the protonated and deuterated samples in Figures 1 and 2, respectively. From a linear least squares fit of the log T_1 versus the log ω_o is obtained the slope, or the frequency dependence of T_1. Extrapolation of this curve to field strengths of the order of the local fields,

about 11.5 kHz for all samples, yield T_1s which are different than T_{1d} by a factor of two to three (see Table 1). Considering that the extrapolation is over three orders of magnitude of the magnetic field, there is good agreement of the spin lattice relaxation time in the laboratory frame with that in the dipolar fields. For the protonated carbohydrates, T_1 may then be associated with motions of segments of the molecules which were identified with the appropriate T_{1d} components (5). In the case of α CD, the T_1 relaxation is due to protons on the outside of the torus cavity. The magnitude of the energy of activation (see next section) tends to indicate that motions of the macrocycle backbone are involved rather than local motions of CH_2OH or OH groups. A similar relaxation mechanism involving chain backbone motions is suggested for dextran. In both cases, the spin diffusion processes and spin lattice relaxation processes must be closely coupled in view of their similar time scales. On the other hand, for β CD and the deuterated samples, there is no spin diffusion bottleneck, as $T_{1d} >> T_2$. Spin diffusion processes occur rapidly compared to spin lattice relaxation processes. For β CD, spin lattice relaxation is due to the motions of the disordered water inside the torus cavity. This fact is shown by T_1 at 11.5 kHz, which is about equal to the long T_{1d} associated with the cavity waters. From the frequency dependence, we suggest a relaxation mechanism which is consistent with the data for β CD and the deuterated samples (see below).

Figure 1. Frequency dependence of T_1 for protonated α CD (A), β CD (B) and dextran B512F (D)

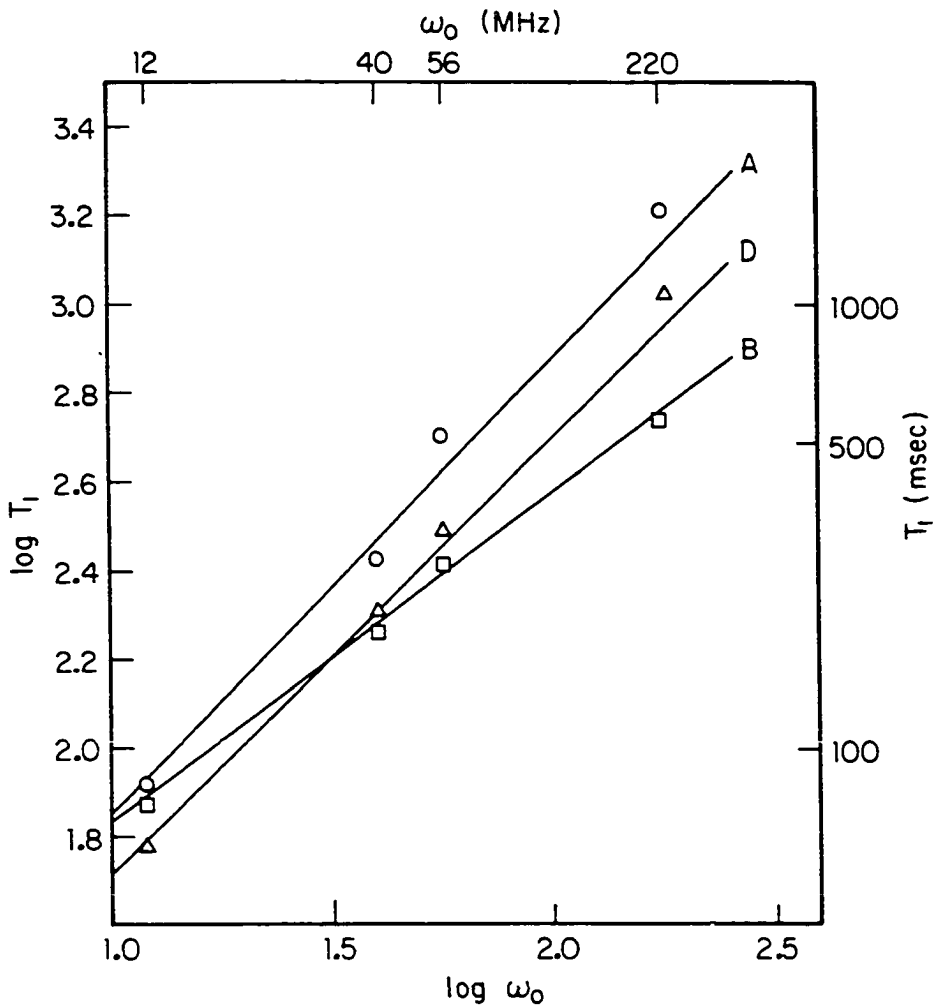
ω0 (MHz)
12
40
56
220
3.4
3.2
3.0
2.8
2.6
2.4
2.2
2.0
1.8
log T1
1000
500
100
T1 (msec)
A
D
B
1.0
1.5
2.0
2.5
log ω0

Figure 2. Frequency dependence of T_1 for deuterated α CD (A), β CD (B) and dextran B512F (D)

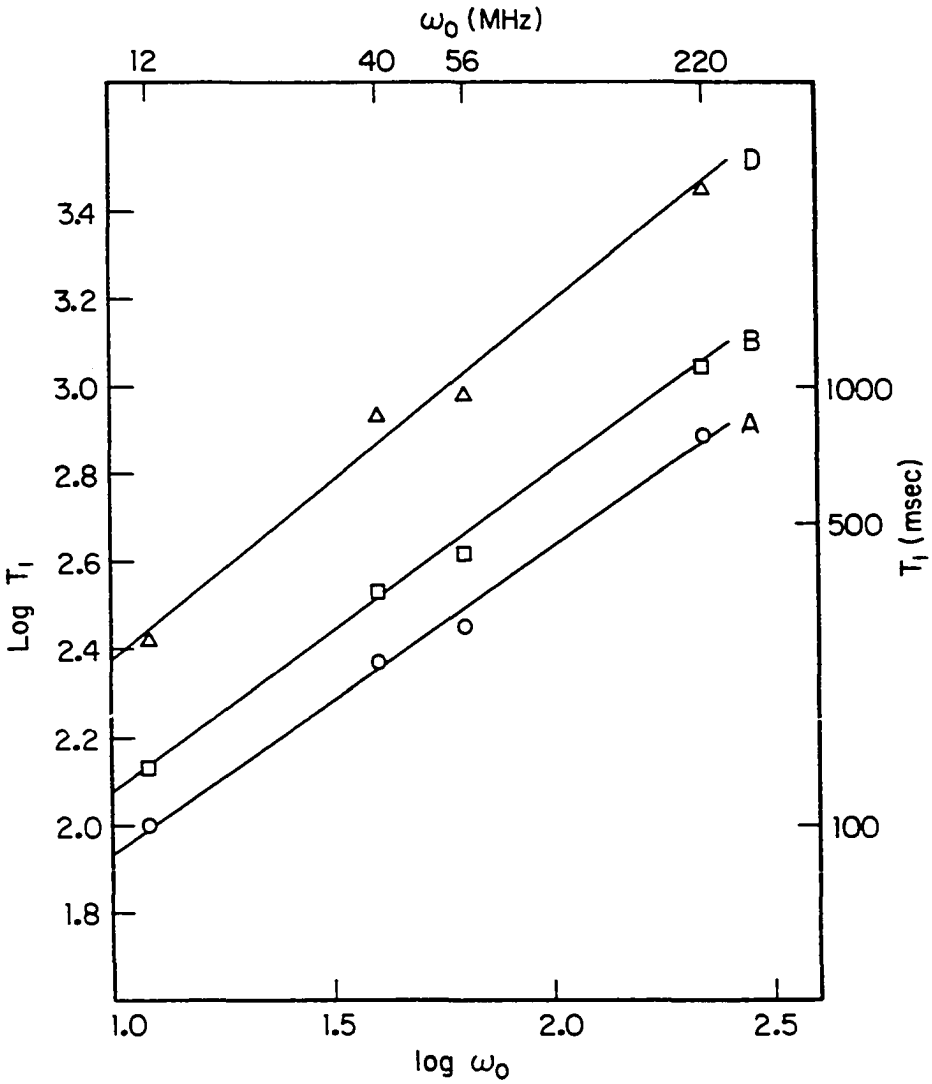
ω_0 (MHz)
12
40
56
220
D
B
A
3.4
3.2
3.0
2.8
2.6
2.4
2.2
2.0
1.8
Log T_1
1000
500
100
T_1 (msec)
1.0
1.5
2.0
2.5
log ω_0

Table 1. T_1 frequency dependence - $T_1 \alpha \omega_o^m$

Compound	m*	T_1 (11.5 kHz)	T_{1d}
α CD	1.03 ± .08	70 μsec	21 μsec (s)
β CD	.69 ± .05	.7 msec	.95 msec (l)
dextran B512F	.99 ± .03	60 μsec	20 μsec (s)
deuterated α CD	.70 ± .02	.8 msec	1.6 msec (l)
deuterated β CD	.73 ± .02	.9 msec	1.9 msec (l)
deuterated dextran B512F	.81 ± .06	1.0 msec	2.7 msec (l)

*Error limit is one standard deviation.

s is for the short T_{1d} component, while l is for the long T_{1d}. T_{1d} for protonated samples is from (5), T_{1d} for deuterated samples are found in Table 4.

At high field (MHz), a single T_1 is observed for all samples. This implies that at this field motions associated with one of the T_{1d} components must be ineffective in the relaxation process. Presumably, spin diffusion from these segments of the molecules would allow a rapid communication on a T_2 time scale to the regions where relaxation occurs, and a spatially averaged T_1 relaxation time would be observed.

In order to interpret the frequency dependence of T_1, a model of the spectral density functions must be chosen (13). The method of the

generalized spectral density functions (14-15), which assumes small step random motions, is appropriate for the carbohydrates studied here. The experimental spectral density functions can be represented by

$$J(\omega_o, t_c) \propto t_c^{1-m} \omega_o^{m}.$$

Several models and their m dependence are listed in Table 2. Temperature studies of T_1 for various carbohydrates (16-17 next section) show that at room temperature, relaxation is between the solid regime, $\omega_o t_c >> 1$, and the intermediate regime $\omega_o t_c = 1$. From Table 1, we note that m is roughly 1 for α CD and dextran, while for β CD and the deuterated samples, m is approximately 3/4. The order fluctuation model, m = 1, (20, see Table 2) leads to $T_1 = 5/2\ T_{1\rho}$, which is not observed for dextran. For β CD and the deuterated samples, the reptation model (21) is in accord with the frequency dependence of T_1. This does not necessarily imply that the relaxation actually occurs through such a mechanism. The reptation model may be envisaged as worm-like displacements of defects along a polymer chain geometrically constrained in a tube. For β CD, we assigned the T_1 relaxation to the disordered water molecules. In the torus cavity, the 6·5 water molecules are distributed over 8 sites (23). Therefore, one might expect highly correlated motions of the water molecules over the sites which would resemble confined polymer distortions as described by reptation. For the deuterated samples, if protons and deuterons are hopping into each others sites, or confined to wells of

hydrogen bonds, a modulation of the dipolar interaction would result in relaxation. Again, collective motions from these small jumps with high frequencies could correspond to chain or backbone fluctuations of the reptation model and provide an appropriate relaxation mechanism. Similar chain fluctuations have been observed on polybutadiene (24) by NMR.

Table 2. T_1 frequency dependence $T_1 \propto \omega_o^m$ for various models

Models		m	references
translation diffusion	solution	1/2	18
defect diffusion	solid	3/2	
rotational diffusion	solution	0	19
	solid	2	
order fluctuation in liquid crystals	isotropic liquid	1/2	20
	nematic phase	1	
reptation		3/4	21,22

Temperature dependence for T_1 of α CD

The temperature dependence of T_1 for α CD is shown in Figure 3. From the slope of the plot log T_1 versus the reciprocal temperature we obtain an apparent energy of activation ε of 1.62 ± .06 kcal/mole for the relaxation processes. It is known that distributions of

correlation times lead to low estimates of the energy of activation as determined by NMR in carbohydrates (16). The real energy of activation, E_A, can be determined (14) from the apparent energy of activation ε, and the frequency dependence, m, of T_1 by equation 1

$$E_A = \frac{\varepsilon}{1-m} \qquad (1)$$

Since this expression diverges at m = 1 we used the standard deviations of the m dependence of αCD to obtain limits on E_A. This yields a lower bound of 15 kcal/mole and an upper bound of 32 kcal/mole. A corrected value of 20 $\pm$ 5 kcal/mole has been inferred from T_1 relaxation in starch (16) using differences between the maximal spin lattice relaxation rates $T_{1\rho}^{-1}$ and T_1^{-1}. In starch, relaxation was associated with chain backbone motion because of the high temperature at which the T_1 minimum occurred. The positive slope in Figure 3 implies that relaxation is characterized by $\omega_o t_c > 1$, which corresponds to the solid regime.

Goldman-Shen experiments

The results of the experiments are shown in Figure 4. After an initial 90_x pulse, the phase coherence of the magnetization decays following two constants: one associated with T_2 (short), the other with T_2 (long). When the second pulse, 90_x is applied after waiting $6T_2$ (short), only the residual magnetization from T_2 (long) is brought back along the Zeeman field. Then, spin diffusion of the magnetization will occur from the mobile domain of the long T_2 to the

rigid domain of the short T_2 on a time scale of T_2 (long) to 10^{-2} T_1. The recovery of the magnetization in the rigid domain is monitored with the third pulse 90_x. The acquisition of the FID following this last pulse is triggered 15 μsec after the last pulse. This was to ensure that the recovery of the probe-receiver-100kHz filter system was complete.

As can be seen from Figure 4, the recovery of the magnetization in the rigid domain was over on a T_2 (long) time scale. The periods between the last two 90° pulses T_2 (short) to 10^{-2} T_1 (data not shown). Under these conditions, the shape of the FID remained essentially constant. This type of fast recovery has been observed for translational diffusion of spins between two domains (7). For the systems studied here, the long T_2 was due to water either in the cavity for α and β CD, or in the structure of dextran. The correlation time for the water motions, or proton jumps must then be smaller than 10 μsec. On almost every collision of the water molecules or protons with the rest of the polysaccharides, magnetization is transferred to the rigid domain where spin diffusion occurs within 10 μsec or T_2 (short). This is in agreement with the temperature dependence of T_2 for α CD as shown in the previous paper. Recovery of the magnetization is then limited by spin diffusion in the rigid domain. Since the water molecules occupy small volumes, about 5-6 Å diameter for the cavity diameter in the CDs, one cannot accurately speak of domains as found in certain commercial polymers (8).

Figure 3. Temperature dependence of T_1 for α CD. Log T_1 versus reciprocal temperature

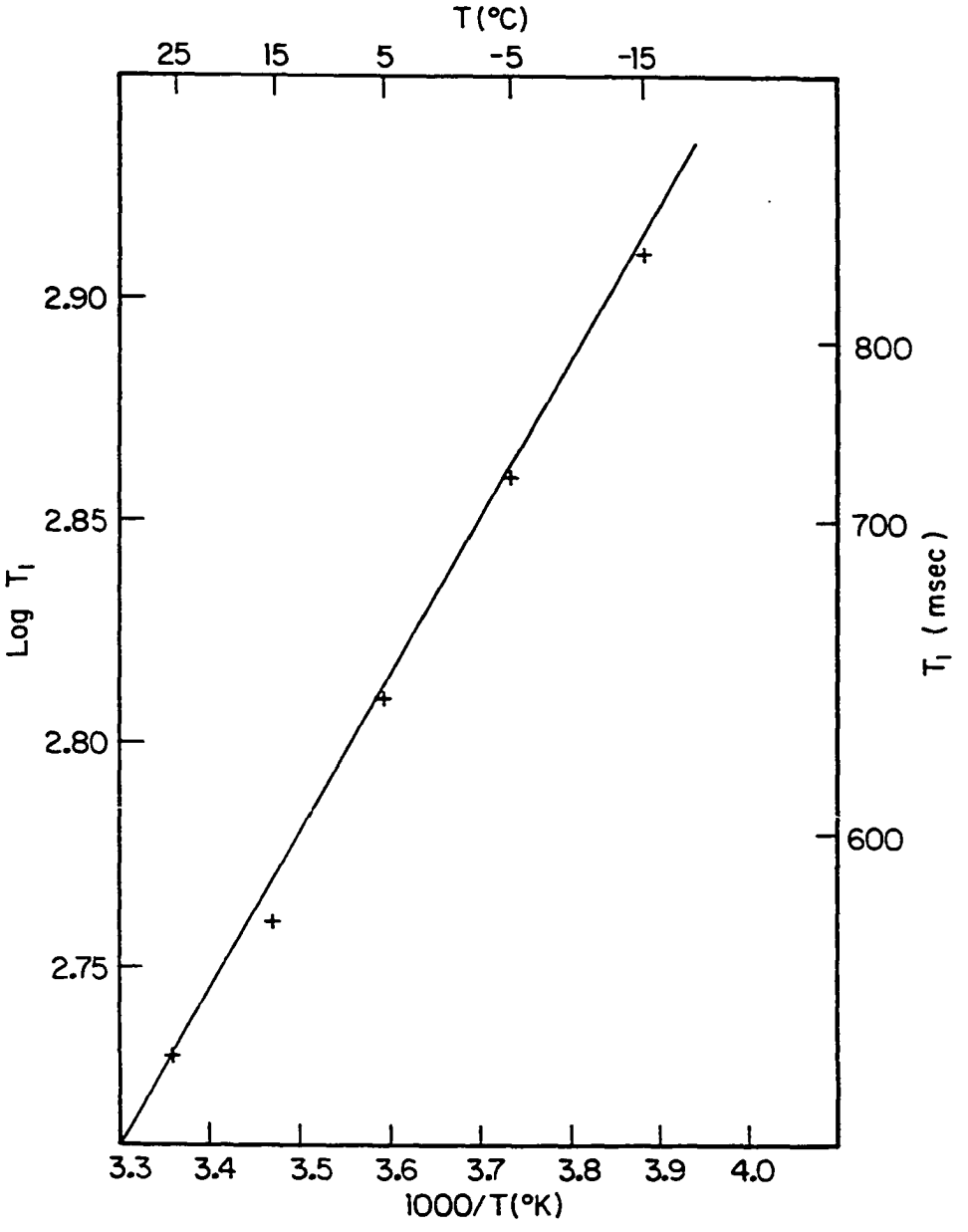
T(°C)
25
15
5
-5
-15
2.90
2.85
2.80
2.75
Log T_1
800
700
600
T_1 (msec)
3.3
3.4
3.5
3.6
3.7
3.8
3.9
4.0
1000/T(°K)

Figure 4. FID following the Goldman-Shen pulse sequence. Acquisition time is 395 μsec. FIDs of deuterated samples on the right, protonated samples on the left. A) α CD, B) β CD, C) dextran B512F

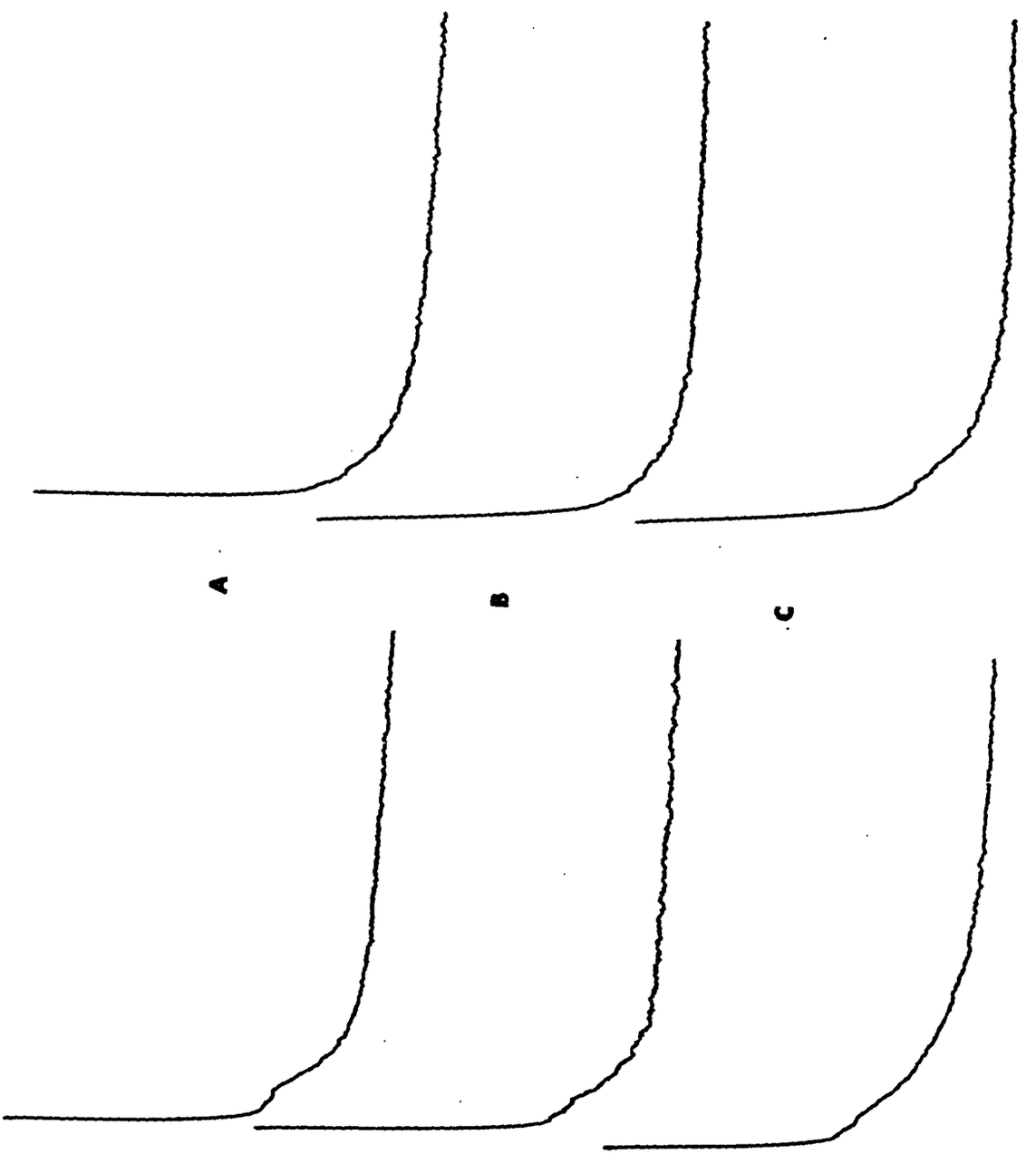
A
B
C

An order of magnitude calculation of the distance over which spin diffusion can occur in the dextran gives an upper limit on the size of domains if many water molecules are concentrated together in the structure. If spin diffusion is modeled by a random walk process (25), then over an interval T_1, the mean distance of diffusion is $s = (2\ DT_1)^{1/2}$, where D is the diffusion coefficient. For a cubic lattice of nearest neighbor protons, Bloembergen (25) has shown that $D = a^2/50T_2$, where a is the lattice distance. For a Gaussian lineshape, the local field $\langle H_L \rangle = \Delta H/\sqrt{12}$ (26), where H is the linewidth at half intensity. From $\langle H_L \rangle = \frac{\gamma^2 h}{r^3}$, where γ is the magnetogyric ratio, h is Planck's constant, we obtain an average r of 2.2 Å for proton separation in the carbohydrates. This value of r and the T_2 from the lineshape gives D, which can be used to calculate the domain size over which spin diffusion occurs. For dextran, we find the domain size to be 100-150 Å, if such structures are found in dextran. Because of the fast recovery even in the Goldman-Shen experiment for dextran, this result implies that water molecules are grouped in small number like the CDs. The domain sized of 100-150 Å in the carbohydrates studied here might imply aggregation of molecules on such a scale. For a pectate gel, MacKay et al. found an upper limit of 100 Å (2) for the rigid and mobile domains.

Multiple quantum coherence spectroscopy in α CD

In Figure 5, we present the double quantum free induction decays obtained in α CD, with the off-resonance Jeener-Brockaert pulse sequence. The preparation and detection period were set equal to the

T_2 (long) to excite the included water molecules. The other protons were selected by having the same interval equal to T_2 (short). The success of the experiments depends on the presence of bilinear spin interactions, such as the dipolar interaction. The fact that we are able to excite this coherence implies that the dipolar interaction contributes to the narrow peak in the frequency spectrum. The order in the local fields due to the carbohydrate protons decays rapidly (Figure 4b) due to proton spin fluctuations. A similar time scale for the decay of transverse magnetization (n = 1) is observed during spin-locking experiments of short duration.

Effects of deuteration

The results of the relaxation measurements are found in Tables 3 and 4. The spectra of these deuterated carbohydrates are similar to those of Figure 3 in the previous paper (5). Surprisingly, no major differences are found in the values of the short T_2s (broad component). If deuteration would lead to uniform distribution of deuterium in the local fields, then one would expect the linewidth, or T_2^{-1} to be scaled by 1/6 due to the smaller magnetogyric ratio of D. On the other hand, only exchangeable protons from hydroxyl groups are replaced (27-28). In D_2O, polysaccharides exchange hydroxyl protons in seconds according to unpublished i.r. spectroscopic evidence (27). From the above T_2 evidence, the non-exchangeable ring and methylene protons must still experience strong dipolar coupling due to spin diffusion. For the long T_2s, slight increases are noted for α and β CD. This does not necessarily imply increased freedom for the

Figure 5. Double quantum coherence free induction decays in α CD. A) excitations of the water molecules in the cavity, expected oscillation period 21 μsec B) excitation of the rest of the protons, expected oscillation period 12.5 μsec

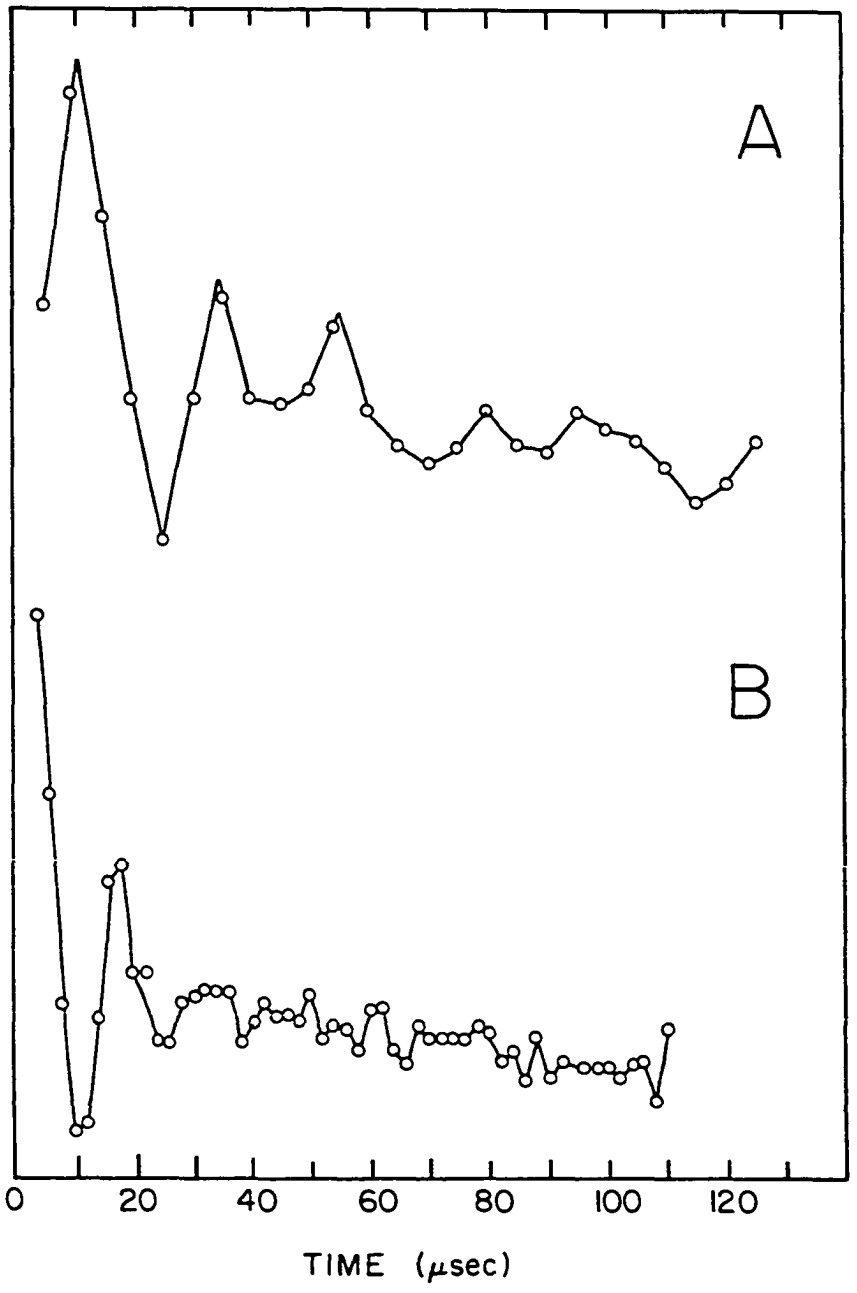
A
B
0
20
40
60
80
100
120
TIME (μsec)

motions of the included water molecules, but could reflect an asymmetry in the local dipolar fields, due to the non-random deuterium distribution. The fact that the proportions of both components of T_2 essentially do not change upon deuteration is an interesting observation. We have not found a satisfactory explanation to account this behavior. Similarly, we unsuccessfully attempted to correlate the various proportions of the two components for the relaxation parameters T_{1d} and $T_{1\rho}$ with different segments of the molecules. This lack of correlation may be due to: 1) different selectivity for exchange at different sites, 2) slower exchange kinetics, or 3) exchange with atmospheric water vapor.

The T_1s increased in all deuterated samples by two- to three-fold. Measurements were characterized by single exponential decays. When the protonated samples from the same stock were stored for several months over drierite, an increase in T_1s of α CD and dextran, and a decrease for β CD were noted with a concurrent decrease in water content as indicated by the decrease in the proportions of the long T_2s. For the deuterated samples under similar conditions, T_1 decreased slightly for all samples while the proportions of the long T_2 increased for α and β CD and decreased for dextran. These variations clearly indicate the participation of water either directly in the relaxation processes or indirectly by altering the segments of the structures. Further experiments with better control of water are needed before definite conclusions can be reached as to the role of water in the relaxation processes as detected by NMR.

Table 3. Spin lattice and spin-spin relaxation times and their relative components

	T_1/msec		T_2/μsec	
α CD	950	100%	9.4	95.0%
			150	5.0%
*	770	100%	10.0	93.4%
			160	6.6%
β CD	1330	100%	9.6	94.3%
			150	5.7%
*	1110	100%	9.6	94.3%
			150	6.6%
dextran B512F	2990	100%	9.6	93.6%
			150	6.4%
*	2830	100%	9.6	94.6%
			150	5.4%

*Kept over drierite for longer periods.

When comparing the relaxation times T_{1d} and $T_{1\rho}$ of the deuterated samples with those of the corresponding protonated systems (5), a general trend is observed for the various components in all samples. For the slow T_{1d}, we note an increase in its value, while it remained

Table 4. Relaxation in dipolar and radio frequency fields and their relative components

	T_{1d}/μsec		$T_{1\rho}$/μsec	
α CD	1600	22.6%	25	19.2%
	18	77.4%	3100	80.8%
β CD	1900	25.9%	3700	100%
	20	74.1%		
dextran B512F	2700	28.0%	21	14.5%
	21	72.0%	4700	85.5%

about the same for the short T_{1d}. A slight decrease was observed in the slow $T_{1\rho}$, while a large decrease was noted for the fast $T_{1\rho}$. Qualitatively, the same picture of the spectral density functions for kHz motions are observed for the deuterated samples as with the protonated samples, if we assume that the dipolar interaction is the main relaxation mechanism. The water protons' spectral density function extends to higher frequency motions than those of the carbohydrate backbone.

It is of interest to compare T_{1d} of 3.5 msec for deuterated cellulose (2) and $T_{1\rho}$ of about 5 msec in a 10 Gauss field for protonated starch (16) to the results obtained here and in the previous paper. For these systems, though the local and global conformations are different, the relaxation times are all of the same

order of magnitude. This implies that the nature of motions in the kHz regime, must not be too different, if relaxation is dominated by the dipolar interactions.

We have measured the magnetization response to a spin locking field with $H_{r.f.} >> H_{local}$. The expected oscillating behavior of $2\omega_{rf}$ is demonstrated in Figure 6 for deuterated α CD. The oscillations dampened with a $T_2' < T_2$ as was the case for the protonated α CD, indicating proton spin fluctuation on this time scale.

Conclusions

A variety of nuclear spin dynamics experiments were applied to protons in α, β CD, dextran and their deuterated analogues. The spin lattice relaxation times T_1 in the laboratory frame were examined as a function of the Larmor frequency ω_o. For α CD and dextran, T_1 is proportional to ω_o, while for β CD and the deuterated samples T_1 $\omega_o^{3/4}$. The latter frequency dependence is consistent with the reptation model involving many high frequency protons or water jumps. Extrapolation of T_1 to low dipolar fields gives values in agreement with measurements of the spin lattice relaxation in dipolar fields, T_{1d}. This permitted assignment of spin lattice relaxation T_1 to certain segments of the molecules. The temperature dependence of T_1 for α CD yielded an apparent energy of activation of 1.62 kcal/mole considering the possibility of distribution of correlation times, a corrected value of the energy of activation in the range 15-30

Figure 6. Spin locking in a 39 Gauss r.f. field for periods of T_2 for deuterated α CD. Initial amplitudes (arbitrary units) versus spin locking time in μsec. Expected period of oscillation 5.7 μsec

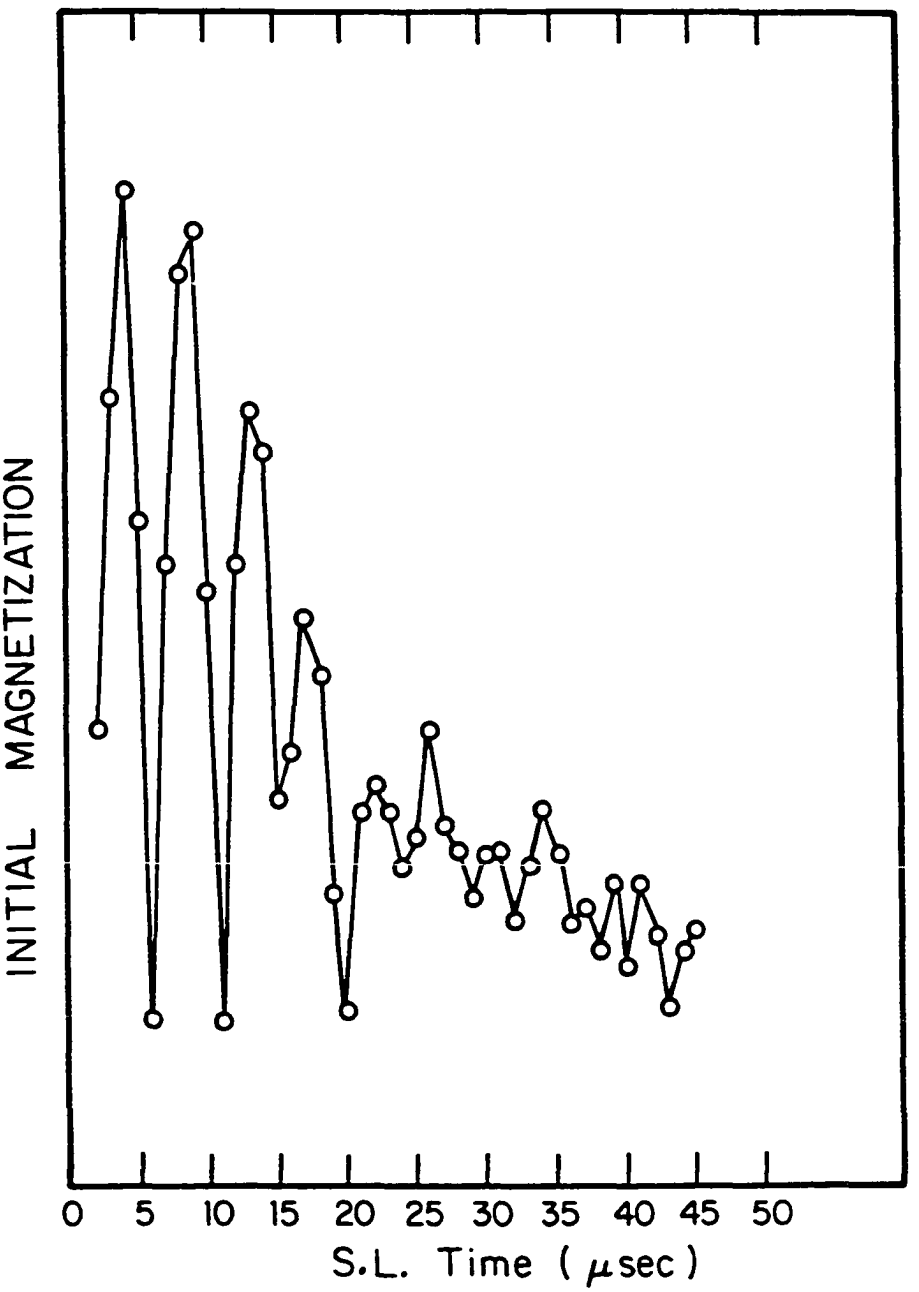
INITIAL MAGNETIZATION
0
5
10
15
20
25
30
35
40
45
50
S.L. Time (μsec)

kcal/mole is obtained, which suggests chain backbone motions as a possible relaxation mechanism in α CD.

The detection of double quantum coherences from the included water molecules in α CD indicates that dipolar coupling is the main interaction responsible for the narrow linewidth component. The results of the Goldman-Shen experiments suggest that water in powders of carbohydrates occurs in small clusters rather than domains. Deuteration of the samples changes the relaxation parameters in an unpredictable fashion. Further experiments with more precise variations in water content and methods of deuteration are required before definite conclusions may be reached for the role of water and exchangeable protons in the relaxation mechanisms.

Acknowledgments

We would like to thank C. G. Fry, J. H. Iwamyia, R. D. Scott and D. R. Torgeson for their help during this work.

References Cited

1. Lacelle, S., R. D. Walker and B. C. Gerstein, (unpublished data), Dept. of Chemistry, ISU).
2. MacKay, A. L., M. Bloom, M. Tepfer and I. E. P. Taylor, Biopolymers 21, 152, (1982).
3. Kaimuma, K. and D. French, Biopolymers 11, 2241, (1972).
4. Sidebotham, R. L., Adv. Carbohydrate Chem. and Biochem, R. S. Tipson, D. Horton (eds.), (Academic Press, New York 1974), Vol. 30, pp. 371-444.
5. Lacelle, S. and B. C. Gerstein, (previous paper, herein).
6. Phua, T. T., B. J. Beaudry, D. T. Peterson, D. R. Torgeson and R. G. Barnes, Phys. Rev. B28, 6227, (1983), and references therein.
7. Goldman, M. and L. Shen, Phys. Rev. 144, 321, (1966).
8. Cheung, T. T. P. and B. C. Gerstein, J. Appl. Phys. 52, 5517, (1981).
9. Cheung, T. T. P., J. Chem. Phys. 76, 1248, (1982).
10. Emid, S., A. Bax, J. Konijnendijk, J. Smidt and A. Pines, Physica 96B, 333, (1979).
11. Emid, S., J. Konijnendijk, J. Smidt and A. Pines, Physica 100B, 215, (1980).
12. Emid, S., J. Smidt and A. Pines, Chem. Phys. Lett. 73, 496, (1980).
13. Noack, F., NMR, Basic Principles and Progress, P. Diehl, E. Fluck, R. Kosfeld (eds.), (Springer-Verlag, New York 1971), Vol. 3, p.84.

14. Lenk, R., Adv. Mol. Relaxation Processes 3, 3, (1972).

15. Lenk, R., Brownian Motion and Spin Relaxation (Elsevier, New York 1977), p. 161-171.

16. Connor, T. M., J. Polymer Science B6, 711, (1968).

17. Adamic, K. and M. Blinc, J. Polymer Science B6, 303, (1968).

18. Hunt, B. I. and J. G. Powles, Proc. Phys. Soc. 88, 513, (1966).

19. Bloembergen, N., E. M. Purcell and R. V. Pound, Phys. Rev. 73, 679, (1948).

20. Blinc, R., D. L. Hogenboom, D. E. O'Reilly and E. M. Peterson, Phys. Rev. Lett. 23, 969, (1969).

21. de Gennes, P. G., J. Chem. Phys. 55, 572, (1971).

22. McBrierty, V. J. and D. C. Douglas, Phys. Repts. 63, 61, (1980).

23. Lindner, K. and W. Saenger, Carbohydrate Research 99, 103, (1981).

24. Martin-Borret, Y., J. P. Cohen-Addad and J. P. Messa, J. Chem. Phys. 58, 1700, (1973).

25. Bloembergen, N., Physica 15, 386, (1949).

26. Cheung, T. T. P. and R. Yaris, J. Chem. Phys. 72, 3604, (1980).

27. Casu, B., M. Reggiani, G. G. Gallo and A. Vigerani, Solution Properties of Natural Polymers, Special Publication No. 23, Chemical Society, pp. 217-226, 1968.

28. Bergeron, R. J. and M. A. Channing, Bioorg. Chem. 5, 437, (1976).

RANDOM MATRIX THEORY IN BIOLOGICAL NUCLEAR MAGNETIC RESONANCE SPECTROSCOPY

Serge Lacelle

From the Ames Laboratory, DOE* and Department of Chemistry
Iowa State University, Ames, Iowa 50011

*Operated for the U. S. Department of Energy by Iowa State University under contract No. W-7405-Eng-82. This research was supported by the Office of Basic Energy Sciences, Chemical Sciences Division.

SECTION III. RANDOM MATRIX THEORY IN BIOLOGICAL NUCLEAR MAGNETIC RESONANCE SPECTROSCOPY

Abstract

The statistical theory of energy levels or random matrix theory is presented in the context of the analysis of chemical shifts of nuclear magnetic resonance (NMR) spectra of large biological systems. Distribution functions for the spacing between nearest-neighbor energy levels are discussed for uncorrelated, correlated, and random superposition of correlated energy levels. Application of this approach to the NMR spectra of a vitamin, an antibiotic, and a protein demonstrates the state of correlation of an ensemble of energy levels that characterizes each system. The detection of coherent and dissipative structures in proteins becomes feasible with this statistical spectroscopic technique.

Introduction

Over the last few years, the increased quantity and greater quality of nuclear magnetic resonance (NMR) data obtained on biological systems, ranging from small metabolites to large macromolecular structures, reflect advances in technique and technology. Most of these studies were done in solution, whereas the NMR biological experiments performed in the solid state have had limited success up to now. Most solution NMR investigations deal with time-independent interactions such as magnetic shielding (chemical shift) and the indirect spin-spin coupling (J- or scalar coupling).

Although time-dependent interactions monitored through relaxation measurements provide dynamic information, they will not be treated explicitly in this work. Here we apply random matrix theory (RMT) (1-3), or the statistical theory of energy levels, to the interpretation of chemical shift data in large biological systems. This theory has been successful in the understanding of spectroscopic data of excited nuclei, atoms, and certain molecular systems (1,4,5) but has never been applied to biological systems. Our purpose is to introduce to the biological community the assumptions, physical content, and results of RMT and to discuss the potential information that can be extracted from such analysis, as well as the inherent limitations of this approach. We examine these points in the Theory and Method section. In Results and Discussion we present an analysis and discussion of NMR data obtained from current literature with examples that include a vitamin, an antibiotic, and a protein. In the Conclusions and Summary, we suggest the application of this technique to some aspects of the problems of irreversibility in biological systems.

Theoretical Background and Method

The motivation for a statistical analysis of the energy level distribution is threefold. First, in large systems where the present methods of NMR are insufficient for a complete assignment of individual resonances, the energy level spacing distribution can characterize the system. Second, the method is general so that the interactions determining the energies or even the nature of the system

need not be known. Finally, even if the assignment of the chemical shift is complete, this signature only describes the average local environment of each nuclear site. This microscopic approach neglects the presence of any correlation between sites. By examining an ensemble of local sites (or energy levels) we obtain a global picture of this many-body system which may indicate the occurrence of mutual or reciprocal relations between its constituents.

We are concerned with the statistical distribution of spacing between nearest-neighbor energy levels in NMR spectra of biomolecules. Let us recall a few basic ideas of probability and statistics. When dealing with an ensemble of values A_i of a property A in a system, one can characterize this sample space with the statistical ensemble average $\langle A \rangle$ (or the first moment), and the second moment describing the fluctuations of A_i about $\langle A \rangle$. The probability of finding a value in the interval $A_i + dA_i$ in the ensemble is given by $P(A_i)dA_i$, where $P(A_i)$ or P is a probability density function satisfying $\Sigma_i P(A_i)dA_i = 1$. Furthermore, we can express the average of a discrete variable, $\langle A \rangle = \Sigma_i A_i P(A_i)$ with the probability P, which can easily be generalized through integration for the case of a continuous variable. The probability density function is loosely called a distribution function in statistical mechanics and characterizes the ensemble as a whole. The constraints employed in defining a representative ensemble are chosen to correspond to the maximal knowledge that we have of the system of interest. RMT permits the interpretation of the functional form of P in terms of qualitative correlation of the investigated

property A. In statistics (6), correlation is a measure of how several variables vary together. Linear covariability of A and B is described by the covariance σ_{AB} given by

$$\sigma_{AB} = \langle AB \rangle - \langle A \rangle \langle B \rangle. \quad (1)$$

A correlation coefficient proportional to the covariance and standard deviation of the random variables can also be defined, but such a quantitative approach is of no concern here. Rather, correlation will imply the familiar and intuitive concept of relation between energy levels; the environment of a local site i is also determined by factors influencing another (or many) sites(s) j. Cooperativity effects in allosteric enzymes and the concerted charge relay mechanism of action of chymotrypsin are biochemical examples of correlation or coherent couplings.

Theoretical distribution functions are available for the results of RMT (2) (Figure 1). The Poisson distribution

$$P(x) = 1/D \exp(-x/D) \quad (2)$$

corresponds to uncorrelated values of the variable x, the energy level spacing (see below), with normalization constant D, while in the correlated case, the Wigner distribution (7) applies and is given by

$$P(x) = \frac{\pi x}{2 D^2} \exp - \frac{(\pi x^2)}{(4 D^2)}. \quad (3)$$

An intermediate condition consists of the random superposition of a few Wigner distributions. This decomposition can indicate a certain

number, n, of correlated states in a system. A large superposition of Wigner functions, $n \to \infty$, leads to the Poisson distribution. In the case of a random superposition of two Wigner distributions, an analytic expression has been derived (8,9) for P given below

$$P(x) = \frac{1}{2D} \exp - \frac{(\pi x^2)}{(8 D^2)} + \frac{(\pi x)}{(8 D^2)} \exp - \frac{(\pi x^2)}{(16 D^2)} \phi \frac{(\sqrt{\pi} x)}{(4 D)}, \quad (4)$$

where ϕ is the complementary error function,

$$\phi(y) = 1 - \frac{2}{\sqrt{\pi}} \int_0^y \exp(-t^2)\, dt. \quad (5)$$

Empirical distributions (9) such as the Porter-Thomas

$$P(x) = 4 x/D^2 \exp(-2x/D) \quad (6)$$

and the normal (Gaussian) distribution

$$P(x) = 1/\sigma(2\pi)^{1/2} \exp[-1/2(x - \mu/\sigma)^2], \quad (7)$$

where μ and σ^2 are the first moment and variance, respectively, have been used in the statistical analysis of energy levels. Because of their empirical origin, the interpretation and/or information content of such distributions have been discussed with respect to specific individual cases.

In spectroscopy, time-independent interactions lead to the experimental determination of characteristic values of the energy of the system, or eigenvalues E_i. The eigenfunctions $|i\rangle$ represent the

stationary states of the system. The nature of this kind of problem is embodied in the Schrodinger time-independent equation

$$H|i\rangle = E_i|i\rangle, \tag{8}$$

where H is the hamiltonian operator corresponding to the energy. In the event where the system possesses a finite number of stationary states, as in NMR, Schrodinger's equation can be "solved" with matrix algebra. The hamiltonian is represented by a matrix with elements H_{ij}, where the diagonal elements ($i = j$) are related to the eigenvalues, and the off-diagonal elements ($i \neq j$) carry information concerning the transition probability between stationary states i and j. Physical symmetry of the system permits a so-called block diagonalization transformation of the hamiltonian which yields irreducible blocks of elements along the diagonal. Instead of working with the original n x n matrix, we can study the eigenvalue distribution function of each block of dimension smaller than n separately, since the elements of different blocks do not mix.

In the statistical theory of energy levels, the elements of the hamiltonian are random variables distributed according to certain assumptions. We suppose the off-diagonal elements are distributed symmetrically about zero mean while the distribution of diagonal elements is taken to be symmetrical, but not necessarily about zero mean. The plausibility of these assumptions and others (2) outside the scope of this paper have been favorably tested with Monte Carlo computer calculations in the derivation of the spacing distribution

Figure 1. Probability density functions, P, for the nearest-neighbor energy level relative spacing x_i (A) Poisson distribution, (B) Wigner distribution, and (C) random superposition of two Wigner distributions

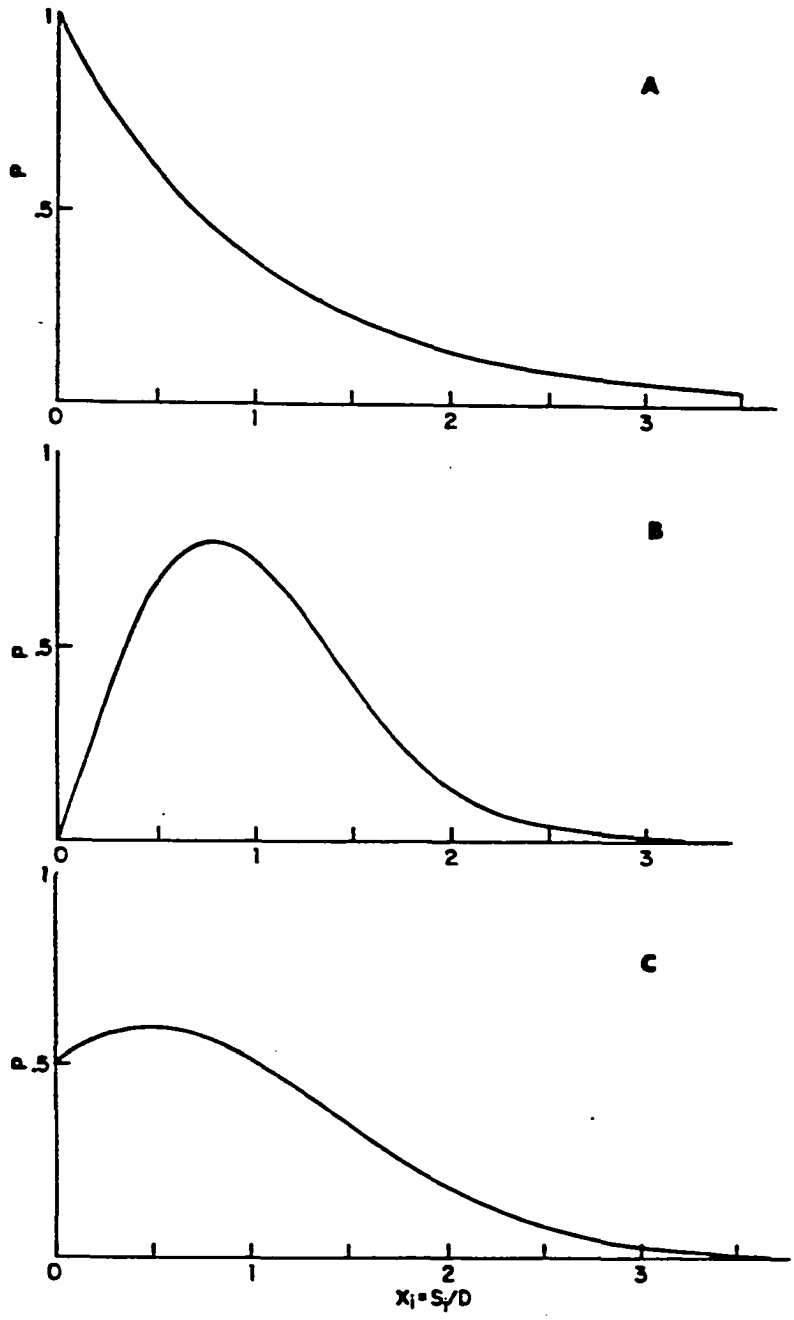
A
B
C
1
.5
0
1
2
3
$X_i = S_i/D$

functions (10, 11).

We wish to treat the chemical shift interaction hamiltonian with RMT. For this interaction the most general hamiltonian (12) is given by $H = -(h/2\pi)\ \mathbf{I}\cdot\overleftrightarrow{\sigma}\cdot\mathbf{B}$, where γ is the magnetogyric ratio; h is Planck's constant; **I**, the spin angular momentum operator; and **B**, the magnetic field. The chemical shift $\overleftrightarrow{\sigma}$ is represented by a second-rank cartesian tensor with nine components σ_{ij}. These can be resolved with symmetry arguments into an isotropic component $\sigma_{iso} = 1/3\Sigma_i\ \sigma_{ii}$, an antisymmetric tensor $\sigma_{ij} = 1/2(\sigma_{ij} - \sigma_{ji})$, and a traceless symmetric tensor $\sigma_{ij} = 1/2(\sigma_{ij} + \sigma_{ji}) - \sigma_{iso}$, with three and five independent components, respectively. In solution, only the isotropic value survives random molecular motions as detected in the NMR spectrum. Under such a circumstance, H^i becomes $-\sigma^i_{iso}\ \omega_o h I_z$, where i denotes a particular site in the system; the energy is $E_i = -\sigma^i_{iso}\ \omega_o$ in frequency units $\omega_o = \gamma\mathbf{B}$. Theories (12) have decomposed σ_{iso} into a paramagnetic and a diamagnetic part, σ_p and σ_d, which depend upon the spatial distribution and orbital angular momentum of the electrons. The interpretation of chemical shifts usually deals with the shielding of a nucleus by surrounding electrons. Any correlation between sites is not obvious from this approach. Chemical shift correlation spectroscopy (13) through scalar coupling is a promising two-dimensional NMR technique that treats correlation of different spins. From the standard NMR spectrum, we obtain qualitative correlation information by analyzing the relative spacing between nearest-neighbor energy levels.

The method consists of ordering the set of energy levels E_i of a system due only to chemical shifts. The nearest-neighbor spacing $S_i = E_{i+1} - E_i$ is obtained for all i sites, from which sample space one establishes the average spacing D. One then computes the relative spacing $x_i = S_i/D$. A histogram of the number of spacings, NS, with value x_i versus x_i permits the comparison of the experimental data with P (x_i). All the distribution functions given here are dependent on a well-behaved spacing average, D. This requirement may be examined by plotting the number of levels N having energy less than or equal to E versus the energy E. A linear plot (constant slope) indicates a uniform energy level density that assures a well-behaved D. In the event of several slopes, the distribution of spacings is obtained separately for the levels belonging to the appropriate energy level density and are plotted on the same histogram (10). The possibility of high-level density or small spacings and low intensity of absorption lines could result in missing certain lines. In NMR, overlapping resonances will usually contribute most to this problem. If the missing levels form a small fraction of the total number of levels, e.g., <5%, we neglect such corrections and assume the overall distribution function remains essentially invariant (10). Quantitative determination of the statistical agreement between the experimentally measured and theoretical distributions is beyond the level of this paper (11). Suffice it to say that nonlinearity must then be introduced in the distribution function, $p \alpha x^q$, which we avoid for the simple cases treated here, the Poisson distribution where

$q = 0$, and the Wigner function with $q = 1$. For a Poisson distribution, the probability of spacing S between an energy level, E, and the adjacent one is S + dS is independent of the spacing and is given by dS/D. The Wigner distribution is linearly dependent on S and the analogous probability is $S\ dS/D^2$. The different behavior of the Poisson and Wigner distributions for small spacings has been explained (2) with group theoretical arguments involving symmetry and level repulsion.

The method can easily be extended in principle for the treatment of time-dependent interactions, H (t). Normally, relaxation measurements are interpreted in terms of a microscopic model of motion. The Wiener-Khintchine theorem shows that the Fourier transform of the autocorrelation function, $\langle H(t) \cdot H(t + \tau) \rangle$ (where the brackets denote an ensemble equilibrium average) yields the spectral density function, $J(\omega)$, thereby giving the frequencies of motions responsible for relaxation. Relaxation rates are directly proportional to $J(\omega)$. An expansion of $J(\omega)$ in terms of eigenvalues and eigenfunctions of a transition operator permits a frequency analysis of relaxation data (14). In the event of a discrete spectrum, one could probe directly the correlation of the different motions in the same way as we have presented it above for static chemical shift interactions.

For large biological systems such as proteins with domains or quaternary structures, the approach has inherent limitations for both static and time-dependent interactions. Continuous distributions and

overlapping of resonance lines cannot be treated with RMT in its present form; one needs a discrete and well-resolved spectrum. Similarly for the power spectrum, $J(\omega)$, continuous distributions of correlation times are often found in large polymeric structures. This problem becomes less important with two-dimensional NMR experiments.

Results and Discussion

The NMR spectrum that can be analyzed by RMT may not display J-coupling since the nearest-neighbor energy level spacing distribution will become a function of chemical shift and the indirect spin-spin interactions. In the detection of rare nuclei, e.g., ^{13}C, ^{15}N, broadband proton decoupling is normally employed, eliminating J-coupling to protons. As for detection of protons, several relatively new two-dimensional NMR techniques (13) permit the separation of different interactions in a spectrum, providing solely chemical shift information.

Recently, Keller et al. (15) assigned most of the resonances of ^{1}H NMR of the trypsin inhibitor homologue K, a protein from snake venom with 57 amino acids. In Figure 2 A, a plot of the number of energy levels N with energy less than or equal to E, versus E, is linear, indicating a well-behaved energy level density. The results of the statistical analysis of the energy level spacing distributions are presented in Figure 3. Here we clearly see the presence of a Poisson distribution, indicating uncorrelated energy levels. In such a large system, one would not expect a correlation of all the energy levels. Tight coupling in the tertiary structure usually involves

only certain segments of the protein, but not necessarily all of the nuclei. Stronger correlations are to be expected in smaller regions of the molecule, such as domains or the secondary structures. Nevertheless, the Poisson distribution characterizes well the ensemble of nuclear energy levels of the trypsin inhibitor. A change in the state of correlation might be expected on binding to trypsin.

A smaller system without distinct domains or secondary structure features might reflect correlation of the tertiary structure involving most nuclei. Cyanocobalamin, or vitamin B_{12}, is well suited to test this proposal. Anton et al. (16) studied this system with ^{13}C NMR and assigned all resonances. Changes in the NMR of the carbonyl and imine carbon regions were monitored by varying the pH, and then compared to analogues. This approach of correlating resonances with several analogues helped in the interpretation of the spectrum. Our analysis of the data is presented in Figures 2 B and 4 for cyanocobalamin only. We assumed the presence of a single energy level density though the curvature in the plot N versus E might indicate the presence of two densities. Surprisingly, the Poisson distribution is in qualitative agreement with the experimental distribution. Therefore, the ^{13}C energy levels are uncorrelated on the NMR time scale. However, this does not exclude correlation of electronic, vibrational, or rotational energy levels which might be important in the functional aspect of the vitamin in vivo.

The structure of alamethicin, an antibiotic that displays interesting interactions with membranes, has been studied in solution

with ^{1}H-two-dimensional NMR techniques by Banerjee et al. (17). Spectroscopic investigations have proposed the existence of secondary structures in the 20 amino acid peptide. The NH_2-terminal region would consist of an α-helix while the COOH-terminus would display an extended β-sheet structure. The presence of two structures implies possible correlation of energy levels within and among secondary structures. The NMR energy level density shows two distinct regions in the N versus E plot (Figure 2 C). To obtain the spacing distribution, a single average spacing D was used in Figure 5 A. When two average spacings D_1 and D_2 were used to treat the data, and their respective relative spacings were plotted on the same histogram (Figure 5 B), the results were very similar to those determined by a single average spacing D. A spacing with a value of 48 standard deviations from D (Figure 2 C) as determined from the other 62 spacings was renormalized to one (s_i = D) in order to prevent the whole distribution from being determined solely by this single aberrant spacing. In both cases, the Poisson and Wigner distributions do not agree with the experimental distributions. The intermediate case of random superposition of two Wigner distributions agrees qualitatively with the data. Equation 4 was developed assuming a single mean spacing D, though Harvey and Hughes (9) expect slight changes in the distribution in the case of two approximately similar energy level densities. From this, one might speculate that a Wigner distribution could be associated with the α-helix region, and another Wigner distribution could be associated with the β-pleated sheet. The

presence of hydrogen bonds that stabilize each structure lends support to the correlation of energy levels in the ^{1}H NMR. From their studies, Banerjee et al. propose a conformation with the first nine amino acids involved in the α-helix, followed by an open spacer of four residues, with the last five residues forming the extended β-sheet. Here, we assumed for simplicity that the first 10 amino acids formed the α-helix and that the last 10 were involved in the extended β-sheet and analyzed the energy level spacing distribution separately, but plotted the results on the same histogram (Figure 5 C). The Wigner distribution is in qualitative agreement with the data that indicates the presence of correlation of spacings. In any case, the ensemble of energy levels of alamethicin can be represented by the random superposition of two Wigner distributions (Equation 5) that correspond to two correlated states.

Conclusions and Summary

The characterization of an ensemble of energy levels by spacing distributions demonstrates the degree of correlation between energy levels. The ^{13}C NMR of vitamin B_{12} and ^{1}H NMR of a trypsin inhibitor both displayed uncorrelated energy levels while the ^{1}H NMR of the antibiotic alamethicin was in qualitative agreement with the random superposition of two Wigner distributions. Presumably, other types of distributions would also characterize biological systems.

In biological NMR, RMT has several advantages for describing a system, or part of it, by a spacing distribution. The existence of channels for either energy transfer or relaxation (18), or hydrogen

Figure 2. Number of energy levels, N, with energy less than or equal to E. All energies are expressed in pp. (A) Trypsin inhibitor homologue K (15), (B) cyanocobalamin (16), (C) alamethicin (17)

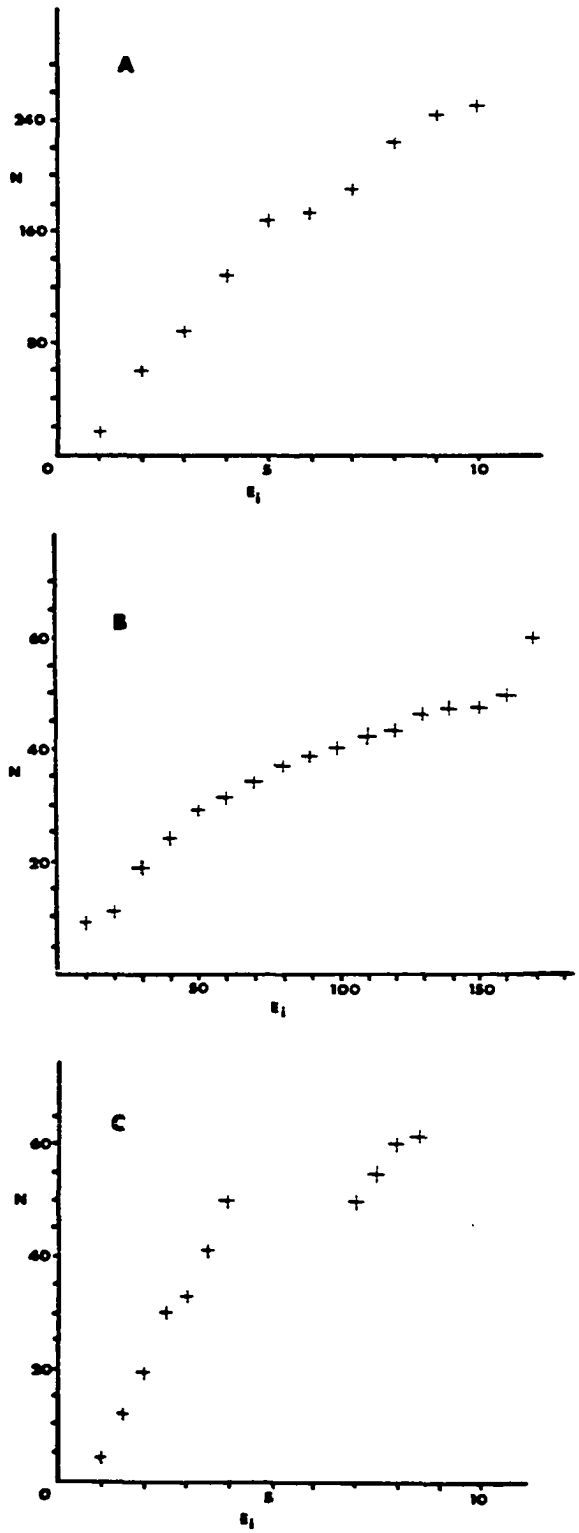
A
240
160
80
N
0
5
10
E_i
B
60
40
20
N
50
100
150
E_i
C
60
40
20
N
0
5
10
E_i

Figure 3. Histogram of the number of spacings, NS, versus the relative spacing x_i for the trypsin inhibitor homologue K (15) superimposed with the Poisson distribution

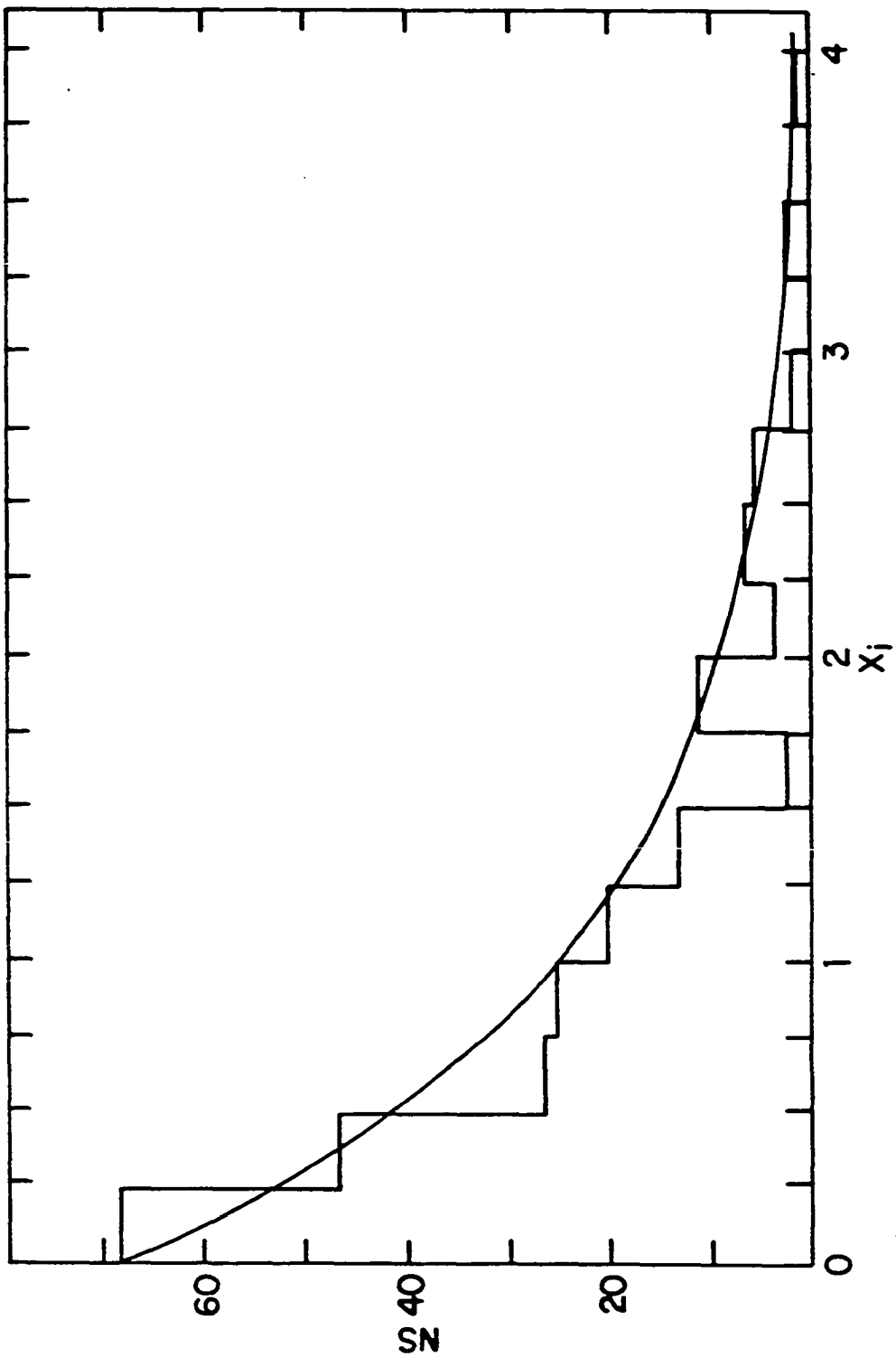
60
40
20
SN
0
1
2
3
4
X_i

Figure 4. Histogram of the number of spacings, NS, versus the relative spacing x_i for cyanocobalamin (16) superimposed with the Poisson distribution

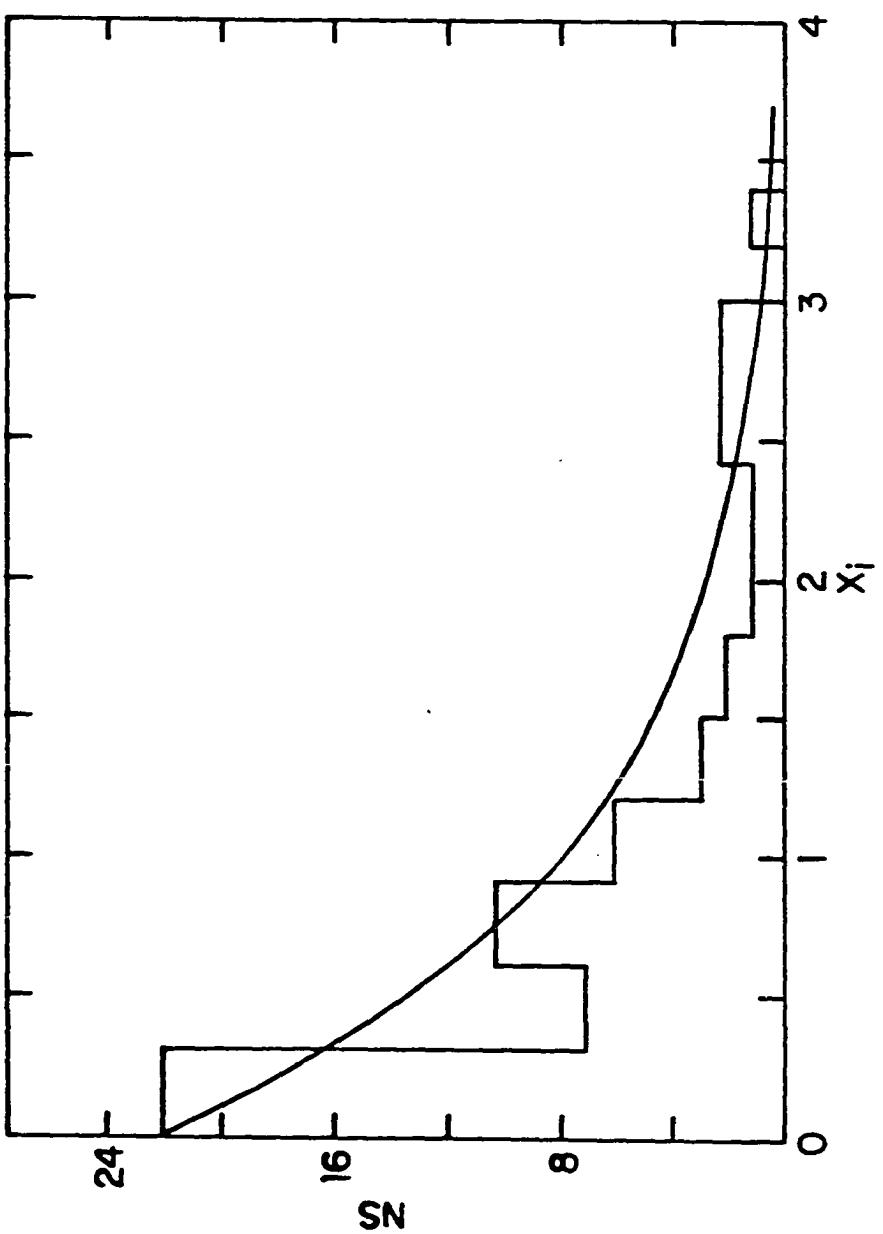
24
16
8
SN
0
1
2
3
4
Xi

Figure 5. Histograms of the number of spacings, NS, versus the relative spacing x_i for alamethicin (17), (A) assuming a single average spacing D, (B) assuming two average spacings D_1 and D_2 (both A and B are superimposed with the distribution function given by Equation 4), (C) separation of α-helix from β-pleated sheet data as explained in the text, superimposed with the Wigner function. In all cases one level is found at $x_i = 7$ (not shown)

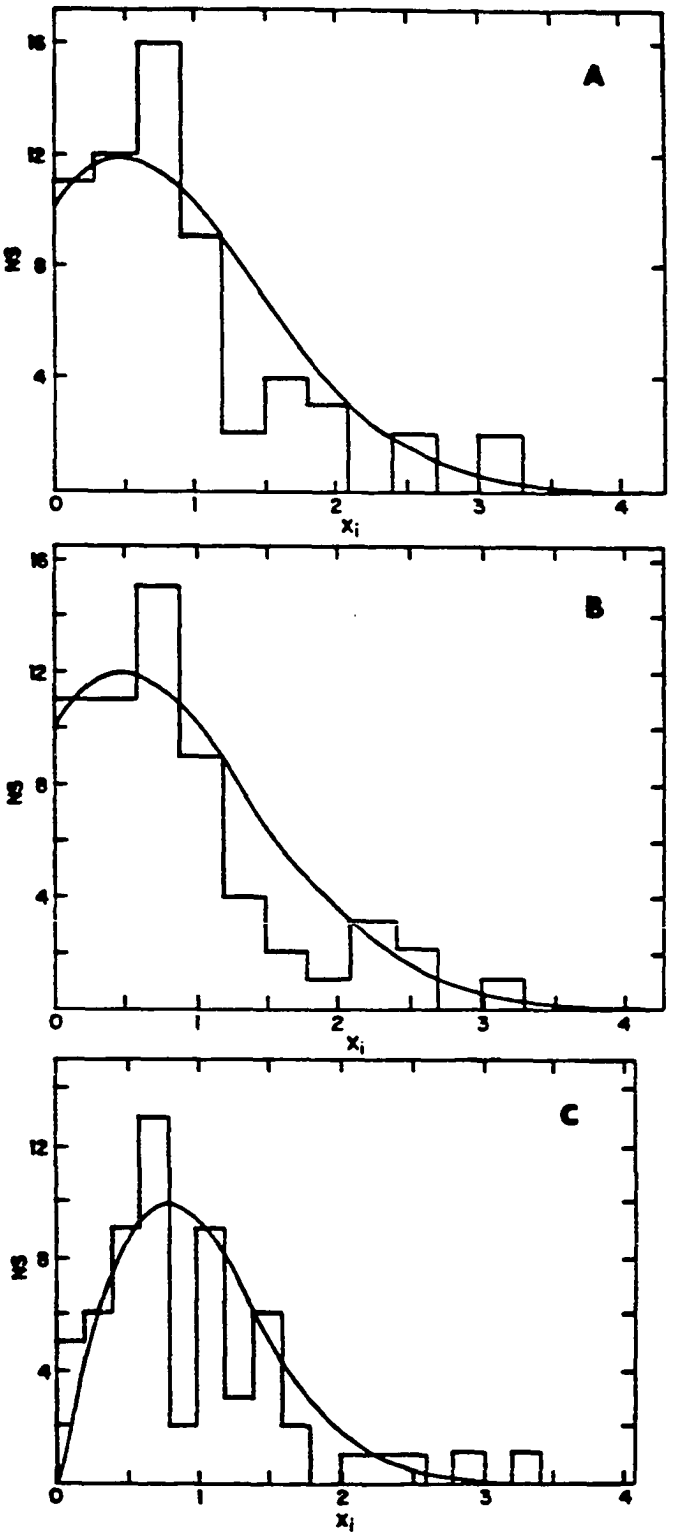
A
B
C
16
12
8
4
0
1
2
3
4
x_i

bond network extending over long range in proteins (19), are dependent on structural or functional correlations (20) of several groups of atoms or amino acids with time- independent and dependent properties. Correlations of this type of many-body collective modes can be conveniently "detected" with the analysis presented here.

Irreversibility in biological systems is ubiquitious. The state of equilibrium is an idealization that is never realized. Rather, stationary or steady states pervade a host of processes that lead to the presence of coherent and dissipative structures. These structures are the building blocks of the biological architecture; biological engineering and design is related to the evolution of these structures. Coherent and dissipative structures and their stability properties play an important role in modern theories of systems that are far from equilibrium (21). The correlated character of these structures and processes can be monitored by RMT analysis of an ensemble of energy levels obtained by NMR.

Acknowledgments

The support and encouragement from Professor B. C. Gerstein, discussions about random matrix theory with Dr. T. T. P. Cheung, and the help of Dr. L. A. Saucke and S. A. Standley in the preparation of the manuscript are gratefully acknowledged. In the preliminary stages of this work, the author was supported by a Postgraduate Scholarship 1979-82 from the Natural Sciences and Engineering Research Council of Canada.

References Cited

1. Porter, C. E. editor, Statistical Theories of Spectra: Fluctuations (Academic Press, New York, 1965).
2. Mehta, M. L., Random Matrices and the Statistical Theory of Energy Levels (Academic Press, New York, 1967).
3. Carmeli, M., Statistical Theory and Random Matrices (Marcel Dekker, New York, 1983).
4. Schaefer, J. and R. Yaris, J. Chem. Phys. 51, 4469, (1969).
5. Haller, E., H. Koppel and L. S. Cederbaum, Chem. Phys. Lett. 101, 215, (1983).
6. Larson, H. J., Introduction to Probability Theory and Statistical Inference. Second ed. (John Wiley and Sons, New York, 1974).
7. Wigner, E. P., Oak Ridge Natl. Lab. Rep. ORNL-2309, 59, (1957).
8. Lane, A. M., Oak Ridge Natl. Lab. Rep. ORNL-2309, 113, (1957).
9. Harvey, J. A. and D. J. Hughes, Phys. Rev. 109, 471, (1957).
10. Porter, C. E. and N. Rosenzweig, Ann. Acad. Sci. Fenn. Ser. A VI 44, 1, (1960).
11. Brody, T. A., J. Flores, J. B. French, P. A. Miller, A. Pandey and S. S. M. Wong, Rev. Mod. Phys. 53, 385, (1981).
12. Abragam, A., The Principles of Nuclear Magnetism (Clarendon Press, Oxford, 1961) p. 170-199.
13. Bax, A., Two-dimensional Nuclear Magnetic Resonance in Liquids (Delft University Press, Boston, 1982), p. 50-98.
14. King, R. and O. Jardetzky, Chem. Phys. Lett. 55, 15, (1978).
15. Keller, R. M., R. Bauman, E. Hunziker-Kurk, F. J. Joubert and K.

Wuthrich, J. Mol. Biol. 163, 623, (1983).

16. Anton, D. L., H. P. C. Hagenkamp, T. E. Walker and N. Maturyoff, Biochemistry 21, 2372, (1982).

17. Banerjee, U., F. P. Tsui, T. N. Balasubramanicon, G. R. Marshall and S. I. Chan, J. Mol. Biol. 165, 757, (1983).

18. Frolich, H., Int. J. Quant. Chem. 2, 641, (1968).

19. Metzler, D. E., Adv. Enzymol. 50, 1, (1979).

20. Wagner, G., A. Pardi and K. Wuthrich, J. Am. Chem. Soc. 105, 5948, (1983).

21. Prigogine, I., From Being to Becoming (Freeman, San Francisco, 1980).

SCALING IN BIOLOGICAL NMR SPECTRAL DISTRIBUTIONS

Serge Lacelle

Ames Laboratory, DOE* and Department of Chemistry
Iowa State University, Ames, Iowa 50011

*Operated for the U. S. Department of Energy by Iowa State University under contract No. W-7405-Eng-82. This research was supported by the Office of Basic Energy Sciences, Chemical Sciences Division.

SECTION IV. SCALING IN BIOLOGICAL NMR SPECTRAL DISTRIBUTIONS

Abstract

A statistical analysis of the distribution of the eigenvalues of the chemical shift interaction as detected by nuclear magnetic resonance (NMR) in large biological systems is presented. The randomness in a sequence of eigenvalues of this interaction in a molecule is discussed in light of random matrix theory, algorithmic complexity theory and fractal geometry. A power law dependence is experimentally observed for the distribution of the number of eigenvalues, N, of the shielding hamiltonian with energy $_i \leq$ E as a function of the energy E. From this distribution, we also obtain a density of states, p(E). This statistical spectroscopic approach served to characterize the chemical shift of segments of biopolymers. These molecular segments are found on a scale intermediate to those defined by local and global molecular structures. The distribution of the log N as a function of the log E is contrasted to that of vibrational states on a percolation cluster. We examine data available from the current literature for two proteins, an antibiotic and a vitamin.

Introduction

In many-body systems, a description of interactions on a microscopic level can be difficult to attain because of the large number of particles involved. The microscopic approach is replaced by

statistical methods to describe the collective behavior of a representative ensemble of systems in statistical mechanics, and by a phenomenological approach in thermodynamics. In the event of discrete energy levels in a many-body system, assignment of quantum numbers to individual levels, based on various models, becomes prohibitive as the number of particles increases. In random matrix theory (1), it is assumed that the local statistical behavior of the energy levels of a large and complicated system with an unknown or unmanageable hamiltonian is represented by that of the eigenvalues of a random matrix. This method permits a qualitative description of the general appearance and the degree of irregularity of the level structure observed experimentally in a spectrum. Statistical properties such as spacings of characteristic values of the magnetic shielding hamiltonian can be studied successfully with NMR spectroscopy (2,3). The extension of this approach to the density of eigenvalues of this interaction in large biological systems is the subject of this paper.

Nearest-neighbor spacing distribution functions representing uncorrelated, correlated, and random superposition of correlated energy levels have been observed for the chemical shift interactions in the spectra of a vitamin, an antibiotic and a protein (3). Such functions represent global properties of energy level ensembles which serve to characterize these systems, in contrast to the usual interpretations of magnetic shielding which describe these systems on microscopic and individual levels. Similarly, the statistical analysis of eigenvalue densities permits "fingerprinting" of molecular

subunits. This analysis will serve to distinguish systems with similar energy spacing distribution functions.

We report on the characterization of the energy level density (or density of stationary states per unit energy interval), for an ensemble of discrete energy levels arising from the chemical shift interaction in large biological systems. The visual complexity of an NMR chemical shift stick spectrum of a protein is displayed in Figure 1, constructed from the data of Keller et al. (4). The purpose of our method is to extract from such a spectrum qualitative information which physically characterizes the system. With the advent of technological and technical advances, it becomes possible to separate and study the different interactions contributing to an NMR spectrum. In this respect, we note that state of the art two-dimensional NMR techniques applied to proteins with known primary structures permits the assignment of up to 250 resonance lines for ^{1}H chemical shift in small proteins (M. W. ~6000) (4). Clearly, these upper limits should increase with progress. The questions then become, how can we handle this huge data base, what does it tell us about these systems, and how can we compare data from one protein to another? Our answer to these questions has been to analyze the collection of chemical shifts from a molecule rather than to treat individual shift of different atoms.

Collective behavior has been observed in polymer chains with ^{1}H NMR. In this case (5), lower temperatures narrowed the ^{1}H dipolar coupling correlation function due to motions, and led to frequency shifts on the order of 2 ppm. The effect of picosecond time scale

structural fluctuations on the ring current contribution in ^{1}H chemical shift has been numerically investigated in a protein (6). Correlations were observed between a time average shift and the shifts calculated from the average structure. The interplay of local and global structural connectivities in small molecules has been demonstrated by graph theoretical methods in the analysis of ^{1}H and ^{13}C chemical shifts (7-9). In favorable cases, the analysis of chemical shifts and spin-spin coupling constants can be simplified if the energy levels are classified according to molecular symmetry properties with group theory (10-11). The above studies all emphasized some global molecular features in the analysis of chemical shifts. In a sense, in the present paper, we try to bridge the local and global properties of chemical shift by demonstrating its scaling behavior between these limits. Such an approach has been successful in many cases: in the analysis of conformational coordinates and properties of proteins on intermediate length scales (12), in understanding long-range characteristics of polymers (13) and critical collective phenomena (14), in unravelling semiclassical energy level structure of bound hamiltonian systems (15), and more generally in the discussion of a variety of natural phenomena (16).

In the Theoretical Background and Method section, we examine some theories of the chemical shift interaction and discuss the importance of density of states. We briefly elaborate on the concept of randomness in a sequence of eigenvalues, and present scaling in the light of fractal geometry. We point out how these themes can be

Figure 1. ^{1}H NMR chemical shift stick spectrum of BTI, constructed from the data of two-dimensional NMR experiments (4). Energy in ppm increases from left (high field) to right (low field)

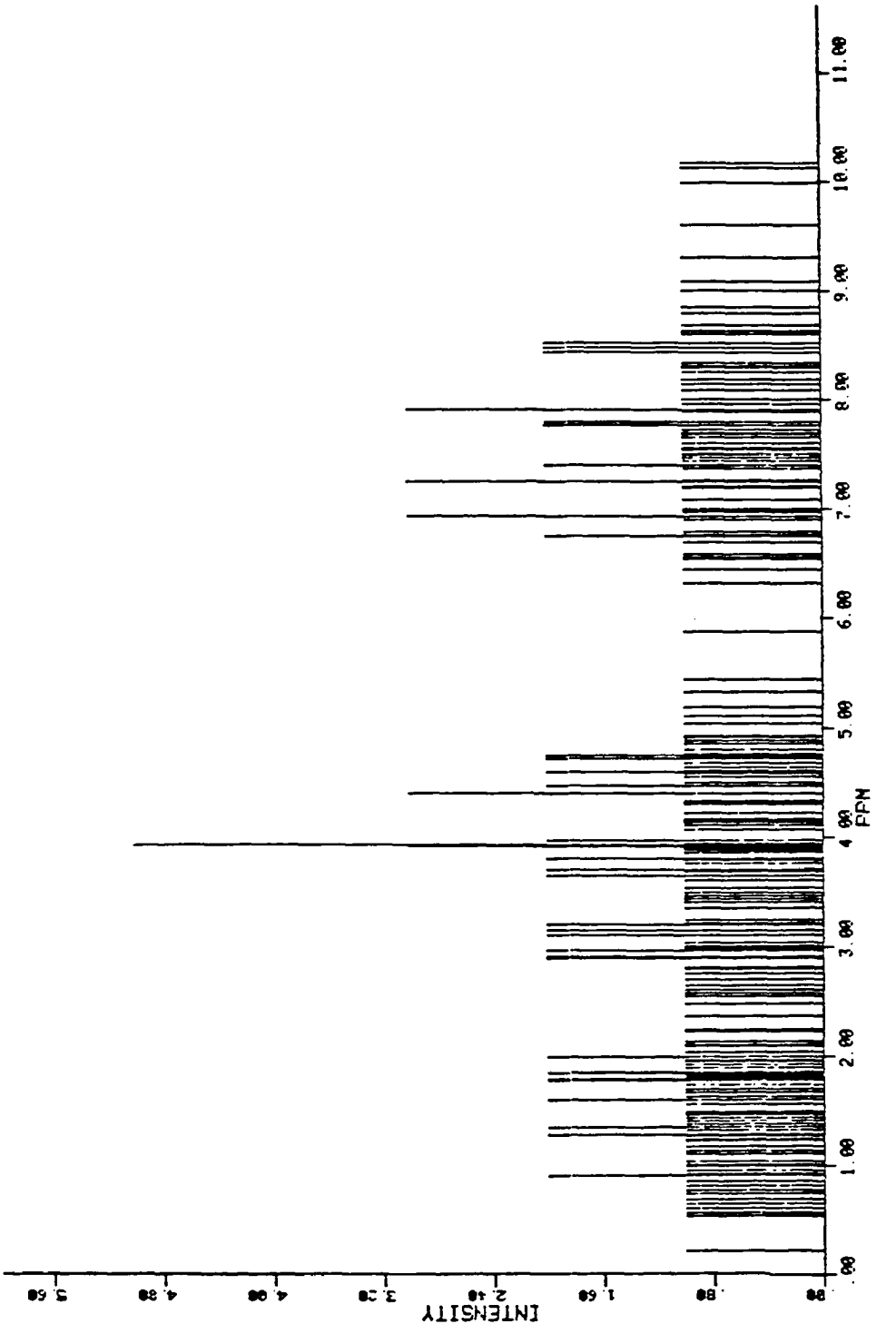
11.00
10.00
9.00
8.00
7.00
6.00
5.00
4.00
3.00
2.00
1.00
.00
PPM
.00
.88
1.68
2.48
3.28
4.08
4.88
5.68
INTENSITY

incorporated in the analysis of discrete NMR chemical shift of large biological systems. This method is then applied to data from current literature in the Results and Discussion. Limitations and a possible extension are presented in the Conclusions and Summary.

Theoretical Background and Method

The nuclear spin hamiltonian of a protein solution in a magnetic field is given by equation 1,

$$H = H_Z + H_{CS} + H_J + H(t) \qquad (1)$$

where H_Z is the Zeeman interaction of magnetic moments with the magnetic field, H_{CS} represents the chemical shift interaction due to induced motions of electrons in the field, H_J is the indirect spin-spin coupling (J or scalar coupling), and H(t) comprises time dependent phenomena such as dipolar relaxation, chemical exchange and radio frequency pulses. In the presence of a strong field, the eigenstates of H_Z are perturbed to 1st and 2nd order by the other interactions present in equation 1. Modern two-dimensional NMR experiments strive to separate these different interactions by "selecting and manipulating" the hamiltonians under which the evolution and detection of the spin system occur. In this spirit, we now only consider H_Z and H_{CS}. It is possible to transform this hamiltonian to an interaction representation known as the rotating frame, where the hamiltonian is time independent. In the present case, this is equivalent to considering only H_{CS}, and to reporting chemical shifts relative to a standard which has a spin precession

frequency equal to that of the rotating frame. The hamiltonian then becomes,

$$H_{CS}^{r} = \sum_{i \text{ sites}} \gamma^{i} \vec{I}^{i} \cdot \overleftrightarrow{\sigma}^{i} \cdot \vec{B} \qquad (2)$$

where the superscript r reminds us that we are in the rotating frame; the sum includes all sites in the molecules, γ is the magnetogyric ratio, $\vec{B}$ is the magnetic field, and $\overleftrightarrow{\sigma}$ is a 2nd rank cartesian tensor representing the chemical shift of site i. In a solution spectrum, we may approximate by considering only the scalar part of the shift tensor, which yields equation 3,

$$H_{CS}^{r} = \sum_{i \text{ sites}} \gamma^{i} I^{i} \cdot \sigma_{iso}{}^{i} \cdot B \qquad (3)$$

where

$$\sigma_{iso}{}^{i} = \frac{1}{3} [\sigma_{11}{}^{i} + \sigma_{22}{}^{i} + \sigma_{33}{}^{i}] = \frac{1}{3} \text{Tr} \overleftrightarrow{\sigma} \qquad (4)$$

The last equation related the magnetic shielding, σ_{iso}, observed in the laboratory (or rotating) frame to that of the components σ_{jj} of the shielding tensor in its principal axis system. Magnetic shielding of nuclei in molecules has been treated by Ramsey (17-20) and leads to a microscopic interpretation of the σ_{kl} in equation 4. Classically speaking, the physical origin of this interaction in a system with no macroscopic electron orbital or spin angular momentum is due to a field produced at the nuclei by the induced motions of electrons in a

magnetic field (17-20). In this treatment, the shielding tensor consists of two parts: a diamagnetic and a paramagnetic part (21-24).

$$\sigma_{\alpha\beta} = \sigma^{d}_{\alpha\beta} + \sigma^{p}_{\sigma\beta} \tag{5}$$

where

$$\sigma^{d}_{\alpha\beta} = \frac{e^2}{2\,mc^2} \langle o| \sum_i \frac{r_i^2\,\delta_{\alpha\beta} - r_{i\alpha}\,r_{i\beta}}{r_i^3} |o\rangle \tag{6}$$

$$\sigma^{p}_{\alpha\beta} = \frac{e^2}{2\,mc^2} \sum_k (E_o - E_k)^{-1} \left[\langle o| \sum_i L_{i\alpha} |k\rangle\langle k| \sum_i \frac{L_{i\alpha}}{r_i^3} |o\rangle + \right.$$

$$\left. \langle o| \sum_i L_{i\beta} |k\rangle\langle k| \sum_i \frac{L_{i\beta}}{r_i^3} |o\rangle \right] \tag{7}$$

The distance from the nucleus of interest to the i^{th} electron is r_i. The α component of the orbital angular momentum operator of electron i about the same nucleus is $L_{i\alpha}$. E_k is the electronic (and vibrational) energy of the state $|k\rangle$ with $|o\rangle$ representing the ground state. The charge and mass of an electron are e and m respectively, while c is the speed of light. Unfortunately, when this theory is applied to molecular systems, σ^d and σ^p both have large contributions, but of opposite sign; this leads to high uncertainty in the resulting σ. For example, ab initio calculations of σ for C ^{17}O and H_2 ^{17}O have an accuracy of about 10-50% (25) with respect to experimental values. This discrepancy can be accounted for by the neglect of relativistic

effects and proper electron correlation energies, and by the lack of knowledge of excited states $|k\rangle$. Numerous approximation schemes (22-24) have been devised to remedy these calculations in order to account for the effects of neighbor anisotropy, ring currents, electric fields and solvents. For complex systems such as proteins, the Ramsey approach leads to severe computational problems.

An appealing treatment of the chemical shift, more in line with that of chemical intuition, has been proposed by Saika and Slichter (26). This treatment provides a diamagnetic correction for the atom (or site) in question, a paramagnetic term for the same atom, and finally a contribution from the electrons of all other atoms. The first two categories find extensive use in emperical NMR structural analysis. Further approximation treatments have been developed to account for the contributions of other atoms (27-28); these form the basis of numerical calculations presented by Hoch et al. (6). From the nature of the physical problem, it is obvious that the chemical shift which results from a many-body interaction cannot presently be "solved" explicitly for cases of interest in biological NMR. For example, in the next section, we analyze the ^{13}C spectrum of vitamin B_{12} with 728 electrons per molecule, and some small inhibitor proteins with almost a thousand atoms. Clearly, one must resort to a qualitative understanding, such as relative spacing distribution functions (3), and density of eigenvalues per unit energy.

The density of states $\rho(E)$ is defined by equation 8, which gives the number of states (or transitions) N, with energy between E and δE.

The notation δE is to represent an infinitesimal

$$N = \rho(E)\,\delta E \tag{8}$$

in the limit of $E \to o$, while emphasizing its finite difference character otherwise. In statistical mechanics, the Laplace transform of $\rho(E)$ with respect to E yields the partition function (29), while the log $\rho(E)\delta E$ is proportional to the entropy of the system (30). Table 1 lists an interesting and important property, the density of characteristic values of hamiltonians for several physical models. The energy (or frequency) dependence is followed by an appropriate dimension. Assuming the following conditions,

$$\rho(E) \alpha E^{S} \tag{9}$$

$$\delta E \alpha E \tag{10}$$

then, $N \alpha E^{S+1}$, so that by plotting the log N versus the log E, one obtains the slope S + 1. A classification of levels with a particular slope or density of states brings about a reduction of the molecules' chemical shift data base. These categories depend on the property of scaling in the sequence of eigenvalues.

The analysis of the distribution of chemical shifts in large biological systems bears strong resemblance to the problem of randomness in other disciplines. Accordingly, we can benefit by briefly examining some general methods that are available for the discussion of randomness in a sequence of energy eigenvalues. These are random matrix theory (1), algorithmic complexity theory (31-32),

and the study of random geometric shapes known as fractals (16).

Table 1. Energy (or frequency) dependence for several models of density of states

Model	s, energy dependence: E^s	Euclidean dimension	Reference
Free particle subject to periodic or boundary conditions, e.g., electron gas in a metal,	-1/2	1	50
particle in a box	1/2	3	51
Photon modes for each polarization in an electromagnetic field	2	3	51
Elastic vibrations and deformations	d-1	d	52, 53
Wigner Semi-Circle Law density of eigenvalues per unit energy of a matrix N x N in a Gaussian ensemble in the limit N -> ∞	1/2, $(C-E^2)^S$	configuration space, N	1, 33
Energy levels of real nuclei	1/2 exp b E^S		33

In random matrix theory (1), one obtains, in principle, the eigenvalues λ of a matrix M (N x N) by solving the determinantal equation 11

$$c(\lambda) = \det (M - I\lambda) \tag{11}$$

For hamiltonians of physical interest, this is equivalent to solving for the real roots of an algebraic equation in λ of degree N. Wigner's semi-circle law (1,33) gives a closed form expression for the density of eigenvalues per unit energy (see Table 1). Dyson (33-34) has proposed a Coulomb gas model of point charges undergoing Brownian motion on an infinite line to account for the local and global distributions of eigenvalues of large matrices. Common distribution functions for the spacing between eigenvalues are the Poisson (uncorrelated case) and the Wigner (correlated case) distributions.

Algorithmic complexity theory deals with the properties of a random sequence of numbers in the context of information theory. The property of complexity is interpreted in terms of the length of a program necessary to generate a sequence of numbers. Maximum complexity is the irreducible case where the length of the program is the same as that of the sequence. In the event of regularity or periodicity in a string of numbers, there will be a reduction of the program and of the information content. Randomness thereby acquires an operational approach. This method has been used (35-37) in order to distinguish between regular and chaotic behavior of motions for the classical limit of quantum systems.

In his provocative book, Mandelbrot (16) has proposed a new and refreshing outlook of irregularity in nature. By examining nature on different scales, he imparts to the reader an awareness of hierarchies of complexity. A random geometrical shape, pattern or continuum is characterized by an effective dimension, the fractal dimension $\bar{d}$,

which reflects non-topological aspects of form (38). Distributions of random shapes, functions, and variables which remain invariant under a change of scale (dilation symmetry) are said to be scaling. Without necessarily involving geometry, scaling can be observed in the distribution of emperical data involving power laws when presented on doubly logarithmic plots (39-44). In geometry, constructions of points on a straight line lead to fractals with $o<\bar{d}<1$, which Mandelbrot calls "Cantor fractal dusts" (45). Since natural objects have finite extension, these shapes are "almost fractals or fractal-like" when they possess scaling properties (46).

Therefore, the distribution of chemical shifts in large biological systems can be modelled by the eigenvalues of random matrices, by a random sequence of numbers, or by a set of points randomly distributed on a line. The use of doubly logarithmic plots will help to demonstrate a degree of regularity in a seemingly irregular spectrum.

Results and Discussion

We examine experimental NMR chemical shift data available from current literature. The investigated systems comprise two small proteins, Bovine Trypsin Inhibitor, BTI (4), Bull Seminal Inhibitor, BSI (47), a vitamin, Cyanocobalamine - B_{12} (48), and an antibiotic Alamethicin (49). For these molecules, with the exception of BSI, the primary, secondary and tertiary structures are well characterized. We attempt to interpret the slopes obtained from the doubly logarithmic plots, log N versus log E, in terms of the tertiary structures.

These plots are presented in Figure 2 for BTI, in Figure 3 for BSI, in Figure 4 for B_{12}, and in Figure 5 for Alamethicin. For each molecule, instead of fitting all the available chemical shift data, a "coarse-grained" distribution of N versus E was used so that the analysis could be easily carried out on a pocket calculator. The number of slopes per plot was kept to a minimum by visually examining the fit and by determining the standard deviation of the slope. We must also keep in mind that we are interested in the scaling of the chemical shift over a distribution which should reflect an intermediate scale rather than a local or global scale property of the sequence of levels. Table II summarizes the slopes and standard deviations calculated from a linear least squares fit, the number of levels or transitions contributing to a particular slope, and the exponent, s, characterizing the density of states dependence on the energy. Most of the standard deviations represent an error of 4 to 11%. When the number of levels is small (~10), we find error limits of 25%.

For both proteins, we may group the distribution of levels according to their energy dependence into two categories. In the case of B_{12} and Alamethicin, three groups of levels are necessary to account for the distribution. All systems display roughly an E^2 dependence at low energies (or high field), except B_{12} which has an $E^{1.1}$ dependence. At higher energies (or low field), we find a crossover to $E^{.9}$ for BTI and BSI, while the distributions for B_{12} and Alamethicin cross over twice to different power laws. The density of

Figure 2. Distribution of the log N versus log E for ^{1}H NMR chemical shift of BTI (4). N represents the number of energy levels (or transitions) with energy $\leq$ E

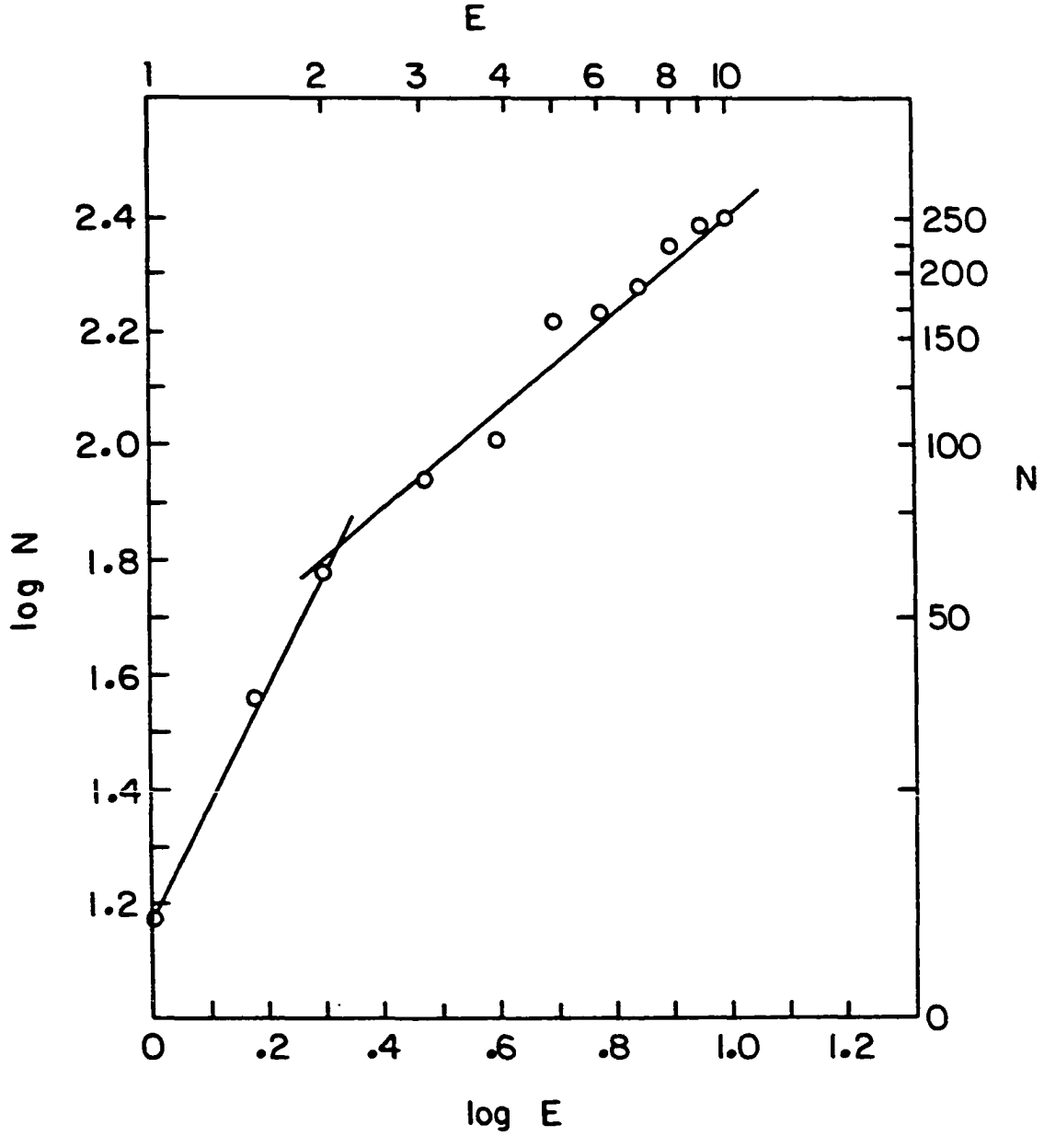
E
1
2
3
4
6
8
10
2.4
2.2
2.0
1.8
1.6
1.4
1.2
log N
250
200
150
100
50
0
N
0
.2
.4
.6
.8
1.0
1.2
log E

Figure 3. Distribution of the log N versus log E for ^{1}H NMR chemical shifts of BSI (47)

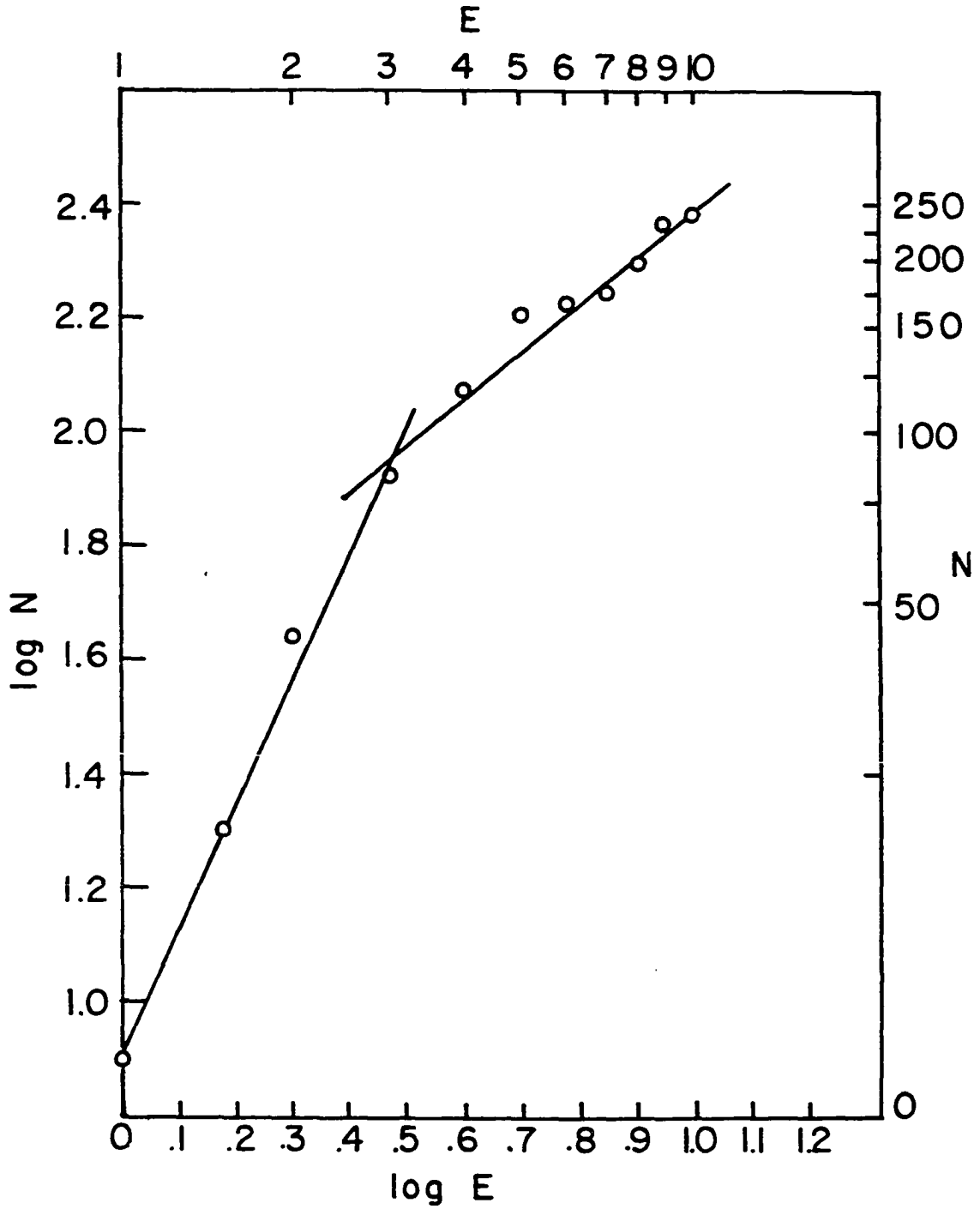
E
1
2
3
4
5
6
7
8
9
10
2.4
2.2
2.0
1.8
1.6
1.4
1.2
1.0
log N
250
200
150
100
50
0
N
0
.1
.2
.3
.4
.5
.6
.7
.8
.9
1.0
1.1
1.2
log E

Figure 4. Distribution of the log N versus log E for ^{13}C NMR chemical shifts of B_{12} (48)

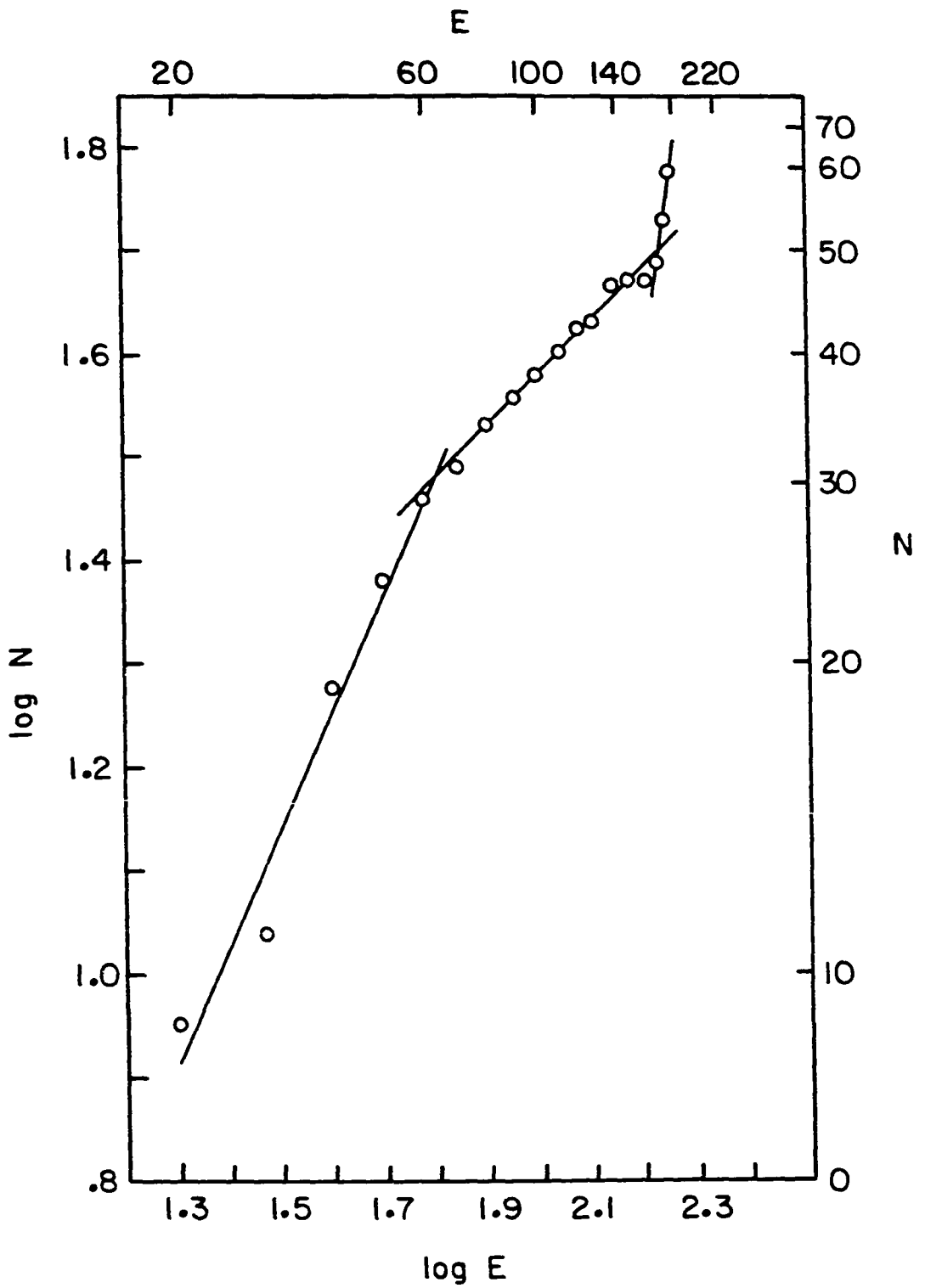
E
20
60
100
140
220
1.8
1.6
1.4
1.2
1.0
.8
log N
70
60
50
40
30
20
10
0
N
1.3
1.5
1.7
1.9
2.1
2.3
log E

Figure 5. Distribution of the log N versus log E for ^{1}H NMR chemical shifts of Alamethicin (49)

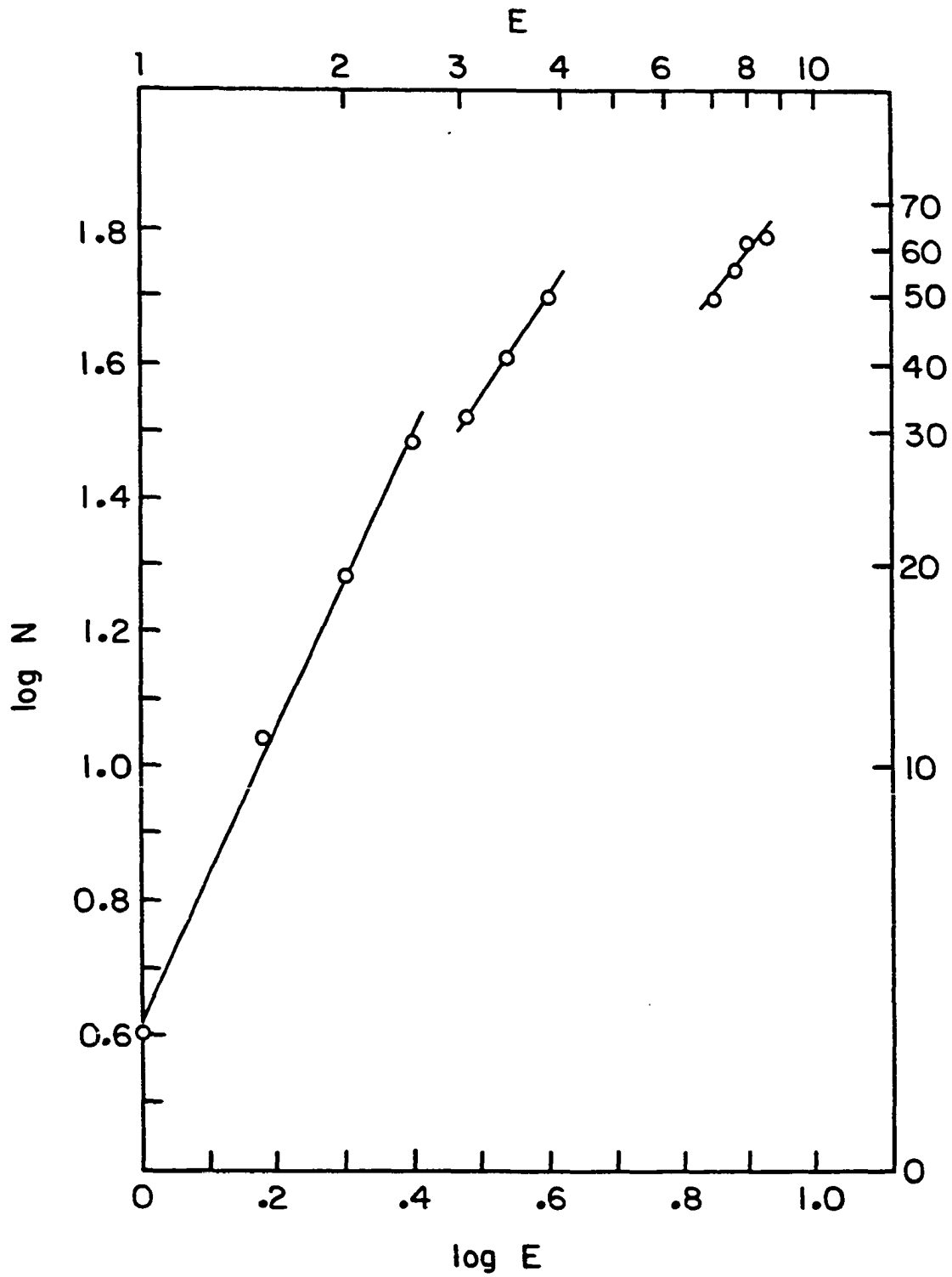
E
1
2
3
4
6
8
10
70
60
50
40
30
20
10
0
1.8
1.6
1.4
1.2
1.0
0.8
0.6
log N
0
.2
.4
.6
.8
1.0
log E

Table 2. Data obtained from doubly logarithmic plots

System	Slope* S+1	Corr†	S‡	Levels	Number of levels
Cyano-cobalamine B12	1.1 ± .1	.979	.10	0-29	29
	.51 ± .02	.996	-.49	29-49	20
	3.4 ± .9	.982	2.4	49-60	11
Alamethicin	2.2 ± .1	.998	1.2	0-30	30
	1.5 ± .0	1.00	.5	30-50	20
	1.2 ± .3	.960	.2	50-62	12
Bovine trypsin inhibitor BTI	2.0 ± .2	.990	1.0	0-60	60
	.90 ± .05	.918	-.10	60-251	191
Bull seminal inhibitor BSI at 18°C	2.2 ± .2	.995	1.2	0-84	84
	.83 ± .10	.977	-.17	84-239	155
Bull seminal inhibitor BSI at 45°C	2.1 ± .2	.993	1.1	0-79	79
	.84 ± .09	.978	-.16	79-239	160

*Error limit on slope is one standard deviation.

†Correlation coefficient from linear least-squares fit.

‡Error limit on s is the same as that of the slope.

states' energy dependence is obtained by subtracting one from the value of the slope of the doubly logarithmic plot (see equations 9, 10 and Table 2).

Crossover is a general feature observed for phonon dispersion in the percolation network model (53-54). For these extended states, at

lower energies, one finds a normal or classical behavior for N(E) and (E) with d being the Euclidean dimension of the system (see Table 1). At higher energies, a crossover occurs to a fractal dimension $\bar{d}$ which characterizes the system. The shape of some hemoproteins at liquid helium temperatures has been shown (55) with ESR relaxation measurements which are proportional to the density of vibrational states, to occupy a space of fractal dimensionality $\bar{d} = 1.65$. Low frequency (40-125 cm^{-1} extended torsional states (librons) with lifetimes of nanoseconds have been observed in crystals of L-alanine (56). Numerical simulations (57) on BTI, using classical dynamics with an harmonic oscillator-type potential predict the occurrence of 350 collective modes in the frequency range 3-200 cm^{-1}. Room temperature corresponds to 210 cm^{-1}. The existence of vibrationally (58) and rotationally (59) excited solitons has been postulated to explain action at a distance through secondary and tertiary structures in proteins. Experimental evidence is lacking for any conformational changes involving extended states and breathing modes as possible mechanisms for internal motions in proteins.

On the time scale of the experimental detection of chemical shifts in proteins, electronic, vibrational and rotational motions are averaged (i.e., fast motional narrowing regime). As seen from equation 7, the paramagnetic part of the chemical shift is proportional to E^{-1}, where E represents electronic and vibrational energy (60). For a particular site, if we average this energy dependence over a density of extended states, we obtain

$$\sigma \sim \int E^{-1} E^{d-1} dE \sim E^{d-1} \qquad (12)$$

Averaging of σ over an energy distribution, in particular the canonical distribution, permits the rationalization of the temperature dependence of σ (20). In the case of chemical equilibrium, chemical exchange effects average σ in a fashion that depend on the rate constant of the process (61).

In light of the percolation cluster model, we examine the structural distribution of atoms according to groups which have the same energy dependence in the doubly logarithmic plots. At low energy, BTI, BSI and Alamethicin all follow roughly E^2, while the distribution of those particular atoms is over the whole molecule, i.e., d = 3. In the case of B_{12}, the initial distribution of ^{13}C shifts follows $E^{1.1}$, of the 30 atoms which contribute to this initial distribution, 26 can be found in the plane defined by the corrin ring, which implied d = 2. The chemical shift average over the extended states of the percolation cluster model predicts an E^{d-1} dependence, with E related to the electronic and vibrational states, and d being the Euclidean geometry. It is an interesting observation that a similar behavior is found for the distribution of chemical shifts at low frequency. At higher energies, the distribution of the chemical shifts crosses over to some fractional power of E for BSI and BTI, while two such crossovers are observed for B_{12} and Alamethicin. Again we note the striking similarity to the predictions of the percolation cluster model.

At this point, we caution the reader that we have not proposed a microscopic interpretation of the scaling of chemical shift, nor have we rationalized the scaling in terms of the percolation cluster model. Indeed, our observations bear a striking resemblance to the predictions of this model, but it is evident that further investigations are needed to elucidate this scaling. The slopes of the doubly logarithmic plots are proportional to the log N/log E and not to log (N/E).

Conclusions and Summary

The distribution of chemical shifts in large biological systems has been shown to follow a power law relationship in the relative energies. For the investigated systems, we observed for the distribution of the log N versus log E a behavior quite analogous to the predictions of a model for vibrational states on a percolation cluster. Indeed, the distribution of chemical shifts at low energies seemed to reflect the dimension of the structure in which the atoms were embedded. Crossover to different power law behavior, with fractional energy exponent is reminiscent of fractal dimension. To understand these empirical observations, further studies are needed.

Our analysis of a collection of chemical shifts in large biological systems is presently limited to spectra with discrete resonances. As two-dimensional NMR techniques evolve, the possibility to unravel the spectra of larger molecules will make the approach presented here and elsewhere (3) more attractive and statistically more reliable. The coarse grained distribution of N versus E smoothed

the data. This kept the analysis simple enough that calculations could be done on a pocket calculator. Instead of smoothing the data, a staircase distribution involving all the available data could be used with appropriate computational facilities.

Extended, coherent and correlated states involving secondary structures, segments or domains of proteins have been suggested in the past, as possible important mechanisms for biological functions. The experimental demonstrations of local to global conformational changes is a difficult task. By considering an ensemble of chemical shifts of a molecule, we have found a degree of regularity in the sequence of those shifts, which suggests that the level sequence might not be as random as one would at first expect. A similar reduction of the chemical shift data base was obtained when an ensemble of spacings was examined. In adopting the approach of examining the levels of an entire molecule rather than individual levels of different atoms, we hope to be able to detect many-body correlated interactions alluded to above. The observed correlations between the initial slopes of the doubly logarithmic plots and the dimension of the systems in which the atoms are imbedded is a first step in that direction.

Acknowledgments

The support and encouragement of Professor B. C. Gerstein, and the help of C. G. Fry are gratefully acknowledged.

References Cited

1. Wigner, E. P., S. I. A. M. Review 9, 1, (1967).

2. Schaeffer, J. and R. Yaris, J. Chem. Phys. 51, 4469, (1969).

3. Lacelle, S., Biophys. J. 46, 181, (1984).

4. Keller, R. M., R. Bauman, E. H. Hunziker-Kurk, F. J. Joubert and K. Wuthrich, J. Mol. Biol. 163, 623, (1983).

5. Lenk, R., Chem. Phys. Lett. 28, 398, (1974).

6. Hoch, J. C., C. M. Dobson and M. Karplus, Biochemistry 21, 1118, (1982).

7. Randic, M., J. Magn. Res. 59, 34, (1984).

8. Mekenyan, O., D. Bonchev and A. T. Balaban, Chem. Phys. Lett. 109, 85, (1984).

9. Randic, M. J. and B. C. Gerstein, J. Magn. Res. 43, 207, (1981).

10. McConnell, H. M., A. D. McLean and C. A. Reilly, J. Chem. Phys. 23, 1152, (1955).

11. Jones, R. G., NMR-Basic Principles and Progress, P. Diehl, E. Fluck, R. Kosfeld (eds.), (Springer Verlag, New York, 1969), Vol. 1, p. 97-174.

12. Rachovsky, S. and H. A. Scheraga, Acc. Chem. Res. 17, 209, (1984).

13. de Gennes, P. G., Scaling Concepts in Polymer Physics (Cornell University Press, Ithaca, 1979).

14. Wilson, K. G., Sci. Am. 241, 158, (1979).

15. Berry, M. V., The Wave-Particle Dualism, S. Diner, D. Fargue, G. Lochak, F. Selleri (eds.), (Reidel, Boston, 1984), p. 231-252.

16. Mandelbrot, B. B., The Fractal Geometry of Nature (Freeman, New York, 1983).

17. Ramsey, N. F., Phys. Rev. 78, 699, (1950).

18. Ramsey, N. F., Phys. Rev. 77, 567, (1950).

19. Ramsey, N. F., Phys. Rev. 83, 540, (1951).

20. Ramsey, N. F., Phys. Rev. 86, 243, (1952).

21. Mehring, M., Principles of High Resolution NMR in Solids, 2nd ed. (Springer-Verlag, Berlin, 1983), p. 233-259.

22. Memory, J. D., Quantum Theory of Magnetic Resonance Parameters (McGraw-Hill, New York, 1968), p. 79-128.

23. Ando, L. and G. A. Webb, Theory of NMR Parameters (Academic Press, New York, 1983), p. 47-82.

24. Harris, R. K., Nuclear Magnetic Resonance Spectroscopy (Pitman, Marshfield, MA, 1983), p. 183-228.

25. Wasylshen, R. E., S. Mooibrock and J. B. MacDonald, J. Chem. Phys. 81, 1057, (1984).

26. Saika, A. and C. P. Slichter, J. Chem. Phys. 22, 26, (1954).

27. McConell, H. M., J. Chem. Phys. 27, 226, (1957).

28. Pople, J. A., Proc. Roy. Soc. A239, 541, (1957).

29. Kubo, R., Statistical Mechanics (North Holland, New York, 1965), p. 102.

30. Kubo, R., Statistical Mechanics (North Holland, New York, 1965), p. 8-11.

31. Kolmogorov, A. N., IEEE Trans. Inf. Theory 14, 662, (1968).

32. Zvonkin, A. K. and L. A. Levin, Russian Math. Surveys 25, 83, (1970).

33. Dyson, F. J., J. Math. Phys. 13, 90, (1972).

34. Dyson, F. J., J. Math. Phys. 3, 1198, (1962).

35. Gasati, G., I. Guarneri and F. Valz-Gris, Phys. Rev. A30, 1586, (1984).

36. Peres, A., Phys. Rev. A30, 504, (1984).

37. Ford, J., Physics Today 35, 40, (1983).

38. Mandelbrot, B. G., in Self-Organization and Dissipative Structures, W. C. Shieve, P. M. Allen (eds.), (Univ. Texas Press, Austin, 1982), p. 91-109.

39. Mandelbrot, B. B., The Fractal Geometry of Nature (Freeman, New York, 1983), p. 341-348.

40. Montroll, E. W. and M. F. Shlesinger, PNAS 79, 3380, (1982).

41. Berger, J. M. and B. B. Mandelbrot, IBM J. of Res. and Dev. 7, 224, (1963).

42. Gerstein, G. L. and B. B. Mandelbrot, Biophys. J. 4, 41, (1964).

43. Mandelbrot, B. B., IEEE Trans. Inf. Theory 13, 289, (1967).

44. Tunaley, J. K. E., J. Appl. Phys. 43, 4777, (1972).

45. Mandelbrot, B. B., The Fractal Geometry of Nature (Freeman, New York, 1983), p. 74-83.

46. Mandelbrot, B. B., The Fractal Geometry of Nature (Freeman, New York, 1983), p. 326-333.

47. Strop, P., G. Wilder and K. Wuthrich, J. Mol. Biol. 166, 641, (1983).

48. Anton, D. L., H. P. C. Hagenkamp, T. E. Walker and N. Maturyoff, Biochemistry 21, 2372, (1982).

49. Banerjee, U., F. P. Tsui, T. N. Balasubramanicon, G. R. Marshall and S. I. Chan, J. Mol. Biol. 165, 757, (1983).

50. Morrison, M. A., T. L. Estle and N. F. Lane, Quantum States of Atoms, Molecules and Solids, (Prentice Hall, Englewood Cliffs, NJ, 1976), p. 443, 552.

51. Merzbacher, E., Quantum Mechanics, 2nd ed., (Wiley, New York, 1970), p. 193, 562.

52. Kittel, C., Introduction to Solid State Physics, 5th ed., (Wiley, New York, 1976), p. 131-136.

53. Rammal, R. and G. Toulouse, J. Physique Lettres, 44, 13, (1983).

54. Alexander, S. and R. Orbach, J. Physique Lettres, 43, 625, (1982).

55. Stapelton, H. J., J. P. Allen, C. P. Flynn, D. G. Stinson and S. R. Kurtz, Phys. Rev. Lett. 45, 1456, (1980).

56. Kosie, T. J., R. E. Cline and D. D. Dlott, Chem. Phys. Lett. 103, 109, (1983).

57. Brooks, T. and M. Karplus, PNAS 80, 6571, (1983).

58. Davydov, A. S., Biology and Quantum Mechanics (Pergamon, New York, 1982), p. 173-178, 185-212.

59. Jardetzky, O. and R. King, Ciba Found. Symp. 93, 291, (1982).

60. Abragan, A., The Principles of Nuclear Magnetism (Oxford Univ. Press, Oxford, 1961), p. 177.

61. Carrington, A. and A. D. McLachlan, Introduction to Magnetic Resonance, (Wiley, New York, 1979), p. 204-213.

CONCLUSIONS

The results of NMR experiments can be interpreted in either the time or frequency domain. NMR relaxation measurements are powerful tools for detection of molecular motions in powders of carbohydrates. The availability of the molecular crystal structures of cyclodextrins aided in the assignment of motions to specific molecular segments. As supported by the data, a distinction was made between the dynamics of protons on the inside or outside of the torus cavity of cyclodextrins. The outside protons had spectral density functions typical of solids, $\omega t >> 1$, while inside protons experience liquid-like motions $\omega t << 1$.

Since fewer details are known regarding the structure of dextran, the interpretation of relaxation measurements is more difficult. This demonstrates a limitation in the use of NMR relaxation measurements. Spectral density functions or correlation functions cannot be calculated from first principles; therefore a model must be selected. Another prerequisite to the analysis of relaxation data is a knowledge of the dominant relaxation mechanism obtained from the structure of the system. The interpretation of relaxation rates is therefore dependent upon a model. A similar situation is encountered in the interpretation of reaction rates of chemical mechanisms. Even if the data are in agreement with the predictions of the model, one cannot prove that the model corresponds to the real situation.

In our studies of carbohydrates, the differences in the ^{1}H relaxation parameters were within an order of magnitude. To complement these measurements, we suggest that ^{13}C relaxation

experiments and r.f. field dependence studies of $T_{1\rho}$ be conducted.

Recent advances in two-dimensional NMR spectroscopy allow the assignment of hundreds of resonances in proteins. In the frequency domain, chemical shift interactions and J couplings have provided fingerprints of molecules. The statistical methods that we applied to the collection of shifts from proteins helped to reduce or classify the information content of their spectra. Mainstream NMR spectroscopy has neglected such approaches in the past. As pointed out by Milan Randic, "these are interesting observations which deserve further attention" (14).

Analysis of distribution functions for the spacing between nearest-neighbor energy levels of chemical shifts provides a method to detect coherent states in biopolymers. These states depend upon spatial and temporal correlations of the structures and functions of these systems. The detection of such states has proven difficult at the level of molecular biology. The ^1H NMR chemical shift spacing distribution in Alamethicin was correlated with the secondary structures present in the molecule. We suggest that subsets of chemical shifts of proteins arising from secondary structures might also be treated in this manner. This is only a first step in use of NMR data to demonstrate correlation of structures in proteins.

The distribution of the number of eigenvalues of the chemical shift of proteins was analyzed on doubly logarithmic plots. It was possible to correlate the slopes of these plots with the dimensional character of the tertiary structures of the molecules. Again, with

larger systems it is suggested that subsets of the chemical shift data could be probed with this method. The crossovers observed in the doubly logarithmic plots deserve further attention. As two-dimensional NMR techniques evolve, and assignment of shifts in larger proteins becomes feasible, the methods proposed in Sections III and IV will certainly be useful in classifying the large data base generated experimentally.

We have shown that large biological systems can be studied in the time or frequency domain by NMR methods. The success of these methods in biophysical chemistry depends upon a clear understanding of the intimate association of theory and experiment.

ADDITIONAL LITERATURE CITED

1. Bloch, F., W. W. Hansen and M. E. Packard, Phys. Rev. 69, 127, (1946).

2. Purcell, E. M., H. C. Torrey and R. V. Pound, Phys. Rev. 69, 37, (1946).

3. Jardetzky, O. and G. C. K. Roberts, NMR in Molecular Biology (Academic Press, New York 1981), p. 3.

4. Jacobsen, B., W. A. Anderson and T. Arnold, Nature, London 173, 772 (1954).

5. Bax, A., Two-Dimensional NMR in Liquids (Reidel, Boston 1982).

6. Mansfield, P. and P. G. Morris, NMR Imaging in Biomedicine (Academic Press, New York 1982).

7. Forshind, E., NMR Basic Principles and Progress, P. Diehl, E. Fluck, R. Kosfeld (eds.), (Springer-Verlag, New York 1971), Vol. 4, p. 145-166.

8. Lenk, R., W. Bernardini, M. Bonzon and H. Greppin, Chem. Phys. Lett. 88, 119, (1982).

9. MacKay, A. L., M. Bloom, M. Tepfer and I. E. P. Taylor, Biopolymers 21, 1521, (1982).

10. Earl, W. L. and D. L. VanderHart, J. Am. Chem. Soc. 102, 3251, (1980).

11. Atalla, R. H., J. C. Gast, D. W. Sindorf, V. J. Bartuska and G. E. Maciel, J. Am. Chem. Soc. 102, 3249, (1980).

12. Jones, R. G., NMR Basic Principles and Progress, P. Diehl, E. Fluck, R. Kosfeld (eds.), (Springer-Verlag, New York 1969), Vol. 1, p. 97-144.

13. Randic, M., J. Magn. Res. 59, 34, (1984) and references therein.

14. Randic, M., personal communication, Dept. of Chemistry, ISU.

REMERCIEMENTS

Je voudrais remercier le Professeur Gerstein pour son encouragement et son support durant mes travaux. L'inspiration des membres de notre groupe de recherche a contribuée énormément à mon éducation au cours des dernières années. Je tiens a remercier Paul Murphy, Peter Cheung, Tom Apple, Gina Hoatson, Mercedes Silva-Crawford, Chuck Fry, Paul Tindall, Joe Iwamyia, Russ Walker and Po-Jen Chu. Je suis reconnaissant au Conseil de recherches en sciences naturelles et en génie du Canada pour une bourse d'étude, 1979-1982. L'excellent travail de Heidi Anderson qui a dactylographiée cette thèse est apprécié énormément. Je voudrais remercier de tout mon coeur Lois et Erin pour l'aide, le support et la patience qu'elles ont démontrées durant ces recherches.